UV-SULFITE BASED ADVANCED REDUCTION TREATMENT OF DISINFECTION BYPRODUCTS AND PERFLUOROOCTANOIC ACID

A Dissertation

by

VENKATA SAI VAMSI BOTLAGUDURU

Submitted to the Office of Graduate and Professional Studies of
Texas A&M University
in partial fulfillment of the requirements for the degree of

DOCTOR OF PHILOSOPHY

Chair of Committee,	Bill Batchelor
Committee Members,	Qi Ying
	Ahmed Abdel-Wahab
	Raghupathy Karthikeyan
Head of Department,	Robin Autenrieth

May 2016

Major Subject: Civil Engineering

ABSTRACT

Advanced reduction processes (ARP) are a class of chemical treatment processes that target oxidized contaminants in water/wastewater. ARPs operate through the generation of reducing radical species such as the hydrated/aqueous electron (e_{aq}^-). UV irradiation of sulfite (SO_3^{2-}) in solution is an effective generation method for e_{aq}^-. The photochemistry of sulfite in solution renders the UV/ SO_3^{2-} ARP advantageous for application to water/wastewater treatment. UV/SO_3^{2-} ARP was successfully tested for application to disinfection byproduct removal and perfluorooctanoic acid (PFOA) defluorination.

Batch experiments were conducted to develop kinetic data for defluorination of PFOA. A pseudo component kinetic model for stepwise defluorination of PFOA was applied to experimental observations of inorganic fluoride to obtain two rate constants for PFOA defluorination. The effectiveness of UV/SO_3^{2-} ARP was tested under UV-L and excimer lamps. Quantum yields for the process were calculated to be in the range of 0.002 to 0.004 mol/Ein. Presence of radical scavengers such as alkalinity lowered the kinetics and quantum yields for the process. Excimer lamp offered improvement in kinetics but required greater energy input, due to low UV conversion efficiency.

Photolytic removal of chlorite (ClO_2^-) was investigated under UV-L lamp. Aqueous chlorite photolysis resulted in a reduced form (Cl^-) and an undesirable oxidized form (chlorate, ClO_3^-). The effect of background water constituents, natural organic matter (NOM) and alkalinity, on photo degradation of chlorite was studied. Results

indicate that NOM significantly reduces chlorate formation by scavenging oxidizing radicals and hindering chlorine dioxide production. The problem of chlorate formation due to high DO in water could be eliminated by applying UV/SO_3^{2-} ARP with high sulfite doses.

Batch kinetic experiments for reduction of bromate (BrO_3^-) with UV/SO_3^{2-} ARP were conducted. A generic kinetic model for functioning of ARPs was applied to understand the effects of process variables on bromate reduction kinetics. Low wavelength excimer lamp improved BrO_3^- reduction kinetics significantly, but required an order of magnitude higher electrical energy as compared to the UV-L lamp. The dual effect of NOM is to scavenge reducing radicals and to filter UV irradiance and these effects were examined to determine if they would be significant limitations for application of UV/SO_3^{2-} ARP to natural waters with high NOM concentrations.

DEDICATION

I dedicate this dissertation work to my family. A special feeling of gratitude to my parents, whose encouragement and ardent support kept me going throughout the enduring process of doctoral study.

ACKNOWLEDGEMENTS

I would like thank my committee chair Dr. Bill Batchelor for his guidance, support, encouragement, and most of all patience throughout the entire process.

I would like to thank my committee members Dr. Qi Ying, Dr. Ahmed Abdel-Wahab and Dr. Raghupathy Karthikeyan, for agreeing to serve on my committee and being generous with their expertise and precious time.

I would like to acknowledge and thank Texas A&M University for giving me the opportunity to conduct my research and providing any assistance requested. Special thanks goes to the friends, colleagues and staff members at TAMU who made the time in graduate school memorable, exciting and a great learning experience.

Thanks to the Qatar National Research Fund and Texas Hazardous Waste Research Center for providing the financial assistance to make this research possible This dissertation was made possible in part by a grant from the Qatar National Research Fund under its National Priorities Research Program award number NPRP 4-1174-2-458.

I would like to thank the city of College Station which became a home away from home for nearly a decade. Aggieland with its trademark features will always be a special place on the planet that shaped and developed my personality.

I thank all the teachers and professors during my academic journey that helped me develop the basic scientific and critical thinking skills.

TABLE OF CONTENTS

Page

LIST OF FIGURES

Page

LIST OF TABLES

Page

CHAPTER I

INTRODUCTION

Chemical redox reactions are the basis for numerous water/wastewater treatment technologies. The ability of redox reactions to chemically transform target contaminants to innocuous forms has enabled their use in diverse treatment processes. Classification of a treatment process as an oxidation or reduction process is based on the nature of the reaction undergone by the target contaminant during the treatment process. If the target contaminant undergoes oxidation, i.e. it loses electrons/increases its oxidation number, the treatment process is considered an oxidation process and vice-versa. Chlorination is one of the most common examples of an oxidation process in water treatment. In drinking water treatment, chlorine (Cl_2) is used to oxidize organic compounds, ferrous iron and manganese that cause taste/odor/color problems. In wastewater treatment, chlorine (Cl_2), ozone (O_3), hydrogen peroxide (H_2O_2) can be applied as oxidizing and disinfecting agents for lowering oxygen demand (BOD/COD), ammonia, ferrous iron and sulfide. These chemicals also improve the performance of biological treatment by oxidizing non-biodegradable and other organic compounds that inhibit bacterial growth. Reduction processes have been directed toward treatment of water contaminated with halogenated/nitrated organics and heavy metals. A typical example of a reduction process is dechlorination of tetrachloroethylene (PCE) with zero valent iron (ZVI, Fe^0). Reducing agents such as ZVI, dithionite ($S_2O_4^{2-}$), bi/sulfite (HSO_3^-/SO_3^{2-}) find

application in treating waters contaminated with chlorinated organics, chromium and nitrate.[1, 2]

Advanced redox processes (AROP) are an improvement of the conventional redox processes. AROPs involve the generation of free radicals by the activation of redox reagents in water. These highly reactive free radicals are the species responsible for oxidation/reduction of the target contaminant. AROPs are characterized by significant increase in overall reaction kinetics and extent of target contaminant destruction.[1-3] Advanced oxidation treatment (AOT) has been an effective technology in reducing the overall COD of wastewaters from industrial sources containing complex organics such as aromatics, alcohols, pesticides and other hydrocarbon contaminants. The principal oxidizing species in most AOTs is the hydroxyl radical (OH·). OH· with an oxidation potential of 2.70 V is a powerful and non-selective radical that is effective against a wide array of target contaminants. Generation of OH· can be achieved through several combinations of oxidizing agents and activating methods.[1-3] Sulfate radical (SO_4^-·) is another powerful but selective oxidizing species (2.5-3.0 V) that is being studied as the basis for several AOTs aimed at disinfection and natural organic matter (NOM) removal.[3] Examples of some AOTs and their generation methods are summarized in Table 1-1.[2, 3] Advanced reduction processes (ARP) are counterparts to AOTs and are in the nascent stage of development. The principal reducing species in ARPs is the hydrated/aqueous electron (e_{aq}^-). The hydrated electron in solution is a free electron surrounded by oriented water molecules. It acts like a single charge anion and a powerful reducing agent, with a reduction potential of -2.9 V.[4] In acidic solutions, the hydrogen

atom (H·), which is the conjugate acid for e_{aq}^-, functions as the principal reactive radical.[5] The generation of hydrated electrons can be achieved through various methods presented in Table 1-2.[3, 5-11]

Table 1-1. Examples of oxidizing radicals and generation methods in AOTs[2, 3, 12]

Oxidizing radical	Generation Process	Stage of Development
Hydroxyl (·OH)	UV/O_3	Commercial
	H_2O_2/O_3	Commercial
	UV/H_2O_2	Commercial
	Fe^{2+}/H_2O_2	Commercial
	$UV/ Fe^{2+}/H_2O_2$	Lab Scale
	UV/TiO_2	Pilot Scale
Sulfate radical ($\cdot SO_4^-$)	$H_2O_2/S_2O_8^{2-}$	Lab Scale
	$UV/S_2O_8^{2-}$	Lab Scale
	$Fe^{2+}/ S_2O_8^{2-}$	Lab Scale
	O_3/HSO_5^-	Lab Scale

Table 1-2. Examples of generation methods for reducing radical in ARPs

Reducing radical	Generation Process	Reported Quantum Yields[3, 5-11] (mol/Ein)
Hydrated electron (e_{aq}^-)	UV/SO_3^{2-}	0.391 (193 nm), 0.108 (248 nm), 0.116 (254 nm)
	UV/I^-	0.497 (193 nm), 0.270 (222 nm), 0.286 (248 nm)
	VUV/H_2O	0.04-0.08 (147 nm), 0.02-0.04 (185 nm)
	$UV/Fe(CN)_6^{4-}$	1.00 (193 nm), 0.674 (248 nm), 0.24 (254 nm)
	$UV/ S_2O_3^{2-}$	0.518 (193 nm), 0.025 (248 nm)
	Electron beam	0.27 (µmol/J)

UV irradiation of sulfite is a generation method for which promising results have been reported at the lab scale in degradation of oxidized contaminants. UV/SO_3^{2-} combination has been successfully used to reduce halogenated organic contaminants such as vinyl chloride, 1,2, DCA, mono-chloro acetic acid and inorganic contaminants such as perchlorate and nitrate.[13-16] The photochemistry of sulfite in solution and the end products of the process renders the UV/sulfite ARP advantageous for application to water/wastewater treatment. Sulfite photochemistry and free radical transformations can be summarized in reactions (1) to (8).[9, 17, 18] In the absence of DO and other oxidized

species, predominant reactions would be (1-1) to (1-3), with sulfate (SO_4^{2-}) as the major end product.

$SO_3^{2-} + hv \rightarrow SO_3^{-}\cdot + e_{aq}^{-}$ (1-1)

$SO_3^{-}\cdot + e_{aq}^{-} \rightarrow SO_3^{2-}$ (1-2)

$SO_3^{-}\cdot + SO_3^{-}\cdot + H_2O \rightarrow SO_4^{2-} + SO_3^{2-} + 2H^{+}$ (1-3)

$SO_3^{-}\cdot + O_2 \rightarrow SO_5^{-}\cdot$ (1-4)

$SO_5^{-}\cdot + HSO_3/SO_3^{2-} \rightarrow HSO_5^{-} + SO_3^{-}\cdot + H^{+}$ (1-5)

$SO_5^{-}\cdot + HSO_3/SO_3^{2-} \rightarrow SO_4^{2-} + SO_4^{-}\cdot + H^{+}$ (1-6)

$SO_4^{-}\cdot + HSO_3/SO_3^{2-} \rightarrow SO_4^{2-} + SO_3^{-}\cdot + H^{+}$ (1-7)

$HSO_5^{-}/SO_5^{2-} + HSO_3/SO_3^{2-} \rightarrow 2SO_4^{2-} + 2H^{+}$ (1-8)

The functioning of an ARP is dependent on four major factors:

i. Type of UV lamp used for irradiation

ii. Characteristics of water matrix

iii. Chemical nature of target contaminant

iv. Nature of reagent used

Any advanced treatment process that utilizes UV irradiation is heavily dependent on characteristics of the UV lamp used for activation of reducing/oxidizing agents. UV lamp characteristics such as emission spectrum, output irradiance and efficiency affect overall performance of the treatment process. The part of electromagnetic spectrum that is classified as UV is between wavelengths 100 and 400 nm, within which the germicidal

portion is between 220 and 300 nm. Typical UV disinfection units and AOTs use low (UV-L) or medium pressure (UV-M) mercury lamps. UV-L lamps have monochromatic emission at 253.7 nm, medium pressure lamps emit a broad range of UV (200-400 nm).[2] Excimer lamps are a new generation of V/UV lamps which can emit quasi-monochromatic V/UV. . These lamps operate by forming excited dimer molecules such as XeCl*, ArCl*, ArF* and KrCl*. Depending on the excimer molecule, these UV lamps produce high energy photons at various V/UV wavelengths (e.g. 172, 193, 207 and 222 nm).[10] Excimer UV lamps have application in surface treatment such as UV curing, etching, film deposition in printing industries Selection of UV lamp for UV/sulfite ARP needs to consider the emission spectrum of the lamp. UV lamps that have an emission spectrum that is closest to or matches with peak absorption wavelength of sulfite or whatever reagent is being used may be best suited. The primary irradiation sources used in previous studies of UV/sulfite process were UV-L and UV-M lamps.[13-16] Considering the absorbance spectrum of sulfite solutions with peak emission around 190-200 nm as previously reported, it is imperative to test the performance of UV/SO_3^{2-} process with an excimer lamp with matching peak emissions around 200 nm.[19] The ability of e_{aq}^- generated from this process to react with both organics and inorganics is of value to development of the ARP.[20] Thus, UV/sulfite ARP needs to be tested for removal of a recalcitrant organic contaminant such as perfluorooctanoic acid (PFOA) and oxidized inorganics such as bromate (BrO_3^-) and chlorite (ClO_2^-).

The research objectives for the current study are described as follows.

1. Test the effectiveness of UV/sulfite ARP for degrading aqueous PFOA, chlorite and bromate
2. Formulate a generic model encapsulating the reactions in a UV/sulfite ARP
3. Study the effect of process variables such as pH, reagent dose and UV irradiance on kinetics of target contaminant removal and product recovery
4. Compare relative performance of low wavelength excimer lamp (222 nm) and high wavelength UV-L lamp (254 nm with respect to kinetics and energy requirement
5. Investigate the effect of interferences and scavengers such as natural organic matter (NOM), nitrate and dissolved oxygen on the UV-Sulfite ARP

CHAPTER II

DEFLUORINATION OF AQUEOUS PERFLUOROOCTANOIC ACID WITH UV-SULFITE ADVANCED REDUCTION PROCESS

Introduction

Perfluorinated chemicals (PFCs) are a group of synthetic substances that have industrial application as surfactants, lubricants, stain/soil repellents and fire retardants. Due to the high energy of carbon-fluorine bonds (552.0 kJ/mol), PFCs have unique physical and chemical properties such as thermal stability and oxidation resistance.[21, 22] The same physiochemical properties that make PFCs valuable in industrial usage, also make them persistent in water bodies and difficult to remove using conventional water/wastewater treatment technologies.[23] Perfluorooctanoic acid (PFOA) and perfluorooctane sulfonic acid (PFOS) are the two primary PFCs that have been reported to accumulate in the aquatic environment and living organisms.[24-27] In the last decade, several studies in the United States (US) have indicated the presence of PFCs even in the blood of the general population.[28] 3M, which used to be largest the manufacturer of these chemicals, terminated production of PFOA and PFOS in 2005.[29] However, due to natural degradation of other fluorinated telomers, PFOA is still found in industrial and domestic wastewaters.[30] PFOA and PFOS are potential human endocrine disruptors and cause developmental and other adverse effects in laboratory animals.[31] The Fourth Conference of the Stockholm Convention classified PFOS and it salts as persistent organic pollutants (POPs).[32]

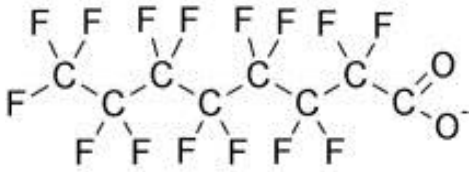

Figure 2-1. Structure of deprotonated PFOA

Fig. 2-1 shows the chemical structure of the deprotonated form of PFOA ($C_8F_{15}O_2$). The major entry routes of PFOA into the environment include wastewater from fluoropolymer manufacturing processes, semiconductor coatings and domestic units.[31] Fate and transport of PFOA in surface waters are dependent primarily on the pH, solubility, bioaccumulation factors, and water partitioning coefficients with respect to sediments (K_{SW}) and soil organic content (K_{OC}). Due to the high energy of carbon-fluorine bonds, PFOA is persistent and has very low natural, photo- and bio-degradability in the aquatic environment.[33] PFOA has a pK_a of -0.5, and exists as a deprotonated anion in most surface waters.[22] Due to its surfactant properties, PFOA has affinity to accumulate at the air-water interface. A study conducted on the relative concentrations of PFOA in the surface, subsurface and micro layer (top 1 mm) of coastal China found enrichment of PFOA in the sea micro layer.[34] Sorption of PFOA onto sediments is a transport process affected by the suspended solids concentrations and particulate organic carbon. Log K_{OC} of PFOA are around 2.5 cm^3/g, which is low compared to other perfluorinated compounds.[35] In aquatic bodies with low suspended

solid concentrations, the primary transport process for PFOA is in the dissolved phase. However, sediments rich in organic content and salinity could show greater sorption of PFOA. This in turn results in greater bioaccumulation in benthic organisms. Several studies in the last decade have reported the occurrence of PFOA in biota of remote regions as well as the Great Lakes region in the US.[36] Partitioning of aqueous PFOA onto the lipids of fish could be one of the reasons for large geographical distribution.

Treatment processes to remove PFOA in wastewaters are being studied with conventional and advanced approaches. The conventional wastewater treatment methods such as activated carbon adsorption were not found to be useful in eliminating PFOA. [23, 37, 38] The majority of studies done on advanced oxidation technologies (AOTs) were also inefficient in degrading PFOA. The principal oxidizing radical in AOTs is the hydroxyl radical (•OH) and it has been reported to not have an affinity to the high energy C-F bond in PFOA.[23, 38] However, some studies indicated an improvement in the effectiveness of Fenton AOT for PFOA, by using alkaline 2-propanol medium or 4-methoxyphenol as a co-substrate for the •OH radical.[39] The presence of oxidants such as persulfate, ferric ion and periodate have also improved the oxidative degradation rate of PFOA.[39-41] This improved degradation of PFOA has been attributed to the formation of PFOA complexes with ferric iron and sulfate radical.[39] However, complete defluorination of PFOA using AOTs has not been made feasible under normal pH conditions.

In the last few years, UV-based photolysis methods were shown to be very promising for PFOA removal. Direct UV photolysis and photochemical oxidation are

the most extensively studied treatment mechanisms for PFOA.[42-45] Direct photolysis of PFOA using UV at 254 nm is not very effective, as PFOA absorbance is very low at that UV wavelength,[44] and the energy of 254 nm photons is insufficient to break the C-F bonds in PFOA. However, PFOA has strong absorption in the vacuum UV (VUV, 10-200 nm) region and this phenomenon has been used to directly photolyze PFOA with 185 nm UV light.[44] Commercial UV lamps used for disinfection emit a major portion of UV light at wavelengths greater than 200 nm, with only a small portion (3–8%) of shorter wavelengths in the VUV region. Additionally, water absorbs VUV at 185 nm with a linear extinction coefficient around 2 cm^{-1} and photolyzes to hydrogen atom (•H) and hydroxyl radicals (•OH).[46] This would interfere with the photolytic defluorination process. Thus, direct photolysis has limitations when being employed for PFOA treatment in wastewater. In a domestic or industrial wastewater, the absorbance of UV light by PFOA will be hindered by the presence of a large number of UV absorbing species such as natural organic matter (NOM) and metal contaminants. The turbidity in wastewaters also scatters UV and limits the amount of irradiation received by target compound.

Advanced Reduction Processes (ARPs) are a recently explored class of treatment processes that operate similar to AOTs in water/wastewater.[47] The principal operating mechanism of ARPs is to generate highly reactive free radicals that reduce oxidized target compounds. The formation of reducing radicals is accomplished by activating reducing agents in solution. Several activating methods such as UV irradiation, high energy electron beam (HEEB), ultrasound and microwave were tested and it was found

that UV light is highly effective in reducing recalcitrant compounds and suitable to fit into a water treatment process.[48, 49] Sulfite, dithionite, sulfide and ferrous iron are some of the chemicals tested as reducing agents.[50] Recent studies on sulfite-UV ARPs indicate that their success in de-chlorination of vinyl chloride, mono-chloro acetic acid and 1,2-DCA.[50, 51] UV irradiation of sulfite solutions leads to production of hydrated electrons (e_{aq}^-) and sulfite radical ($^{\bullet}SO_3^-$) as shown in reaction (2-1).[52-54] This reaction can be reversed (reaction (2-2)) and the sulfite radical can react with itself (reaction (2-3)). The hydrated electron is a strong reductant with standard reduction potential of -2.9 V and an affinity toward halogenated organics.[5] Sulfite radical can act as an oxidant or reductant depending on the characteristics of other species in solution.

$$SO_3^{2-} + hv \rightarrow {}^{\bullet}SO_3^- + e_{aq}^- \qquad (2\text{-}1)$$

$$^{\bullet}SO_3^- + e_{aq}^- \rightarrow SO_3^{2-} \qquad (2\text{-}2)$$

$$^{\bullet}SO_3^- + {}^{\bullet}SO_3^- + H_2O \rightarrow SO_4^{2-} + SO_3^{2-} + 2H^+ \qquad (2\text{-}3)$$

Several combinations of reducing agents and activating methods have been tested to defluorinate PFOA. The generation of hydrated electrons is key in such approaches. Laser flash photolysis of $K_4Fe(CN)_6$ and UV activation of KI were reported to be successful in reductive defluorination of PFOA.[55, 56] However, these methods are limited in their development as a wastewater treatment process due to toxicity and regulation of chemicals involved. In addition, some of these treatment processes involve reaction conditions with highly acidic pH, formation of metal complexes and production of

gaseous fluoroalkane byproducts.[32, 42, 43] It is therefore desirable to select an efficient treatment process for PFOA that could be scaled up with minimal limitations. Summary of methods based on photochemical reduction that have been tested for PFOA removal and their performance is described in Table 2-1.

The combination of sulfite and UV light offers a chemically benign and operationally simple approach to PFOA degradation. It has been tested to be highly effective in defluorination of PFOA [57]. Defluorination around 90% was reported after 24 h reaction time in anoxic water systems. The defluorination process of PFOA proceeded through formation of several short-chain perfluorinated carboxylic acids, perfluorinated alkyl sulfonates and partially fluorinated organics. Hydrated electron generated from sulfite irradiation was identified as the reducing radical that attacks fluorinated compounds to release free fluoride in water.[57] The current research aims to build on previous studies of UV/sulfite ARP for PFOA and develop quantitative parameters that define the process.

Table 2-1. Summary of successful PFOA defluorination methods

Reagent	Activation method	Optimum Conditions	Maximum defluorination	Reference
Sulfite (SO_3^{2-})	UV	Neutral to high pH, Anoxic water system, e_{aq}^-	90%	57
Ferric iron (Fe^{3+})	UV	Bubbling of molecular O_2	48%	58
Ferrous iron (Fe^{2+})	UV	Acidic pH 2-3,	100%	59
Potassium iodide (KI)	UV	Alkaline pH 9, e_{aq}^-	100%	56
Periodate (IO_4^-)	VUV	e_{aq}^- generation	25%	60
Fenton (Fe^{2+}-H_2O_2)	UV	Acidic pH, OH•	53%	61
Ferric iron (Fe^{3+})	VUV	Acidic pH 3-4, OH•	50%	62

The objectives of the current research are:

i. Investigate the effect of process variables (pH, sulfite concentration and type of UV lamp) on PFOA defluorination in a batch reactor system.
ii. Apply a mechanistic kinetic model to study the effect of process variables on defluorination rate constants
iii. Study the effect of radical scavengers such as alkalinity and nitrate on PFOA defluorination
iv. Estimate the energy requirements of UV-sulfite ARP for PFOA removal

Methodology

UV Setup

Two monochromatic UV lamps were used to activate sulfite in solution. A UV surface disinfector setup, UVS-236 DS, was purchased from Lumalier (Memphis, TN, USA). The setup was equipped with a Philips TUV PL-L36W/4P low pressure mercury lamp that emits UV at 254 nm. This Philips germicidal lamp does not emit at 185 nm and is representative of a typical UV lamp commonly used in water/wastewater disinfection. The characteristics of UV-L lamp are described in Table 2-2 and the emission spectrum is shown in Fig. 2-2.

Table 2-2. Characteristics of UV-L lamp

Lamp	Type	Length (cm)	Input Power (W)	Output UV-C Power (W)	Amps	Volts	Lifetime (h)
PLL36W/TUV	Low Pressure (Hg)	41.5	36.0	12.0	0.44	105	9000

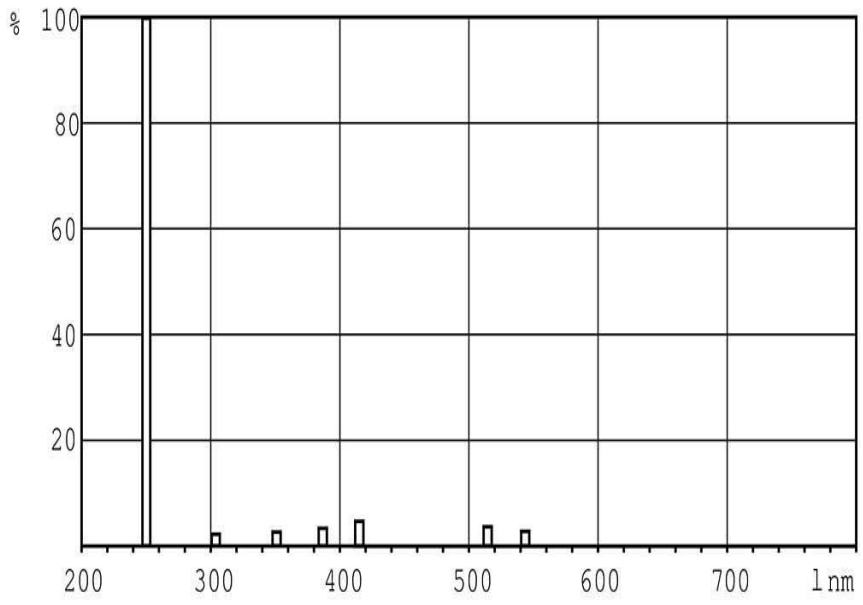

Figure 2-2. Emission spectrum for UV-L lamp

A second UV lamp that emits monochromatic UV at 222 nm was purchased from Institute of High-Current Electronics, Russian Academy of Sciences, Tomsk, Russia. This lamp produces UV due to the formation of excited dimer of Krypton Chloride (KrCl). The energy requirements and dimensions of the excimer lamp is detailed in Table 2-3. Emission spectrum for the excimer lamp is shown in Fig. 2-3.

Table 2-3. Characteristics of UV-KrCl excimer lamp

Excimer molecule	KrCl*
Wavelength, λ (max) (nm)	222
Dimension of output window (cm)	6×10
Power consumption (W)	45
Radiant exitance (mW/cm^2)	17
Power requirements (V)	110±5, 60 Hz
Lifetime (h)	8000
Dimension (cm)	25×8×8

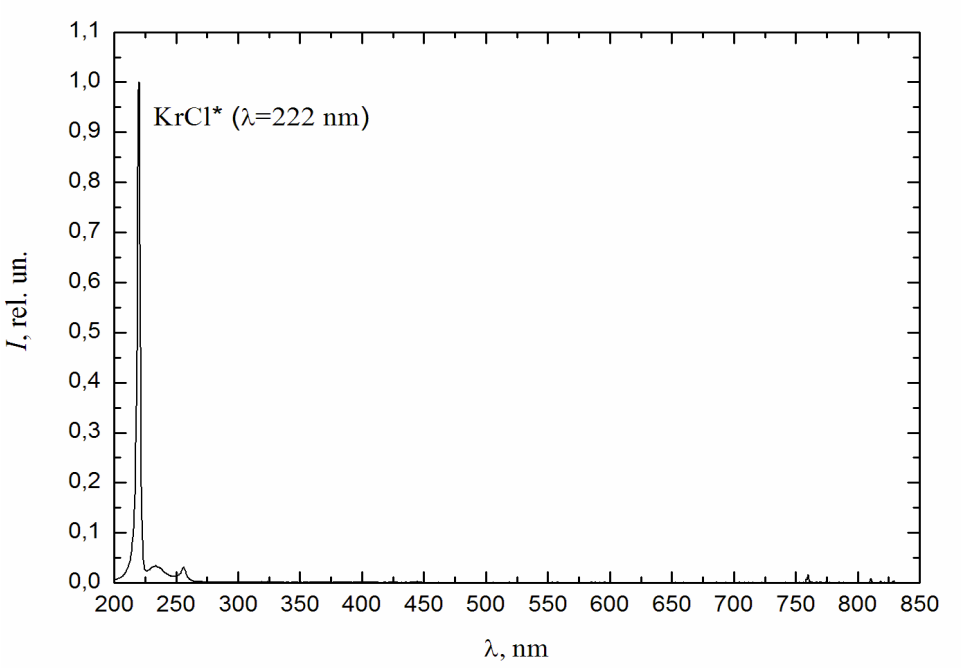

Figure 2-3. Emission spectrum for UV-KrCl excimer lamp

Two separate enclosures were built to house the UV-L and UV-KrCl lamps. A representation of the enclosures is provided in Fig. 2-4. The UV enclosure was simulating a bench scale UV apparatus used in water disinfection studies. However, the UV beam was not perfectly collimated due to space constraints within the UV enclosure. The UV lamps were fixed onto the enclosure and directly on top of the reactor with experimental solution. A petri dish with a volume of 100 mL and depth of 1.3 cm was placed on a magnetic stirrer and directly below the UV lamp. To ensure a completely mixed condition, the stirrer was on a fixed speed throughout the experimental time. UV intensities at surface of the petri dish were measured with a UVC 512 light meter calibrated at 254 nm (Professional Equipment, Janesville, WI, USA). UV irradiance

measurements reported in the current study may require correction factors when extrapolated to pilot scale and large scale UV treatment systems. UV irradiation undergoes reflection and refraction at the air/water interface and at the bottom of the petri dish. It was reported that not accounting for reflection and refraction effects could result in errors up to 25% in calculating UV dose requirements for disinfection studies. [63, 64] Following are the major correction factors suggested by previous studies on bench scale UV disinfection.[63, 64]

Reflection Factor (RF): UV light emitted from the lamp passes from air to water medium, in the current reactor. Due to a difference in refractive index of the two mediums, a fraction of UV light is reflected off the interface. The fraction reflected is also dependent on the angle of incidence. UV disinfection studies at bench scale involve collimated beam apparatus, where UV light is assumed to be normally incident. For UV lamps with emission spectrum in the wavelength range of 200-300 nm, the RF value suggested is 0.025.

Petri Factor (PF): The UV irradiance measured by the UVC 512 light meter is over the area of 0.5 cm^2 centered on the petri dish. But, UV irradiance will vary over the surface area of the water sample in the petri dish. PF is a correction factor defined as the ratio of average of the incident UV irradiance over the area of the petri dish to the irradiance at the center. PF accounts for variance in UV over the surface area. For a collimated beam setup, PF is in the range of 0.9 to 1.0.

Divergence Factor (DF): For non-collimated UV setup, divergence of the UV beam increases significantly with the distance between UV lamp and the water sample. UV

irradiance decreases with distance from the lamp and the DF assumes that the decrease is proportional to the inverse square of the distance from the UV lamp. DF averages the inverse square function over the depth of the reactor.

The effect of UV reflection from the walls and bottom of the reactor would require the application of fluid dynamics approach to modeling UV irradiances distribution in the reactor. The current reactor, a petri dish would have different UV distribution pattern from a pilot/large scale reactor. Some studies have focused on developing computational tools for obtaining a discrete ordinates radiation model that simulates UV radiation patterns around UV-L lamp in a rectangular chamber filled with water. Results from these studies indicate that consideration of wall reflection improved the accuracy of model predictions on the UV irradiance distribution.[63, 64]

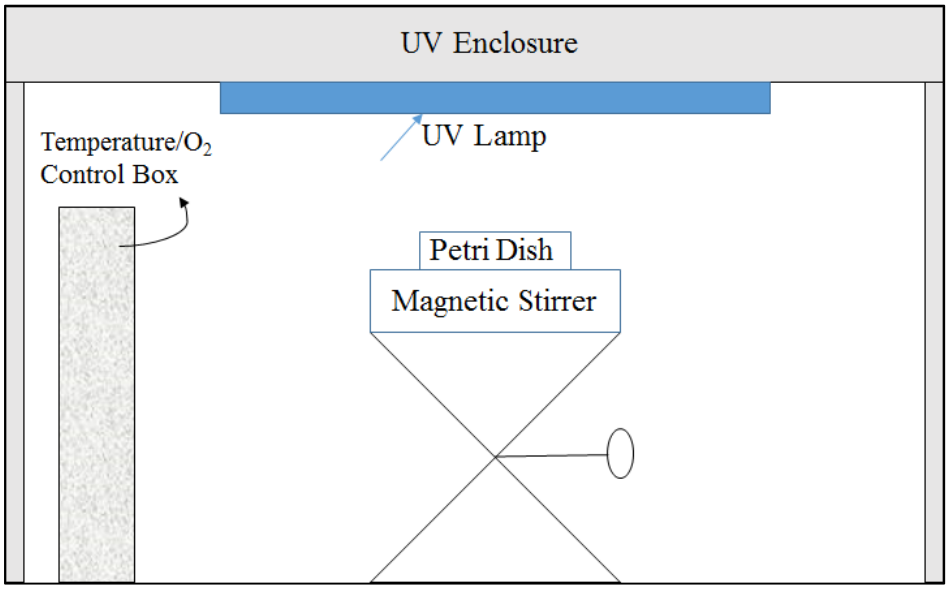

Figure 2-4. Frontal view of UV enclosure

UV absorption spectrum of PFOA and sulfite were measured with Agilent 8453 UV-visible spectroscopy system. Quartz cuvettes of 1 cm path length and 4 mL sample volume were used to determine molar extinction coefficients of target and reductant.

Chemical reagents

Potassium fluoride, acetate, nitrate, and formate (1000 mg/L) of Ion Chromatography (IC) standard grade were purchased from Inorganic Ventures (Christiansburg, VA, USA). Sodium sulfite (anhydrous, 98.6%) was obtained from Avantor Performance Materials (Center Valley, PA, USA). Buffers were prepared from potassium phosphate (anhydrous, 97%), potassium hydrogen phosphate (anhydrous, 98%), potassium di-hydrogen phosphate (99%) and phosphoric acid (85%) purchased from Alfa Aesar (Ward Hill, MA, USA). PFOA solid (anhydrous, 98.6%) was purchased from Alfa Aesar (Ward Hill, MA, USA).

Anaerobic chamber

All chemical solutions were prepared and experiments conducted inside an anaerobic chamber (Coy Laboratory Products Inc.). The chamber atmosphere was maintained at 95% nitrogen (N_2) and 5% hydrogen (H_2). Trace oxygen in the chamber was removed by a palladium catalyst connected to a recirculating fan, as shown in Fig. 2-4. The catalyst reacted with H_2 in the chamber atmosphere and converted trace levels of oxygen to water vapor. Oxygen levels were monitored with an Oxygen and Hydrogen Analyzer (Coy Laboratory Products Inc.) and a resazurin indicator. Deionized water (ultra-pure 18 MΩ·cm) was deoxygenated by purging with 99.99% N_2 for 2 h. This deoxygenated deionized water was allowed to equilibrate with the atmosphere in the anaerobic

chamber for 12 h. All chemicals sensitive to oxidation were stored in the chamber throughout the time period of the experiments.

Fluoride analysis

Analyses for inorganic fluoride and anions of organic acids, formic and acetic acid were conducted on a Dionex DX-500 ion chromatography system. A hydroxide selective anion exchange column IonPac AS19 of dimensions 4 x 250 mm and a guard column AG19 of dimensions 4 x 50 mm were used to separate fluoride, formate and acetate ions. A 10-mM sodium hydroxide solution at a flow rate of 1 mL/min was used as the eluent. Sample vials (0.5 mL) were used in the AS-40 auto sampler with a sample injection loop of 200 µL. The DX-500 was equipped with a GP 40 gradient pump, CD 20 conductivity detector and AERS 500 (4 mm) suppressor. The principal interferences for fluoride analysis would be the overlap of fluoride and formate/acetate peaks and presence of high sulfite concentrations. To counter this, calibration standards of fluoride were prepared with equal concentrations of formic and acetic acids. Characteristics of anion analysis using the method described above are summarized in Table 2-4.

Table 2-4. Anion analysis method

Anion	Method detection limit (µg/L)	Retention time (min)
Fluoride	25	5.4
Acetate	120	6.0
Formate	70	6.4

The factors/process variables studied include: type of UV lamp, pH, sulfite dose, alkalinity and nitrate. The responses measured were max defluorination ratio, rate constants, quantum yield, time for 50% defluorination and electrical efficiency per order (E_{EO}).

Data analysis – quantitative parameters

Defluorination ratio

In order to explain the effect of process variables on defluorination of PFOA, quantitative parameters that describe rate and efficiency of defluorination need to be developed. Defluorination ratio, which is a measure of extent of fluorine removed from organic compounds, is calculated as in equation 2-1.

$$DeF_t = \frac{C_{F,t}}{PFOA_0.15} \quad \text{2-1}$$

DeF_t is the defluorination ratio at time t,

$C_{F,t}$ is the inorganic fluoride concentration in mol/L at time t

$PFOA_0$ is the initial concentration of PFOA, in mol/L

Defluorination ratios of experiential data are plotted across time to observe the extent to which fluorinated organics are removed at a given time in an experiment. Quantitative determination of rate constants can be made by developing a semi-mechanistic kinetic model for PFOA defluorination. This model is based on the principal mechanism by which PFOA releases inorganic fluoride, but uses a pseudo-component, rather than actual chemical intermediates. As reported in previous studies of PFOA degradation, hydrated electrons from photolysis of sulfite, attack fluorine attached to carbon. This results in a stepwise breakup of PFOA to less fluorinated and shorter chain carboxylic acids.[40, 57, 59, 62] These compounds are further reduced by hydrated electrons releasing inorganic fluoride at every step. This phenomenon of stepwise reduction of PFOA is simplified to a single step and accounted for in the following one pseudo-component model.

One pseudo-component model (k_1, k_2)

The model assumes that PFOA represented by compound A, reacts with hydrated electrons generated by sulfite irradiation and breaks down to a pseudo compound, B and fluoride ions (F). Compound B reacts with hydrated electrons to further release the remaining fluoride. Previous research into PFOA degradation suggests the mechanism to

be step wise reductive defluorination in which the carbon–fluorine bonds adjacent to carboxylic groups are cleaved.[45, 57, 65]

Model reactions [1] and [2] are the basic steps in the model. Both model reactions are assumed to be first order with respect to compounds A and B. Detailed derivation of the model is provided in appendix A.

$A + m_1\ e_{aq}^- \rightarrow B + n\ F$ [1]

Rate of reaction, $r_1 = k_1\ [A]$

It is assumed that r_1 is first order reaction. So, the concentration of A at any time t, in a batch reactor can be calculated as, $[A] = [A]^0\ \exp(-k_1 t)$

k_1 is the first order rate constant and,

[A] is the molar concentration of PFOA at any time 't'

$[A]_0$ represents the initial molar concentration of PFOA

$B + m_2\ e_{aq}^- \rightarrow C + (15\text{-}n)\ F$ [2]

Rate of reaction, $r_2 = k_2\ [B]$

k_2 is the first order rate constant and,

[B] represents the molar concentration of a pseudo component formed from PFOA reduction

In the real system, multiple compounds/steps are involved in reductive defluorination. The total fluoride (F_t) in the system is present as

a. Fluoride attached to PFOA, A
b. Fluoride attached to pseudo component, B
c. Inorganic fluoride, F

Conducting a material balance for fluoride in a batch reactor with reactions described by these rate equations, concentration of fluoride at any time can be calculated as in equation 2-2:

$$F = 15[A]_0 - 15[A]_0 e^{-k_1 t} - n\left\{\frac{k_1[A]_0}{(k_2 - k_1)}\right\}\left(e^{-k_1 t} - e^{-k_2 t}\right) \qquad 2\text{-}2$$

'n' can vary depending on number of fluorine atoms attached to pseudo compound B. An iterative process was used to select 'n' value as 9, so as to minimize the errors between model and experimental data (residual plot added in Appendix A). The values for k_1 and k_2 were obtained by fitting fluoride concentration data to equation 2-2. Non-linear least squares regression using Levenberg-Marquardt algorithm in MATLAB was used to get estimates and 95% confidence intervals for k_1 and k_2. These rate constants provide a quantitative measure of defluorination kinetics.

Generic ARP model

Degradation of contaminants to intermediate products and complete reduction to innocuous end products by UV/Sulfite ARP is complex and involves multiple photolytic and chemical steps. The overall kinetics (rate of removal) of a specific target can be described by identifying the major reactions occurring in an ARP and developing rate equations for each reaction. This generic ARP model is useful in describing the effect of process variables on rate constants k_1 and k_2 obtained from the one pseudo component model. The major reactions occurring in an ARP and their respective rate equations are specified in Table 2-5.

Table 2-5. Basic reactions/steps involved in a UV/Sulfite ARP.

Steps	Reaction	Reactions	Rate equations
A.	Photolysis of target	Target + hν → Products	$r_A = \phi_T I_{avg} \epsilon_T C_T$
B.	Photolysis of sulfite	Sulfite + hν → R	$r_B = \phi_S I_{avg} \epsilon_S C_S$
C.	Target radical reaction	Target + R → Products	$r_C = k_{TR} C_T C_R$
D.	Scavenging of radicals	Scavengers + R → Products	$r_D = k_{ScR} C_{SC} C_R$

r_A, r_B, r_C and r_D are rates of individual reactions in an ARP,

ϕ_T and ϕ_S are quantum yields for photolysis of target and sulfite,

$\varepsilon_{,T}$ and ε_S are molar extinction coefficients for target and sulfite ($\log_e$ base),

C_T, C_S, C_R and C_{SC} are concentrations of target, sulfite, reducing radicals and scavengers

k_{TR} and k_{SCR} are pseudo first order rate constants for target-radical and scavenge- radical reactions. I_{avg} is the average UV irradiance in the reactor, which can be calculated as in equation 2-3.

$$I_{avg} = \frac{I_0\left(1-e^{(-\alpha L)}\right)}{\alpha L} \qquad 2\text{-}3$$

$$\alpha = \sum_{1}^{n} \varepsilon_i C_i \qquad 2\text{-}4$$

$\varepsilon_{,i}$ is the $\log_e$ base based molar extinction coefficient

C_i is concentration of UV absorbing species i,

I_0 is the incident UV irradiance measured at top of the reactor,

L is the depth of the reactor

Step A describes direct photolysis of target compound by UV absorption.

Step B describes photolysis of sulfite to produce reducing radicals i.e. hydrated electrons, according to reaction (2-1).

Step C accounts for reduction of target by reaction with reducing radicals.

Step D accounts for all of the scavengers such as carbonate, nitrate or dissolved organic matter that may consume reducing radicals in solution.

Assuming a stationary state for concentration of radicals in which the derivative is negligible relative to the rates, the following expression can be obtained,

$$\frac{dC_R}{dt} = r_B - (r_C + r_D) = 0 \qquad 2\text{-}5$$

$$\phi_S I_{avg} \varepsilon_S C_S = k_{TR} C_T C_R + k_{SCR} C_{SC} C_R \qquad 2\text{-}6$$

Thus, concentration of reducing radicals is

$$C_R = \left\{ \frac{\phi_S I_{avg} \varepsilon_S C_S}{k_{TR} C_T + k_{SCR} C_{SC}} \right\} \qquad 2\text{-}7$$

As target compound is removed by reactions A and C, the overall removal rate of target can be calculated as,

$$\frac{dC_T}{dt} = -\left(r_A + r_C\right) \qquad 2\text{-}8$$

$$\frac{dC_T}{dt} = -\left(\phi_T I_{avg} \varepsilon_T C_T + k_{TR} C_T C_R\right) \qquad 2\text{-}9$$

Substituting the expression for C_R from equation 2-7 and conducting a material balance on the target in a batch reactor, a generic equation for how the concentration of target changes in the UV/Sulfite ARP can be expressed as,

$$\frac{dC_T}{dt} = -\left\{\phi_T I_{avg} \varepsilon_T C_T + k_{TR} C_T \left[\frac{\phi_S I_{avg} \varepsilon_S C_S}{k_{TR} C_T + k_{SCR} C_{SC}}\right]\right\} \qquad 2\text{-}10$$

From the one pseudo component model, degradation of PFOA is assumed to follow first order kinetics as,

$$\frac{dA}{dt} = -k_1 A$$

From the above equations, the apparent first order rate constant (k_1) can be expressed as

$$k_1 = \left\{\phi_T I_{avg} \varepsilon_T + \left[\frac{k_{TR} \phi_S I_{avg} \varepsilon_S C_S}{k_{TR} C_T + k_{SCR} C_{SC}}\right]\right\} \qquad 2\text{-}11$$

Time for 90% defluorination (t_{90})

Using the values k_1 and k_2 obtained from the one pseudo component model, the time required for removal of 90% of organic fluorine (t_{90}) can be estimated by equation 2-12. This is the time required to achieve one order of magnitude reduction or 1-log removal of the target compound.

$$1.5[A]_0 - 15[A]_0 e^{-k_1 t_{90}} - n\left\{k_1[A]_0 / (k_2 - k_1)\right\}\left(e^{-k_1 t_{90}} - e^{-k_2 t_{90}}\right) = 0 \qquad 2\text{-}12$$

Initial Quantum yield (ϕ_0)

The efficiency of UV-Sulfite ARP was determined by calculating initial quantum yield for removal of PFOA (ϕ_0). The quantum yield for a photochemical reaction is the ratio of the rate of the reaction to the rate of photon absorption. In the current system, photons are absorbed primarily by sulfite in solution to produce hydrated electrons, which further reduce the target. The quantum yield for photolysis of sulfite (ϕ_S), depends on pH and is reported to be around 0.03 mol/Ein at pH 11 for UV-L lamp.[48] The hydrated electrons generated from sulfite photolysis react with and remove PFOA and other short chained fluorinated organics. So, quantum yield for PFOA removal is expressed as molecules of PFOA removed per Einstein of UV photon absorbed by sulfite. The following equation is used to calculate quantum yield (ϕ_0) at initial conditions when the rate of the reaction can be described as first-order. It also assumes that the reactor is well mixed and applies the Beer-Lambert law to calculate the average photon flux throughout the reactor when sulfite is the only compound absorbing light.

ϕ = [rate of reaction] / [rate of UV absorption]

$$\phi_0 = \frac{k_1[A]_0}{\frac{I_0}{L}(1-e^{-\varepsilon_S C_S L})} \qquad 2\text{-}13$$

k_1 is the initial rate constant for PFOA reduction,

L is the depth of the reactor,

$[A]_0$ is the initial PFOA concentration,

$\varepsilon_{,S}$ and C_S are molar extinction coefficient and concentration of sulfite,

I_0 is the flux of incident UV photons, Ein/m^2-s

Energy requirement (E_{EO})

The key factor determining the effectiveness of ARPs is the ability to generate highly potent chemical reductants such as the hydrated electrons (e_{aq}^-). Despite the fact that many combinations of ARPs have been tested to be very successful at the lab scale, their development and full scale commercialization depends on estimating the cost of hydrated electron generation. Since most ARPs involve UV lamps to activate reagents, they are electric energy intensive and energy could be a major fraction of the operating costs. Thus, estimates for energy requirement are necessary to compare different ARPs and provide the necessary data for scaling them up. Although, a number of factors such as environmental regulations, effluent quality goals and operational ease are considered in selecting a treatment technology, economics plays a decisive role. The following equations describe the procedure for estimating energy requirement for PFOA degradation using the UV/Sulfite ARP.

Electrical efficiency per order (E_{EO}) is the electrical energy required to degrade a target contaminant by one order of magnitude in a unit volume of contaminated water. For a batch reactor, E_{EO} can be calculated as in equation 2-14. E_{EO} is used as a standard measure for estimating energy requirements in AOTs. When kinetics of contaminant removal are first order, the E_{EO} will be constant over different initial concentrations.[66]

$$E_{EO} = \frac{P.t}{\log(\frac{C_0}{C_f})V} \qquad 2\text{-}14$$

P is the input power of the UV lamp needed to produce light energy absorbed in the reactor,

t is the time of UV lamp operation,

V is the volume of water treated,

C_0 and C_f are the initial and final concentrations of the contaminant

The power variable P, normalized by volume can be expressed as P_v and E_{EO} can be modified as

$$E_{EO} = \frac{P_V . t}{\log\left(\frac{C_0}{C_f}\right)} \qquad 2\text{-}15$$

The power of the UV lamp needed to produce light energy absorbed in the reactor, $P_{V,absorbed}$ can be calculated as,

$P_{V,absorbed}$ = $P_{V,applied}$ * fraction of UV absorbed

$$P_{V,absorbed} = \frac{I_0^{'}}{L}(1 - e^{-\sum \varepsilon_i C_i L}) \qquad 2\text{-}16$$

$I^{'}_0$ is the incident UV irradiance,

L is the depth of the reactor,

ϵ_i is the $\log_e$ based molar extinction coefficient of UV absorbing species i,

C_i is the concentration of species i,

The power applied needs to be adjusted as per the efficiencies of UV lamps specified in Table 2-6.

$P_V = P_{V,\ absorbed} / (\eta)$

η is efficiency of the UV lamp

EEO for PFOA removal is calculated as in equation 2-17,

$$E_{EO} = P_V . t_{90} \quad \text{2-17}$$

The power input and maximum UV output of the two UV lamps used in the current study are specified in Table 2-6.

Table 2-6. Power ratings and UV output of UV Lamps

Lamp Type	Input Power (W)	UV output (W)	Energy of photon (kJ/Ein)	Efficiency (η)
UV-KrCl	45	1.02	539.3	0.02
UV-L	36	12	471.4	0.33

Results and discussion

Photolysis of PFOA

Fig. 2-5 presents defluorination ratios of PFOA under direct photolysis with UV-L and UV-KrCl lamps. UV-L lamp does not produce any measureable extent of defluorination, whereas the excimer lamp photolyzes PFOA and results in significant concentration of inorganic fluoride over the irradiation time. Defluorination approaches 80% after 4 h of irradiation. Rate constants k_1 and k_2 were obtained from fitting the experimental data in Fig. 2-5 to the one pseudo component model in equation 2-2. The rate constants and model goodness of fit parameters are detailed in Table 2-7. k_1 ($0.96 \pm 0.09\ h^{-1}$) represents the pseudo first order rate constant for degradation of PFOA. k_2

($0.32 \pm 0.04\ h^{-1}$) represents the overall rate constant for degradation of short-chained and less fluorinated carboxylic acids formed from PFOA photolysis. Previous research into PFOA degradation suggests the mechanism to be step wise reductive defluorination in which the carbon–fluorine bonds adjacent to carboxylic groups are cleaved.[45, 57, 65] As, k_1 and k_2 are representative of the defluorination rates for the target PFOA and its subsequent less fluorinated products, the difference in k_1 and k_2 values indicates that defluorination rates are proportional to the length of carbon chain and extent of fluorination. This phenomenon is consistent with reduction of chlorinated organics, where the rate of de-chlorination decreases as the degree of chlorination reduces. The first order rate constants reported for PFOA photolysis with VUV at 185 nm are around 0.702 to 0.816 h^{-1}. The excimer lamp operating at 222 nm, has lower absorption cross section in water and unlike VUV irradiation, does not photolyze water to produce hydrogen atom (•H) and hydroxyl radicals (•OH).[46, 67] Thus, it may be more suitable for direct photolytic treatment. Formic acid and acetic acid were detected on the ion chromatograms. These products were consistent with reported photolysis of PFOA with VUV irradiation.[45]

The photon energy of 222 nm UV light (539.3 kJ/Ein) is 14% higher than that of 254 nm light (471.4 kJ/Ein). However, the photon flux supplied by the UV-L lamp in the current setup (2.864×10^{-8} Ein/s-cm^2) is more than double the flux supplied by excimer lamp (1.205×10^{-8} Ein/s-cm^2). The inability of the UV-L lamp to degrade PFOA is a due to the absorbance pattern of PFOA. As depicted in Fig. 2-6 and Table 2-8, PFOA absorbs 222 nm UV with an extinction coefficient (log_{10} base) of 88.9 $M^{-1}cm^{-1}$, whereas

UV_{254} absorption is negligible. Higher energy of 222 nm photons coupled with higher absorption produces the difference in defluorination patterns. The data demonstrate that UV at 222 nm from the excimer lamp is capable of cleaving the carbon–fluorine carbon-carbon bonds. Initial quantum yield for direct photolysis, which is a measure of efficiency, can be calculated to be 0.035 mol/Ein. This value was calculated from the slope of defluorination curve between 0 and 1 hr.

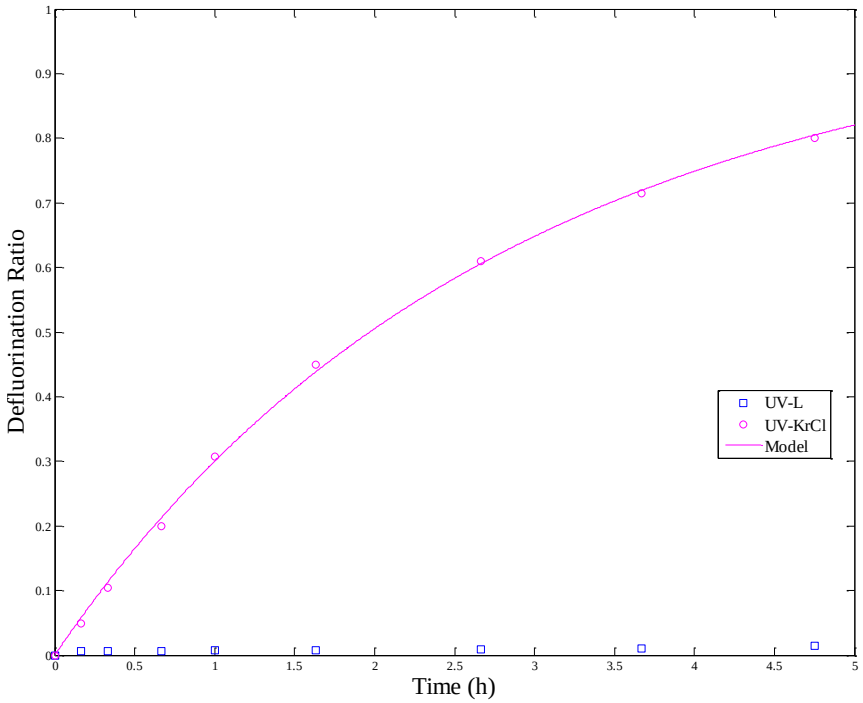

Figure 2-5. PFOA photolysis with UV-L and UV-KrCl lamps at pH 7.2, $[PFOA]_0$ = 0.02 mM, UV-L irradiance = 13.5 mW/cm^2, UV-KrCl irradiance = 6.5 mW/cm^2

Table 2-7. Rate Constants and model goodness of fit parameters for PFOA photolysis, $[PFOA]_0$ = 0.02 mM, UV-L irradiance = 13.5 mW/cm^2, UV-KrCl irradiance = 6.5 mW/cm^2

UV Lamp	Rate constant k_1 (hour^{-1})	95% CI	Rate Constant k_2 (hour^{-1})	95% CI	SSE	RMSE	R^2	$C_{V\ RMSE}$
UV-L	-	-	-	-	-	-	-	-
UV-KrCl	0.96	0.09	0.32	0.04	8.22 E-04	1.08 E-02	0.998	0.03

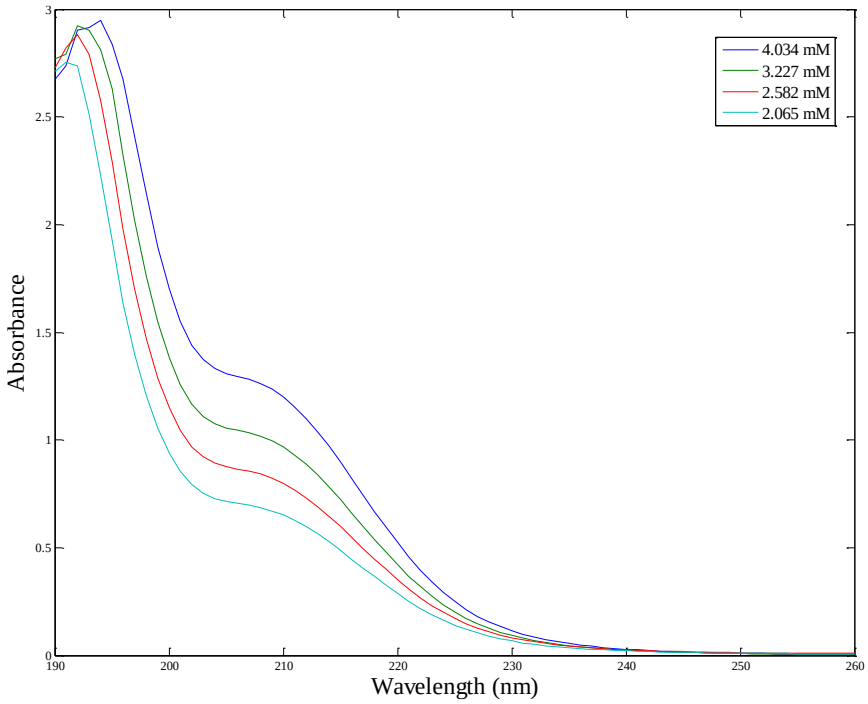

Figure 2-6. PFOA absorption spectra for different concentrations at pH 7.2

Table 2-8. Molar extinction coefficient of PFOA solutions

pH	Concentration range (mM)	Molar absorptivity at 222 nm ($\log_{10}$ **base**) (M^{-1} cm^{-1})	Molar absorptivity at 254 nm ($\log_{10}$ **base**) (M^{-1} cm^{-1})
7.2	2.065 to 4.034	88.9	-

Effect of pH

UV Light Absorption

Absorption spectra for sulfite at pH 7.2, 9.0 and 10.3 are presented in Fig. 2-7, 2-8, 2-9 and 2-10. As sulfite speciation is dependent on pKa values of sulfurous acid (1.9 and 7.2), the relative fractions of sulfurous acid (H_2SO_3), bisulfite (HSO_3^-), and sulfite (SO_3^{2-}) vary with solutions pH. The ability of each of these species to absorb UV light varies, so the overall molar extinction coefficient of the solution also varies with pH. The data are shown in Table 2-9. At highly alkaline pH, SO_3^{2-} is the dominant species and would produce e_{aq}^-, according to reaction (2-1). Under moderately acidic conditions, bisulfite would be the dominant specie and it absorbs UV light and produces hydrogen radical according to the following reaction.[54]

$$HSO_3^- + h\nu \rightarrow \bullet SO_3^- + \bullet H \qquad (2\text{-}4)$$

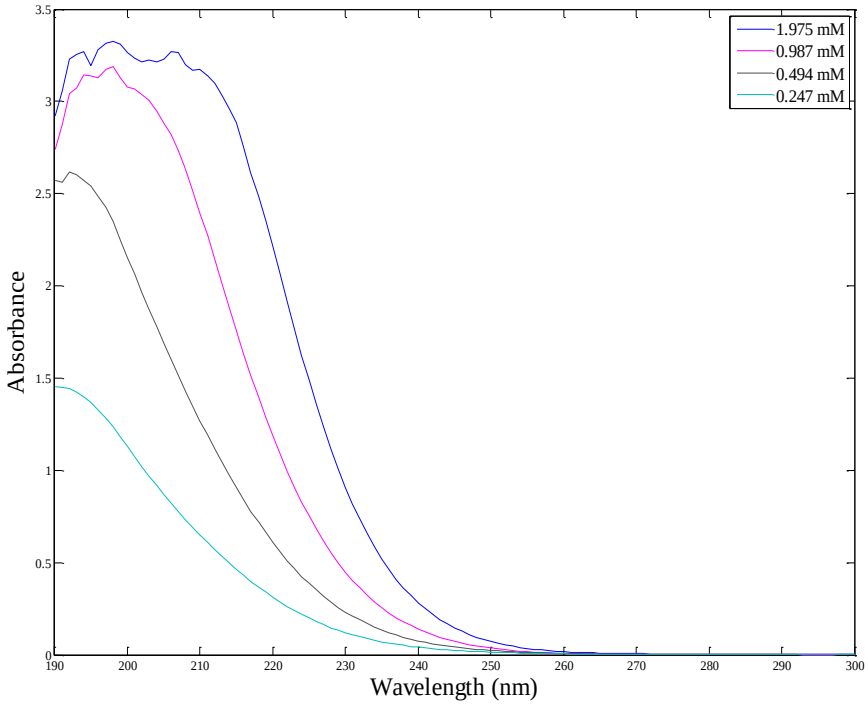

Figure 2-7. Sulfite absorption spectra for different concentrations at pH 7.2

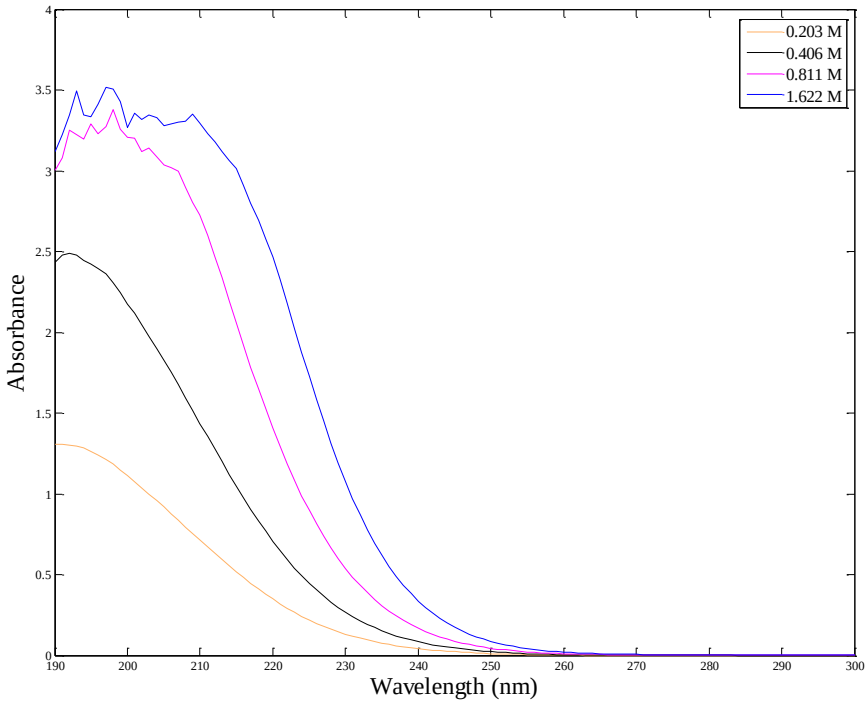

Figure 2-8. Sulfite absorption spectra for different concentrations at pH 9.0

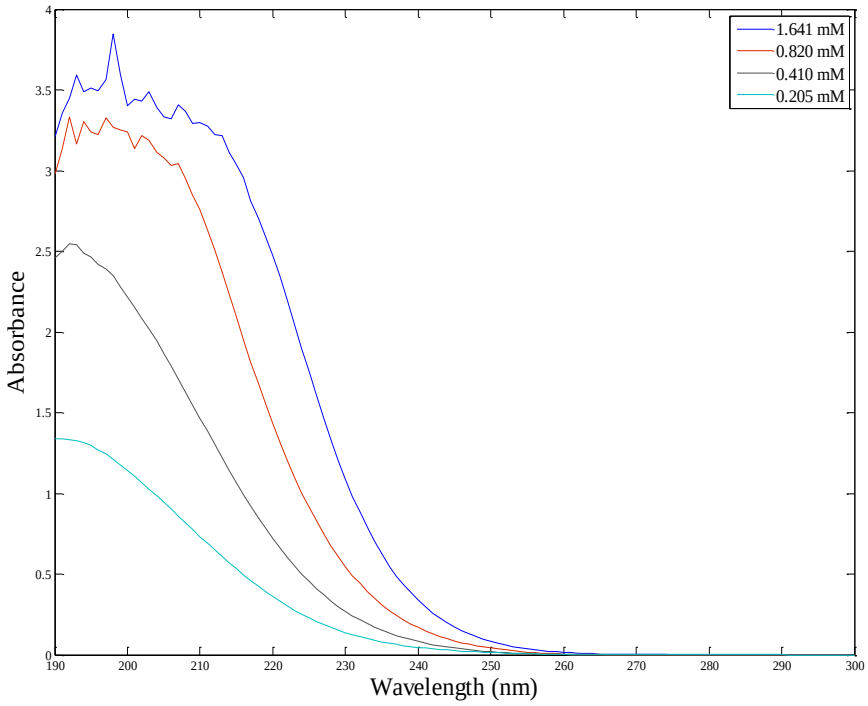

Figure 2-9. Sulfite absorption spectra for different concentrations at pH 10.3

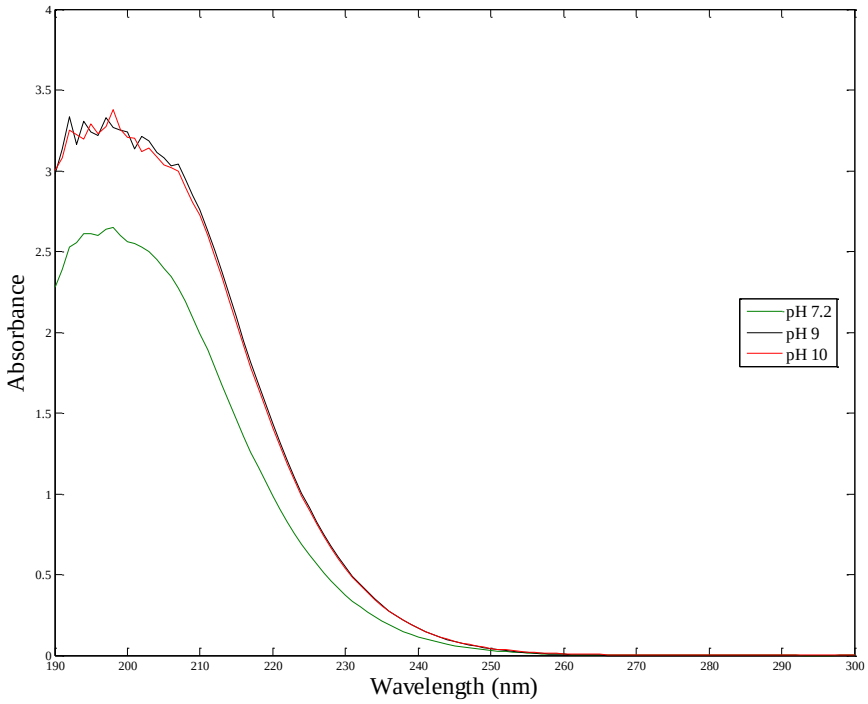

Figure 2-10. Sulfite absorption spectra at different pH, and [S(IV)] = 0.00164 M

Table 2-9. Molar absorptivity of sulfite solutions at different pH and UV wavelengths

pH	Ionization fraction of $[SO_3^{2-}]$	Molar absorptivity at 222 nm, (log_{10} base) (M^{-1} cm^{-1})	Molar absorptivity at 254 nm, (log_{10} base) (M^{-1} cm^{-1})
7.2	0.454	955	16.7
9.0	0.981	1316	21.2
10.3	1.000	1324	22.3

Defluorination with UV-L lamp

Defluorination ratios of PFOA with UV-L lamp at various pH are presented in Fig. 2-11. No measurable fluoride was detected at pH 5. Maximum defluorination around 80% was attained after 3 h of irradiation at pH 9.0 and 10.3. The kinetic model in equation 2-2 was fitted to the fluoride concentrations observed over time and rate constants k_1 and k_2 were obtained using the assumption that the value of "n" was 9. The rate constants and model goodness of fit parameters are shown in Table 2-10. Defluorination rate constants k_1 and k_2 at different pH are presented in Fig. 2-12 and 2-13. The error bars presented in Fig. 2-12 and 2-13 represent the confidence interval for the rate constants obtained by fitting the one-pseudo component model. At low pH, SO_3^{2-} concentration is very low and the principal S(IV) specie present is HSO_3^-. Bisulfite

does not absorb UV effectively and produces hydrogen radical ($^{\bullet}H$) upon UV irradiation. Therefore, the rate of hydrated electrons formation and PFOA defluorination is negligible. As pH increases, the concentration of SO_3^{2-} rises and correspondingly the rate of formation of hydrated electrons is higher. This phenomenon translates to higher rate constants k_1 and k_2 at pH 7.2, 9.0 and 10.3. Lack of fluoride release at pH 5 indicates that $^{\bullet}H$ lacks affinity towards fluorinated organics.

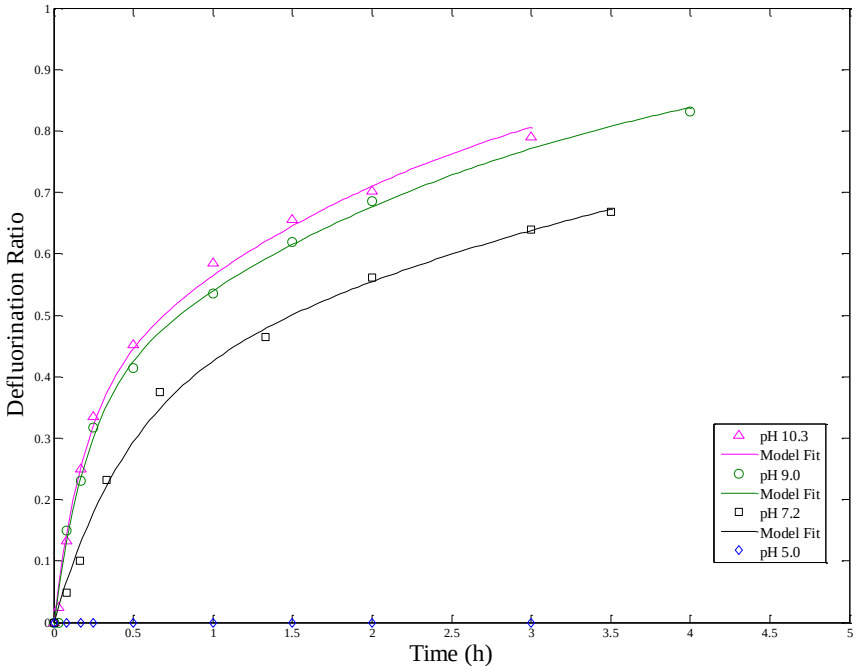

Figure 2-11. PFOA defluorination with UV-L lamp at different pH, $[PFOA]_0$ = 0.02 mM, sulfite dose = 7.2 mM, UV-L irradiance = 13.5 mW/cm^2

Table 2-10. Rate Constants and model goodness of fit parameters for PFOA defluorination with UV-L lamp at different pH, $[PFOA]_0$ = 0.02 mM, sulfite dose = 7.2 mM, UV-L irradiance = 13.5 mW/cm^2

pH	Rate constant k_1 (hour^{-1})	95% CI	Rate Constant k_2 (hour^{-1})	95% CI	SSE	RMSE	R^2	$C_{V\ RMSE}$
5.0	0	0	0	0	-	-	-	-
7.2	2.40	0.44	0.20	0.03	2.63 E-03	1.94 E-02	0.995	0.06
9.0	4.68	0.47	0.34	0.03	1.10 E-03	1.17 E-02	0.995	0.03
10.3	5.24	0.83	0.39	0.05	2.72 E-03	1.84 E-02	0.997	0.05

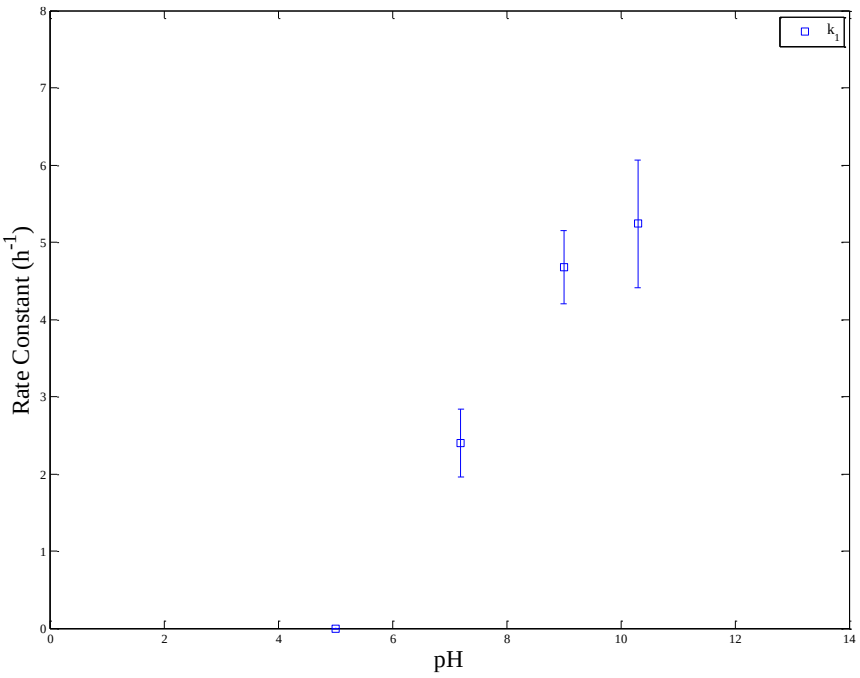

Figure 2-12. Effect of pH on initial defluorination rate constant (k_1) with UV-L lamp, $[PFOA]_0$ = 0.02 mM, sulfite dose = 7.2 mM, UV-L irradiance = 13.5 mW/cm^2

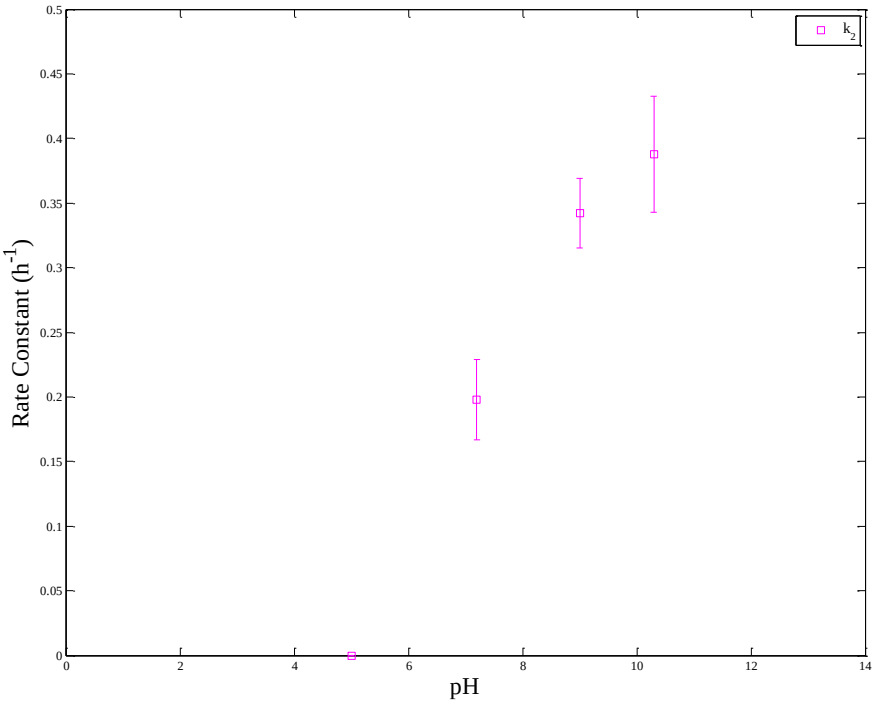

Figure 2-13. Effect of pH on secondary defluorination rate constant (k_2) with UV-L lamp, $[PFOA]_0$ = 0.02 mM, sulfite dose = 7.2 mM, UV-L irradiance = 13.5 mW/cm^2

Defluorination with UV-KrCL lamp

Defluorination ratios of PFOA with UV-KrCl lamp at various pH are presented in Fig. 2-14. pH did not have a significant impact on kinetics of defluorination, as presented in Fig. 2-15 and 2-16. The error bars presented in Fig. 2-15 and 2-16 represent the confidence interval for the rate constants obtained by fitting the one-pseudo component model. The rate constants and model goodness of fit parameters are shown in Table 2-11. This behavior is due to high molar absorptivity of sulfite at 222 nm UV, as

shown in Table 2-9. The fraction of UV_{222} absorbed by sulfite, calculated as in equation 2-12, is 100% at most alkaline pH. So, changing pH will not affect light absorption and aqueous electron production. This results in negligible changes in k_1 and k_2 with pH.

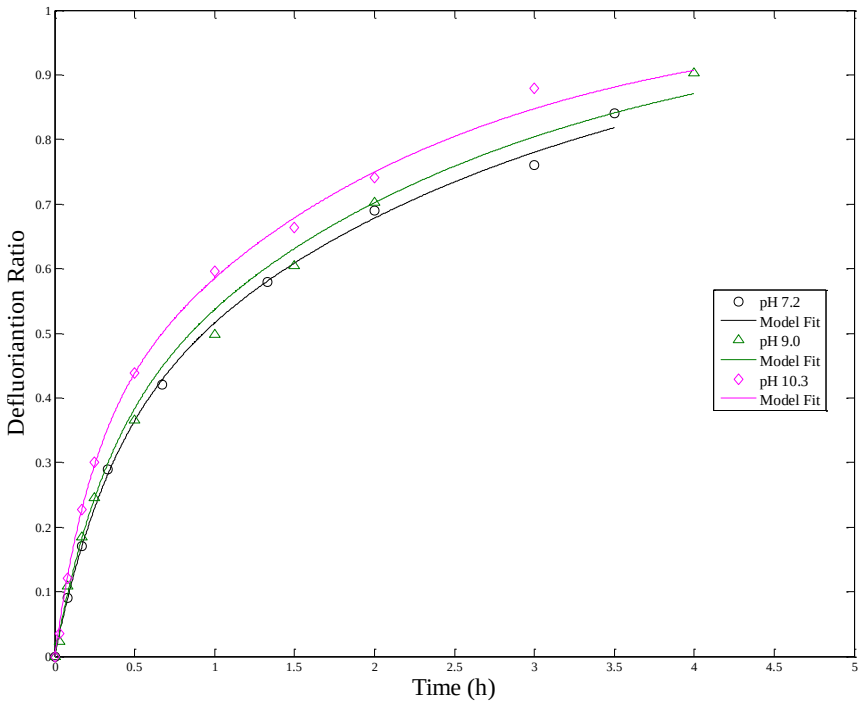

Figure 2-14. PFOA defluorination with UV-KrCl lamp at different pH, $[PFOA]_0$ = 0.02 mM, sulfite dose = 7.2 mM, UV irradiance = 6.5 mW/cm^2

Table 2-11. Rate Constants and model goodness of fit parameters for PFOA defluorination with UV-KrCl lamp at different pH, $[PFOA]_0$ = 0.02 mM, sulfite dose = 7.2 mM, UV irradiance = 6.5 mW/cm^2

pH	Rate constant k_1 (hour^{-1})	95% CI	Rate Constant k_2 (hour^{-1})	95% CI	SSE	RMSE	R^2	C_V RMSE
7.2	3.05	0.36	0.38	0.03	1.18 E-03	1.30 E-02	0.998	0.03
9.0	3.32	0.62	0.42	0.07	3.93 E-03	2.22 E-02	0.995	0.06
10.3	4.45	0.54	0.50	0.04	1.66 E-03	1.44 E-02	0.998	0.04

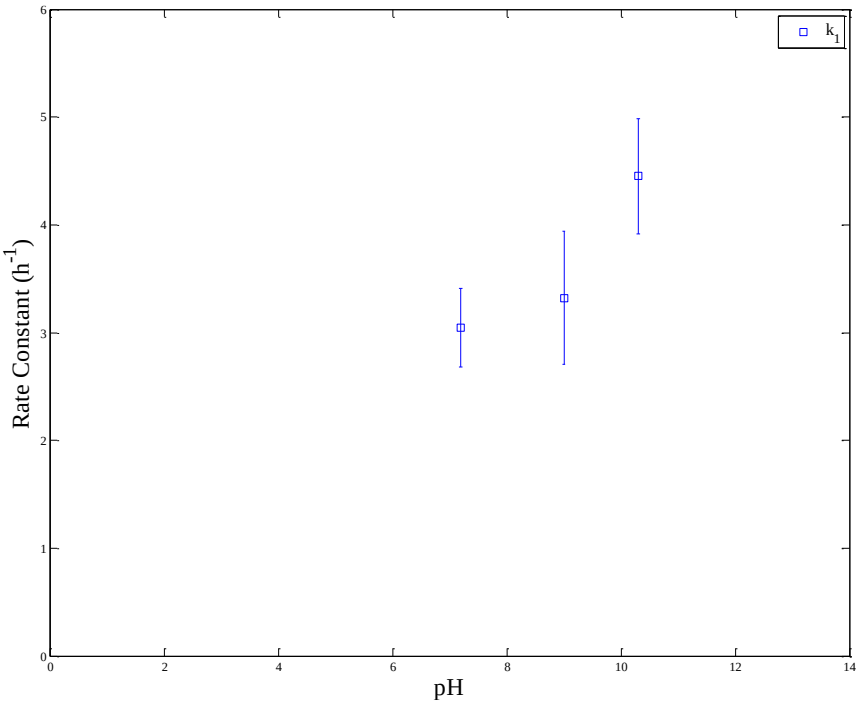

Figure 2-15. Effect of pH on initial defluorination rate constant (k_1) with UV-KrCl lamp $[PFOA]_0$ = 0.02 mM, sulfite dose = 7.2 mM, UV irradiance = 6.5 mW/cm^2

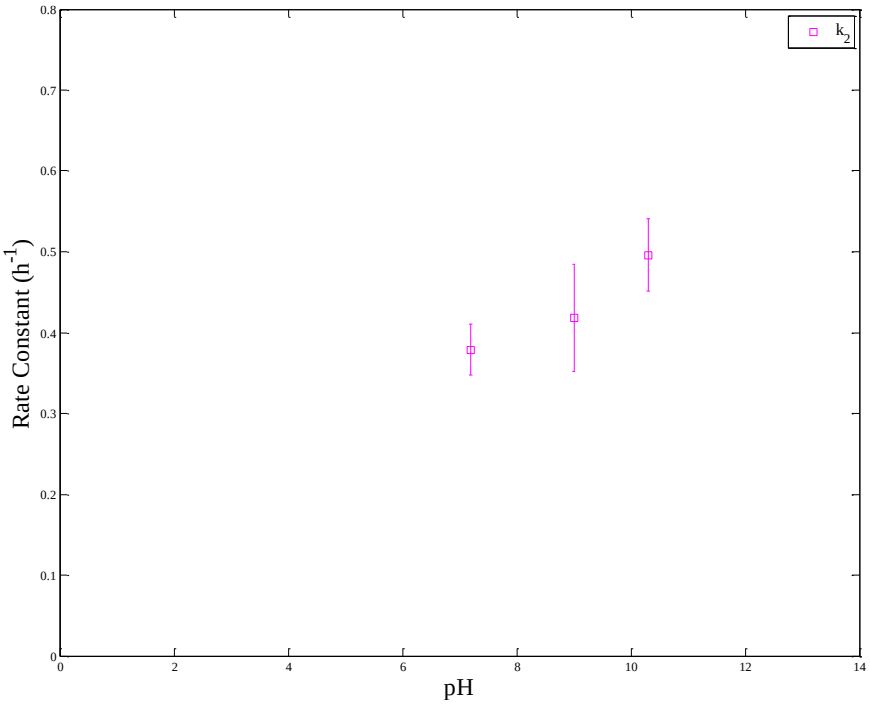

Figure 2-16. Effect of pH on secondary defluorination rate constant (k_2) with UV-KrCl lamp $[PFOA]_0$ = 0.02 mM, sulfite dose = 7.2 mM, UV irradiance = 6.5 mW/cm^2

Effect of sulfite dose

UV-L lamp

Defluorination ratios of PFOA at different concentrations of sulfite are presented in Fig. 2-17. The range of sulfite doses tested was from 1.8 mM to 14.4 mM. Since, the system was buffered at pH 10.3, the most dominant species of S(IV) is SO_3^{2-}. The UV irradiance measured at top of the reactor was 13.5 mW/cm^2. Maximum defluorination

around 80% was attained after 4 h of irradiation at the highest sulfite dose. The kinetic model in equation 2-2 was fitted to the fluoride concentrations observed over time and rate constants k_1 and k_2 were obtained. The rate constants and model goodness of fit parameters are shown in Table 2-12. The dependence of rate constants, k_1 and k_2 on sulfite dose can be evaluated by considering the generic model for target reduction in UV/Sulfite ARP. According to equation 2-7, initial rate constant can be expressed as a function of sulfite concentration. At 254 nm UV, molar extinction coefficient of PFOA is negligible, and thereby photolysis of PFOA need not be considered as a reaction pathway for PFOA degradation. The principal mechanism for PFOA defluorination is by reaction with hydrated electrons. Thus, equation 2-7 can be simplified as

$$k_1 = \left\{ \left[\frac{k_{TR}\phi_S I_{avg} \varepsilon_S C_S}{k_{TR}C_T + k_{SCR}C_{SC}} \right] \right\} \qquad 2\text{-}18$$

Substituting the equation for I_{avg} from equation 2-3, in equation 2-18, initial pseudo first order rate constant can be modified as,

$$k_1 = \frac{k_{TR}}{k_{TR}C_T + k_{SCR}C_{SC}} \left[\frac{\phi_S I_0 (1 - e^{-(\varepsilon_S C_S L)})}{L} \right] \qquad 2\text{-}19$$

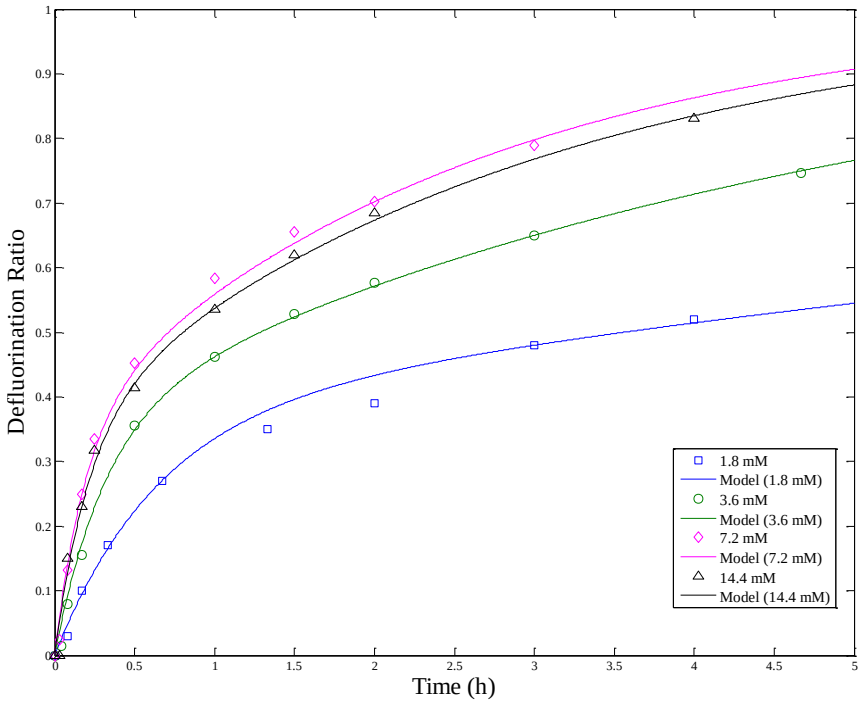

Figure 2-17. PFOA defluorination with UV-L lamp and different concentrations of sulfite, $[PFOA]_0$=0.02 mM, UV-L irradiance = 13.5 mW/cm^2, pH = 10.3

Table 2-12. Rate Constants for PFOA defluorination with UV-L lamp and different concentrations of sulfite, pH=10.3

Sulfite Dose (mM)	k_1 ($hour^{-1}$)	95% CI	k_2 ($hour^{-1}$)	95% CI	SSE	RMSE	R^2	C_V RMSE
1.80	1.57	0.16	0.06	0.01	7.60 E-04	1.04 E-02	0.997	0.04
3.60	3.21	0.24	0.20	0.01	4.29 E-04	7.32 E-03	0.999	0.02
7.20	5.24	0.83	0.39	0.05	2.72 E-03	1.84 E-02	0.996	0.05
14.4	4.68	0.47	0.34	0.03	1.10 E-03	1.17 E-02	0.999	0.03

Equations 2-18 and 2-19 predict that the rate constant k_1 would be proportional to the concentration of sulfite and average UV irradiance in the reactor. This relationship would be analogous for decay of all short chained and less fluorinated carboxylic acids formed from PFOA reduction. The error bars presented in Fig. 2-18 and 2-19 represent

the confidence interval for the rate constants obtained by fitting the one-pseudo component model. From the data in Fig. 2-18 and Fig. 2-19, the dependence of rate constants k_1 and k_2 on sulfite concentrations appears to be linear and in accordance with equation 2-18 for lower sulfite levels from 1.8 mM to 7.2 mM. At these low sulfite concentrations, little light would be absorbed, so the average UV irradiance would not depend on sulfite concentration but would be approximately equal to the incident UV irradiance. With this substitution, equation 2-18 predicts a proportionality between the rate constant and sulfite concentration as observed in Fig. 2-18 and 2-19 at low sulfite concentrations. However, at a sulfite dose of 14.4 mM, the rate constants no longer seem to be proportional to concentration of sulfite. This behavior could be due to increased rate of scavenging of hydrated electrons by sulfite according to reaction 2-2.

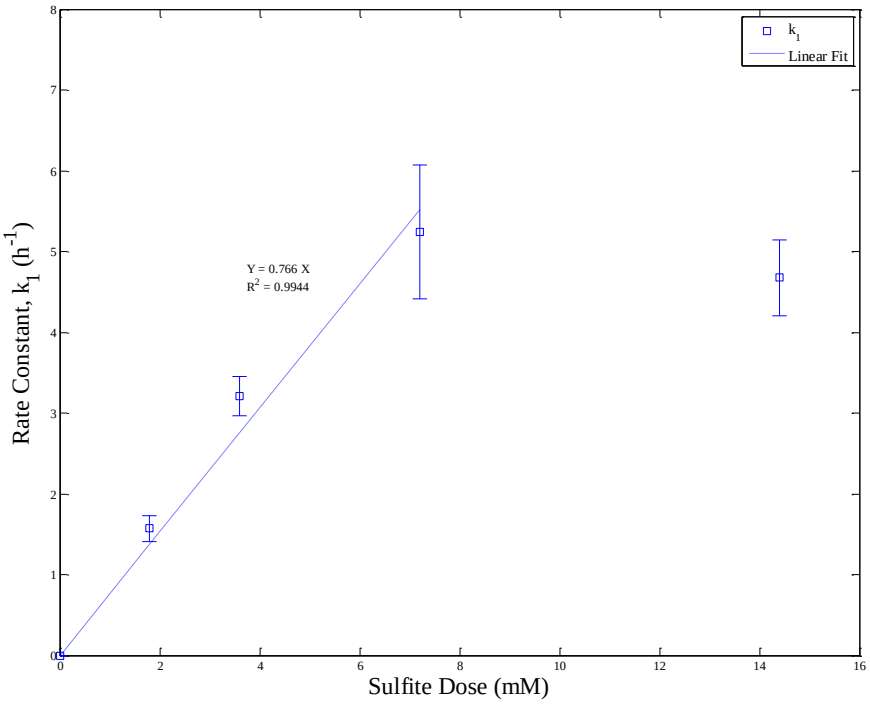

Figure 2-18. Effect of sulfite dose on initial rate constant for PFOA degradation with UV-L lamp, $[PFOA]_0$ = 0.02 mM, UV-L irradiance = 13.5 mW/cm^2, pH = 10.3

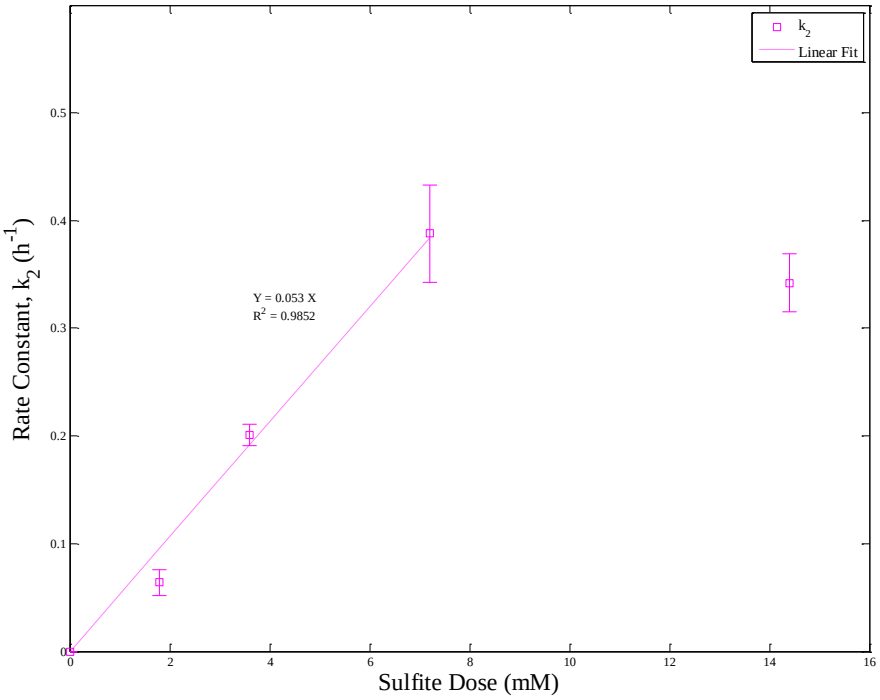

Figure 2-19. Effect of sulfite dose on secondary defluorination rate constant (k_2) for with UV-L lamp, $[PFOA]_0$ = 0.02 mM, UV-L irradiance = 13.5 mW/cm^2, pH = 10.3

Simplifying equation 2-19 could also explain the plateauing of defluorination rates at high sulfite concentrations. As sulfite concentration increases, the fraction of UV absorbed in the reactor represented by ($1-e^{-\varepsilon CL}$) approaches unity and equation 2-19 could be modified as,

$$k_1 = \frac{k_{TR}}{k_{TR}C_T + k_{SCR}C_{SC}}\left[\frac{\phi_S I_0}{L}\right] \qquad 2\text{-}20$$

Thus, at very high sulfite concentrations, defluorination rate constants are no longer proportional to sulfite concentration. In order to identify the optimum sulfite dose, it is necessary to calculate the fraction of UV being absorbed in the reactor. Fig. 2-20 presents the rate constants against the fraction of UV absorbed.

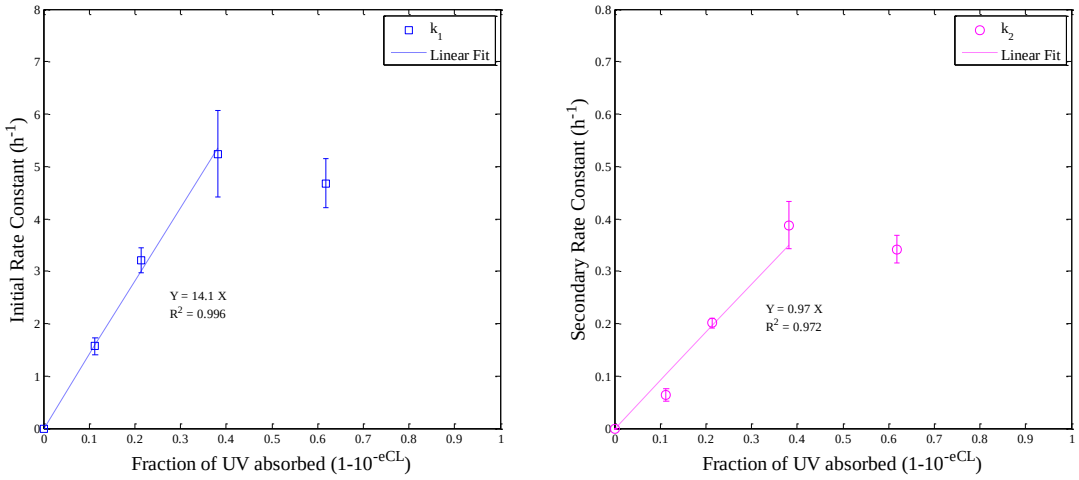

Figure 2-20. Variation in rate constants with fraction of UV_{254} absorbed, $[PFOA]_0$ = 0.02 mM, UV-L irradiance = 13.5 mW/cm^2, pH = 10.3

In Fig. 2-20, initial rate constant k_1 is plotted on the graph on left and k_2 on right. The linear relation from equation 2-19 holds good for both k_1 and k_2 at low UV absorption fractions. When the fraction of UV absorbed is low, increasing sulfite doses would lead to proportional increases in rate constants. Under high UV absorption conditions, the distribution of UV irradiance across the depth of the reactor may not be uniform. The reactor used in the study has a depth of 1.3 cm. When sulfite concentration is very high, the top layer of solution receives more UV irradiation than the bottom layer. Even though the reactor is placed on a magnetic stirrer, in order to simulate a completely mixed condition, the rate of mixing needs to keep up with rate of UV absorption and radicals production. The assumption of a completely mixed reactor, which was used to calculate average UV irradiance in the reactor in equation 2-3 may not hold when the time scale of the reactions is much less than the time needed to move water from the top to the bottom of the reactor. The top layer of solution in the reactor absorbs maximum photons and photon flux at bottom of the reactor may be reduced. In such a scenario, defluorination rates would be variable across the depth of the reactor. If UV distribution across the reactor is nonhomogeneous defluorination rate may be affected. Additionally, the measurement of inorganic fluorine may involve experimental errors that manifest in the calculated rate constants, k_1 and k_2. A combination of these factors can serve as an explanation for a reduction of defluorination rate at higher sulfite doses.

UV-KrCl lamp

Defluorination of PFOA with excimer lamp, at varying concentrations of sulfite are presented in Fig. 2-21. The range of sulfite doses tested was from 1.8 mM to 14.4 mM. The kinetic model in equation 2-2 was fitted to the fluoride concentrations observed over time and rate constants k_1 and k_2 were obtained. The rate constants and model goodness of fit parameters are shown in Table 2-13. As the excimer lamp supplies UV at 222 nm, the molar extinction coefficient of sulfite is significantly higher than the value at 254 nm. This higher ε_S value, ensures that the fraction of UV absorbed in the reactor approaches unity. As presented in Table 2-14, even at the lowest sulfite concentration of 1.8 mM, 100% of 222 nm photons are absorbed by sulfite in solution. Fig. 2-22 presents the effect of increasing sulfite concentrations on initial rate constant k_1. Unlike the UV-L lamp, initial rate constant for PFOA degradation decreases with increasing sulfite doses. This inverse relationship can be explained by considering equation 2-20. When fraction of UV absorbed approaches 1, k_1 is no longer proportional to sulfite concentration. In addition, sulfite acts as scavenger of hydrated electrons, represented by C_{SC} in equation 2-20. An increase in scavenger concentration inversely impacts k_1. However it should be noted that reduction of PFOA by hydrated electrons has faster kinetics than direct photolysis.

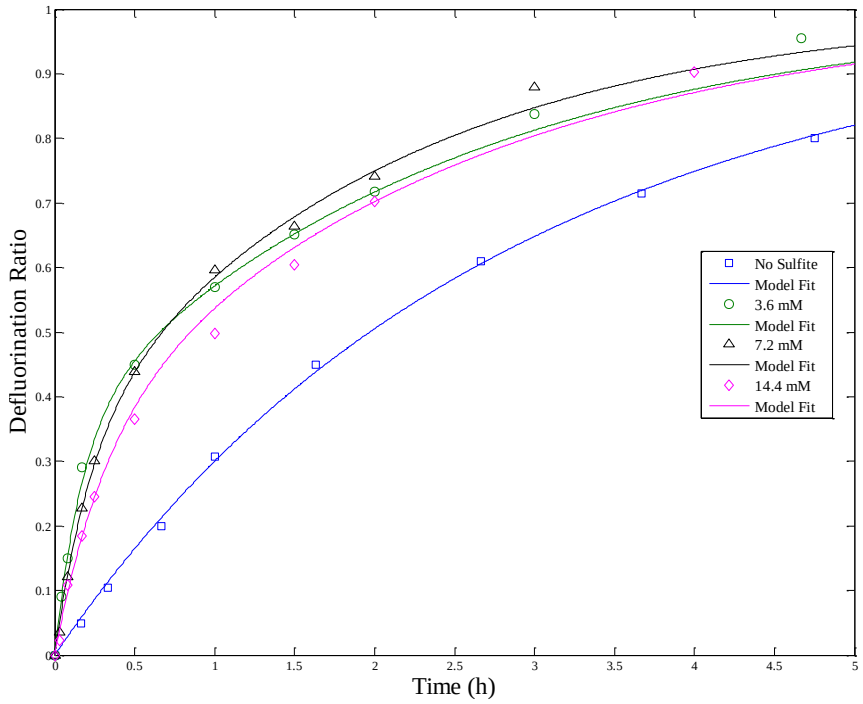

Figure 2-21. PFOA defluorination with UV-KrCl lamp and different concentrations of sulfite, $[PFOA]_0$ = 0.02 mM, UV irradiance = 6.5 mW/cm^2, pH = 10.3

Table 2-13. Rate Constants for PFOA defluorination with UV-KrCl lamp and different concentrations of sulfite, pH 10.3

Sulfite Dose (mM)	Rate constant k_1 ($hour^{-1}$)	95% CI	Rate Constant k_2 ($hour^{-1}$)	95% CI	SSE	RMSE	R^2	C_V RMSE
0.00	0.96	0.09	0.32	0.04	8.22 E-04	1.08 E-02	0.999	0.03
3.60	5.82	0.58	0.41	0.02	7.79 E-04	9.87 E-03	0.999	0.02
7.20	4.45	0.54	0.50	0.04	1.66 E-03	1.44 E-02	0.998	0.04
14.4	3.32	0.62	0.42	0.07	3.93 E-03	2.22 E-02	0.995	0.06

Table 2-14. Fraction of UV absorbed at different doses of sulfite

Sulfite Dose	Fraction of UV absorbed at 222 nm	Fraction of UV absorbed at 254 nm
1.8	1.00	0.11
3.6	1.00	0.21
7.2	1.00	0.38
14.4	1.00	0.62

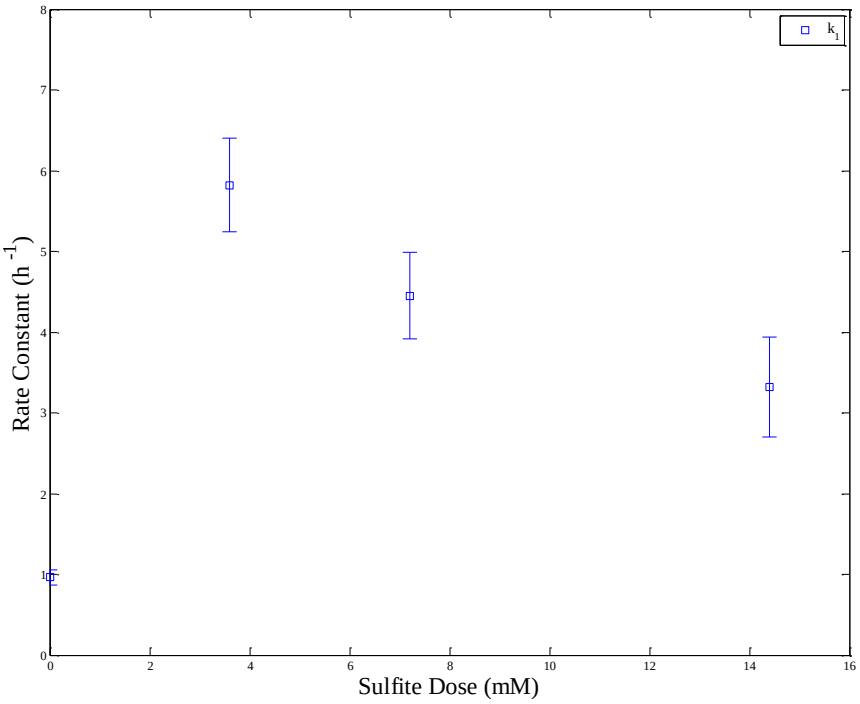

Figure 2-22. Effect of sulfite dose on initial defluorination rate constant (k_1) with UV-KrCl lamp, $[PFOA]_0$ = 0.02 mM, UV irradiance = 6.5 mW/cm^2, pH = 10.3

Fig. 2-23 presents the secondary rate constant k_2 as a function of sulfite concentrations. The error bars presented in Fig. 2-22 and 2-23 represent the confidence interval for the rate constants obtained by fitting the one-pseudo component model. Unlike k_1, k_2 does not decrease with increasing sulfite dose. k_2 is representative of rate of defluorination of PFOA degradation products. Due to continuous photolysis of sulfite at 222 nm, the concentration of sulfite in the reactor $C_{S,}$ is constantly decreasing. The rate of this reaction can be expressed as,

Rate of photolysis = ϕ_S I_{avg} $\epsilon_{S,222}$ C_S

Due to a reduced C_S, the fraction of UV absorbed also reduces with reaction time and k_2 follows the relation in equation 2-20. Thus, secondary rate constant dose not decrease with increasing sulfite dose.

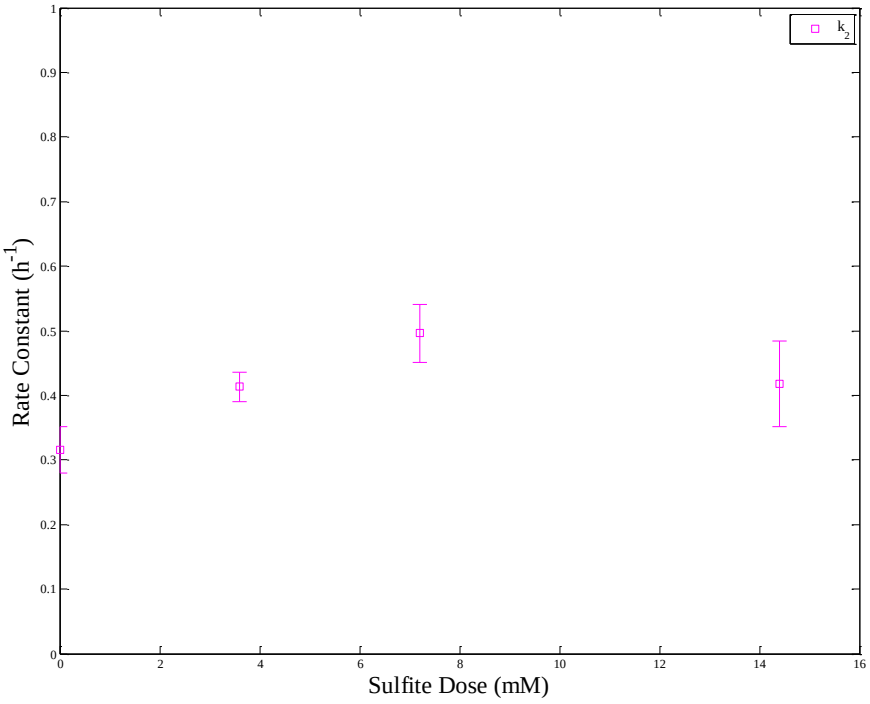

Figure 2-23. Effect of sulfite dose on secondary defluorination rate constant (k_2) with UV-KrCl lamp, $[PFOA]_0$ = 0.02 mM, UV irradiance = 6.5 mW/cm^2, pH = 10.3

Effect of alkalinity

UV-L lamp

Fig. 2-24 and 2-25 present the effect of alkalinity on initial and secondary rate constants for defluorination with the UV-L lamp. The error bars presented in Fig. 2-25 represent the confidence interval for the rate constants obtained by fitting the one-pseudo component model. Alkalinity in the range of 0 to 100 ppm as $CaCO_3$ was added to the solution using sodium bicarbonate. Bicarbonate and carbonate are strong scavengers of oxidizing radicals such as hydroxyl radicals (·OH).[68] Hydrated electrons, the principal species responsible for reductive defluorination, are not scavenged by bi/carbonate, and have longer half-lives.[68-71] However rate constants obtained from the one pseudo component model suggest that addition of alkalinity significantly reduces defluorination rate of PFOA and its less fluorinated intermediates. This effect could be due to formation of an intermediate species that scavenges hydrated electrons. Bi/carbonate could react with $^{\bullet}SO_3^-$ (reduction potential 0.75 V) produced from sulfite photolysis and generate the highly electrophilic carbonate radical ($^{\bullet}CO_3^-$). The rate constant for reaction of carbonate radical with hydrated electrons is reported to be 4.9×10^9 $M^{-1}S^{-1}$.[70] The following set of reactions could explain the lowering of defluorination rates with increasing alkalinity.[68, 71]

$$^{\bullet}SO_3^- + CO_3^{2-} \rightarrow {}^{\bullet}CO_3^- + SO_3^{2-} \quad (2\text{-}5)$$

$$^{\bullet}SO_3^- + HCO_3^- \rightarrow {}^{\bullet}HCO_3 + SO_3^{2-} \quad (2\text{-}6)$$

$$^{\bullet}CO_3^- + e_{aq}^- \rightarrow CO_3^{2-} \quad (2\text{-}7)$$

$$^{\bullet}HCO_3 + e_{aq}^- \rightarrow HCO_3^- \quad (2\text{-}8)$$

The dependence of defluorination rate on the concentration of carbonate can also be mathematically understood from the generic ARP model as simplified in equation 2-21. The rate of target removal is inversely related to concentration of scavenging species, C_{SC}. When this model is applied to PFOA degradation, the rate of target removal can be expressed as rate of defluorination. Thus, the dependence of initial and secondary rate constants of defluorination on alkalinity are in accordance with equation 2-21. All of the terms in equation 2-21, except C_{SC} do not vary within the experimental conditions. Thus, defluorination rate can be simplified as being inversely related to scavenger concentration. Addition of 25 ppm $CaCO_3$ resulted in 60% reduction of k_1 and 40% reduction in k_2. In natural water, total alkalinity is typically around several hundred mg/L as $CaCO_3$, which would greatly impact PFOA defluorination with the UV-L lamp. From this data, it can be inferred that pretreatment of water for bi/carbonate removal may be necessary to facilitate efficient PFOA kinetics.

$$\frac{dC_T}{dt} = -\left[\frac{k_{TR}C_T\phi_S I_{avg}\varepsilon_S C_S}{k_{TR}C_T + k_{SCR}C_{SC}}\right] \qquad 2\text{-}21$$

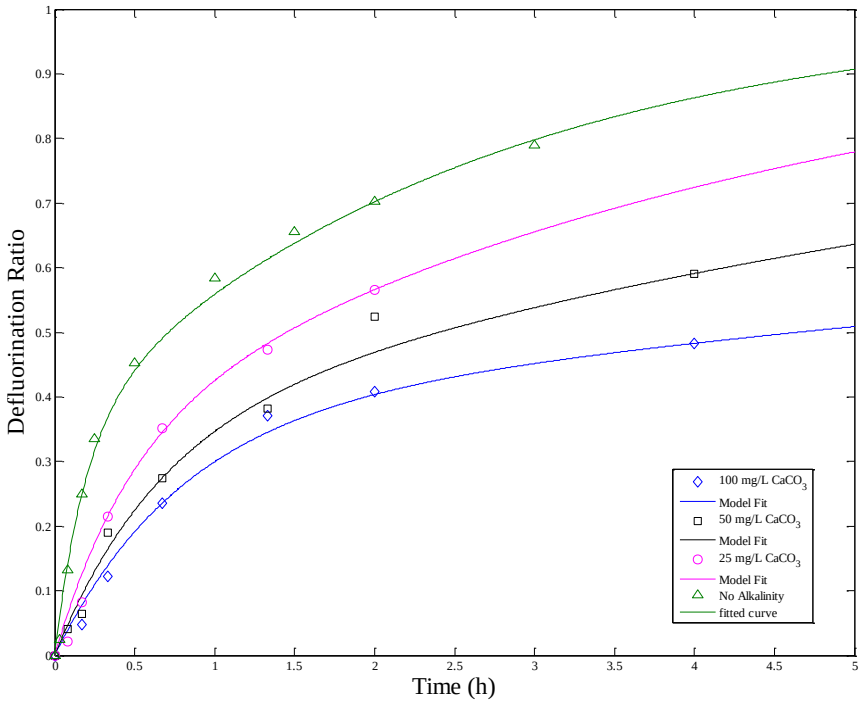

Figure 2-24. Effect of alkalinity on PFOA defluorination with UV-L lamp, $[PFOA]_0$ = 0.02 mM, UV-L irradiance = 13.5 mW/cm^2, $[S(IV)]_0$ = 7.2 mM, pH=10.3

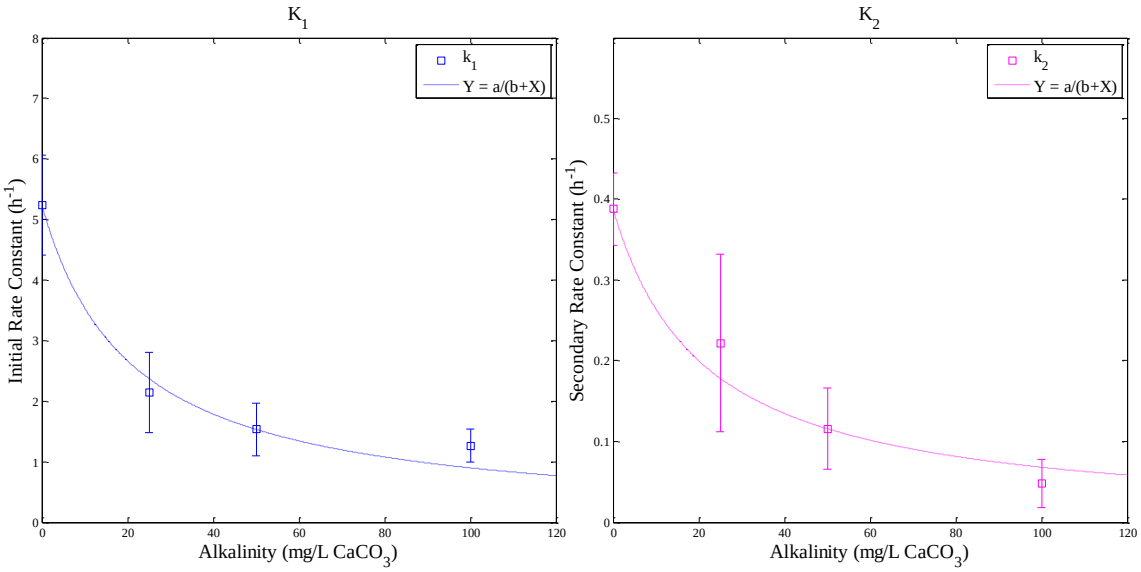

Figure 2-25. Effect of alkalinity on PFOA defluorination rate constants with UV-L lamp, $[PFOA]_0$ = 0.02 mM, UV-L irradiance = 13.5 mW/cm^2, $[S(IV)]_0$ = 7.2 mM, pH=10.3

UV-KrCl lamp

Fig. 2-26 and 2-27 present the effect of alkalinity on initial and secondary rate constants for defluorination with excimer lamp. The error bars presented in Fig. 2-27 represent the confidence interval for the rate constants obtained by fitting the one-pseudo component model. For PFOA defluorination with the excimer lamp, a 40% reduction in initial rate constant was observed with 25 ppm of alkalinity. But additional increase in

alkalinity didn't have a significant effect on k_1. The secondary rate constant k_2 did not show any trend with increasing alkalinity. Overall, the effect of alkalinity was less pronounced when the excimer lamp is used for PFOA removal. This could be due to direct photolysis of PFOA under 222 nm irradiation. When the total sulfite concentration in the system decreases, PFOA absorbs UV and defluorination rate is dominated by the part of equation 2-22 ($\phi_T I_{avg} \varepsilon_T$) that describes direct photolysis. k_2 values, which represent first order decay of intermediates formed by PFOA reduction, are obtained from experimental measurements that were taken when sulfite concentration is reduced by photolysis. Assuming a quantum yield of 0.03 for sulfite photolysis, the concentration sulfite in the reactor would be insignificant relative to initial dose.[48] During this phase, photolysis of PFOA and intermediates under excimer lamp could be the dominant defluorination mechanism. Hence, k_2 values don't show any trend with alkalinity addition. This behavior is different from the UV-L lamp, where photolysis of PFOA is negligible. This dual mechanism for defluorination under the excimer lamp offers greater adaptability to alkalinity in the treatment process.

$$\frac{dC_T}{dt} = -\left\{ \phi_T I_{avg} \varepsilon_T C_T + k_{TR} C_T \left[\frac{\phi_S I_{avg} \varepsilon_S C_S}{k_{TR} C_T + k_{SCR} C_{SC}} \right] \right\} \qquad 2\text{-}22$$

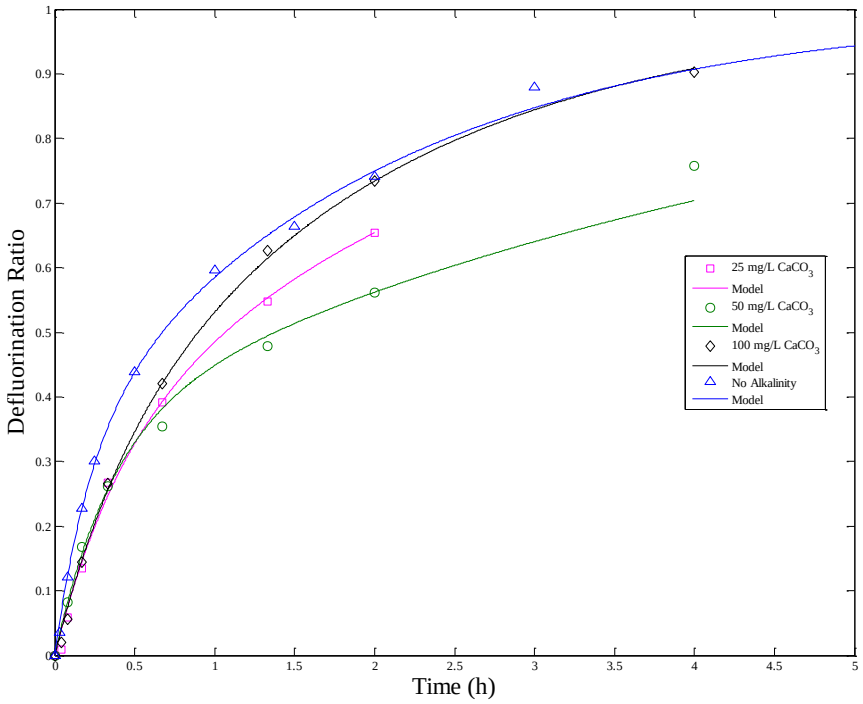

Figure 2-26. Effect of alkalinity on PFOA defluorination with UV-KrCl lamp, $[PFOA]_0$ = 0.02 mM, UV-KrCl irradiance = 6.5 mW/cm^2, $[S(IV)]_0$ = 7.2 mM, pH=10.3

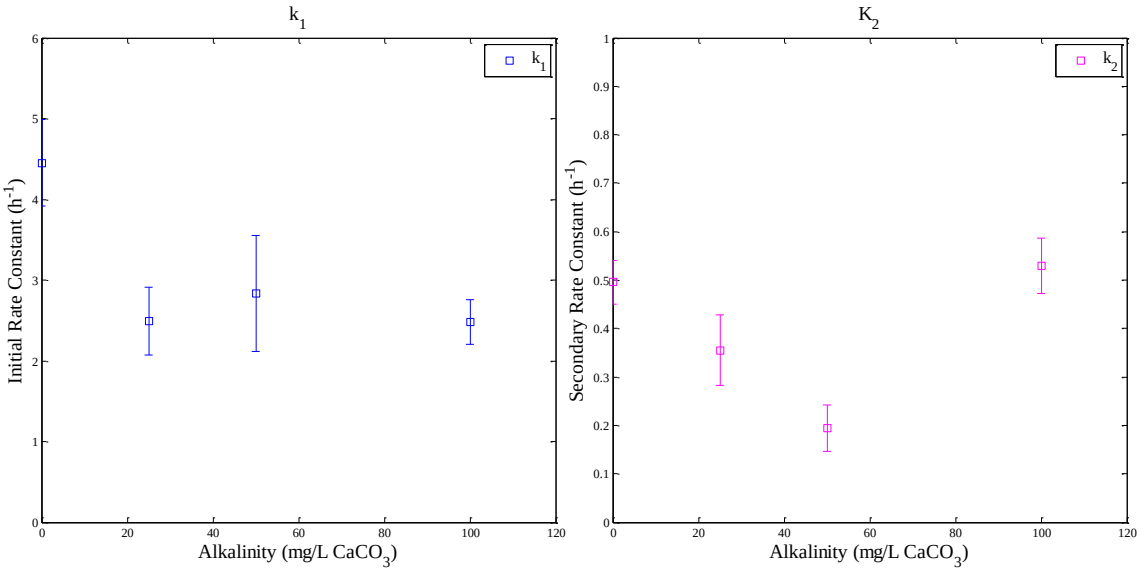

Figure 2-27. Effect of alkalinity on PFOA defluorination rate constants with UV-KrCl lamp, $[PFOA]_0$ = 0.02 mM, UV-KrCl irradiance = 6.5 mW/cm^2, $[S(IV)]_0$ = 7.2 mM, pH=10.3

Effect of nitrate

As shown in Fig. 2-28 and 2-29, the addition of nitrate resulted in decreasing the initial defluorination rate constant, k_1 with the UV-L lamp. This decrease is due to the scavenging of e_{aq}^- by NO_3^- according to reaction (9).[57, 72] The unstable species, $\bullet NO_3^{2-}$ is further reduced to nitrite.

$NO_3^- + e_{aq}^- \rightarrow \bullet NO_3^{2-}$ (2-9)

As presented in Fig. 2-29, nitrate (10 mg/L) addition did not significantly impact k_2. The pseudo first order rate constant for nitrate reduction with UV-L/sulfite ARP are reported to be around 10 hr^{-1}, for a sulfite dose of 8.4 mM and UV irradiance of 4 mW/cm^2.[49] Assuming similar removal patterns and projecting nitrate reduction rates for the current experimental conditions, nitrate could be completely reduced within 2 h of irradiation. Thus, impact of nitrate on scavenging of e_{aq}^-, is more pronounced on k_1 than on k_2. The pattern in Fig. 2-29 lend support to this argument. The error bars presented in Fig. 2-29 represent the confidence interval for the rate constants obtained by fitting the one-pseudo component model.

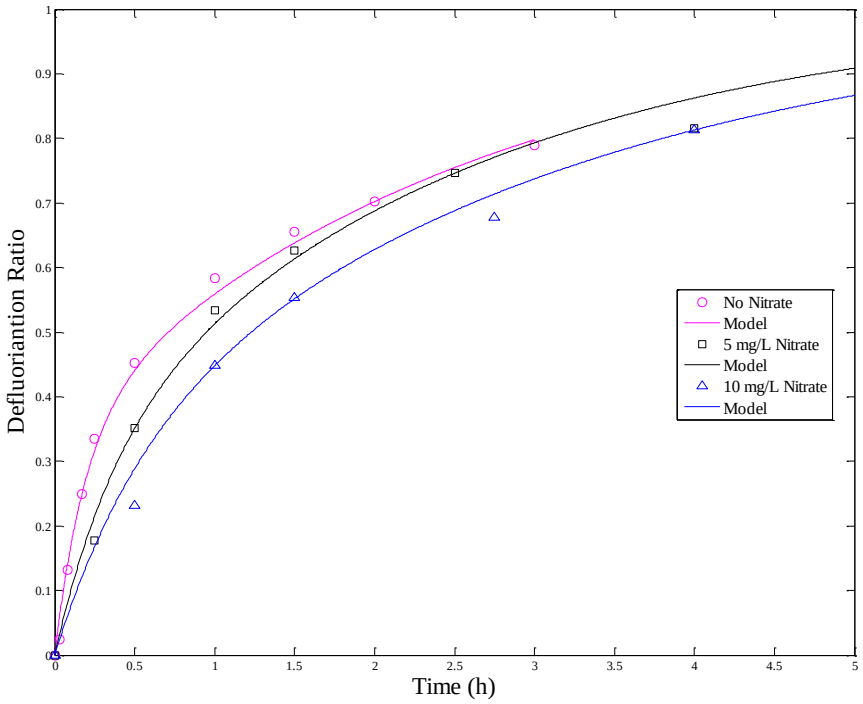

Figure 2-28. Effect of nitrate on PFOA defluorination with UV-L lamp, $[PFOA]_0$ = 0.02 mM, UV-L irradiance = 13.5 mW/cm^2, $[S(IV)]_0$ = 7.2 mM, pH=10.3

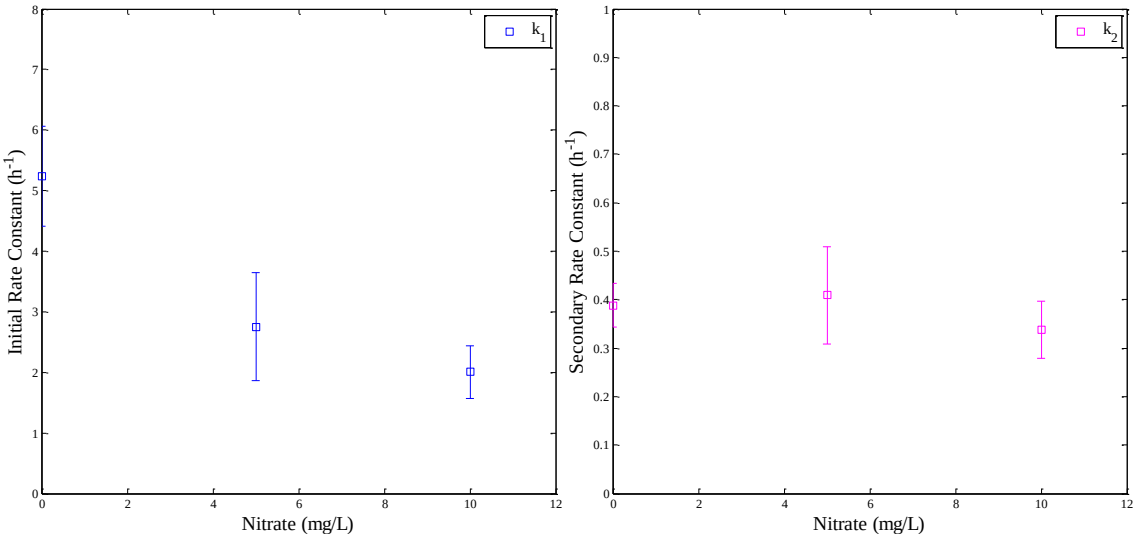

Figure 2-29. Effect of nitrate on PFOA defluorination rate constants with UV-L lamp, $[PFOA]_0$ = 0.02 mM, UV-L irradiance = 13.5 mW/cm^2, $[S(IV)]_0$ = 7.2 mM, pH=10.3

UV-KrCl lamp

Under the excimer lamp, in addition to scavenging effect, nitrate absorbs UV_{222} and forms nitrite. Nitrite is also a scavenger of electrons, as in reactions (2-10) and (-11).[57, 72]

$NO_3^- + hv \rightarrow NO_2^- + 0.5O_2$ (2-10)

$NO2- + e_{aq}^- \rightarrow \bullet (NO_2)^{2-}$ (2-11)

The effect of nitrate addition on the first defluorination rate constant was less pronounced with the excimer lamp than with the UV-L lamp, as shown in Fig. 2-30. This may be due to the additional mechanism for PFOA removal by direct photolysis with the excimer lamp. Similar to the UV-L lamp, addition of nitrate had a greater impact on initial rate of PFOA defluorination, than on secondary rate. The effect of nitrate addition on k_1 and k_2 is presented in Fig. 2-31. The error bars presented in Fig. 2-31 represent the confidence interval for the rate constants obtained by fitting the one-pseudo component model.

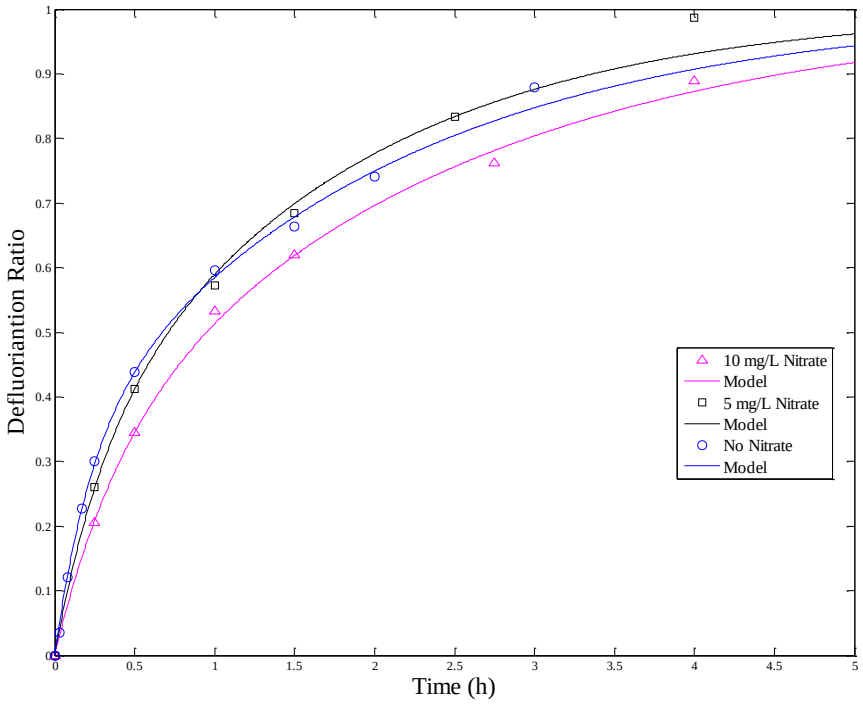

Figure 2-30. Effect of nitrate on PFOA defluorination with UV-KrCl lamp, $[PFOA]_0$ = 0.02 mM, UV-KrCl irradiance = 6.5 mW/cm^2, $[S(IV)]_0$ = 7.2 mM, pH=10.3

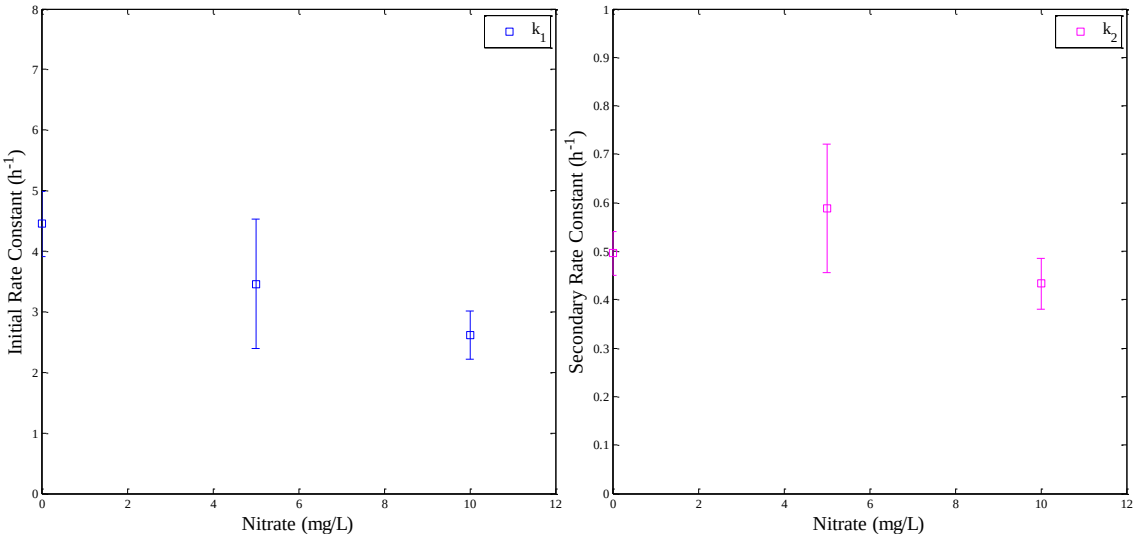

Figure 2-31. Effect of nitrate on PFOA defluorination rate constants with UV-KrCl lamp $[PFOA]_0$ = 0.02 mM, UV-KrCl irradiance = 6.5 mW/cm^2, $[S(IV)]_0$ = 7.2 mM, pH=10.3

Quantum yield analysis

Initial quantum yields were calculated according to equation 2-23. Fig. 2-32 and 2-33 present initial quantum yields for UV-L and UV-KrCl lamps, as a function of sulfite dose and alkalinity. Quantum yield is a measurement of the efficiency of a photochemical reaction. The photons supplied by both lamps are absorbed by sulfite, which results in production of hydrated electrons. A greater fraction of photons supplied

by the excimer lamp (222 nm) are absorbed by sulfite, than photons supplied by the UV-L lamp, due to higher molar absorptivity of sulfite at 222 nm than at 254 nm. However, as the fraction of UV absorbed increases, rate of sulfite photolysis will increase proportionally and this results in higher rate of defluorination. This phenomenon should result in comparable quantum yields for UV-L and excimer lamp. As presented in Fig. 2-32, quantum yield for both lamps are similar across sulfite doses.

From equation 2-6 and 2-23, higher sulfite concentrations would also lead to increased rate of UV absorption and sulfite photolysis. However, at high concentrations of sulfite, self-scavenging of radicals occurs according to reaction (3). This self-scavenging could lower the initial quantum yield for PFOA removal. This physical phenomenon can be mathematically expressed by modifying the rate equation described in equation 2-6. As the rate of PFOA photolysis is negligible relative to sulfite, equation 2-6 is simplified and used with the fundamental definition of quantum yield to obtain equation 2-24. All terms except C_{SC} in equation 2-24 are constant under current experimental conditions. Sulfite in the absence of any external scavengers and at sufficiently high doses would act as the scavenger whose concentration is represented by C_{SC}. An increase in C_{SC} would thereby cause a reduction in quantum yield. Data presented in Fig. 2-32 show a decreasing trend in quantum yields with higher sulfite concentrations. Further evidence of the scavenging effect can be observed when an external scavenger such as alkalinity is added to the system. Fig. 2-33 presents the effect of alkalinity on quantum yield for both lamps. The data in Fig. 2-33 show a greater effect of alkalinity which acts as C_{SC} in equation 2-24 and impacts the efficiency of the UV/Sulfite ARP.

$$\phi_{initial} = \frac{k_1 PFOA_0}{\frac{I_0}{L}(1 - e^{-\sum \varepsilon_S C_S L})} \qquad 2\text{-}23$$

$$\phi = \frac{k_{TR} C_T \phi_S}{k_{TR} C_T + k_{SCR} C_{SC}} \qquad 2\text{-}24$$

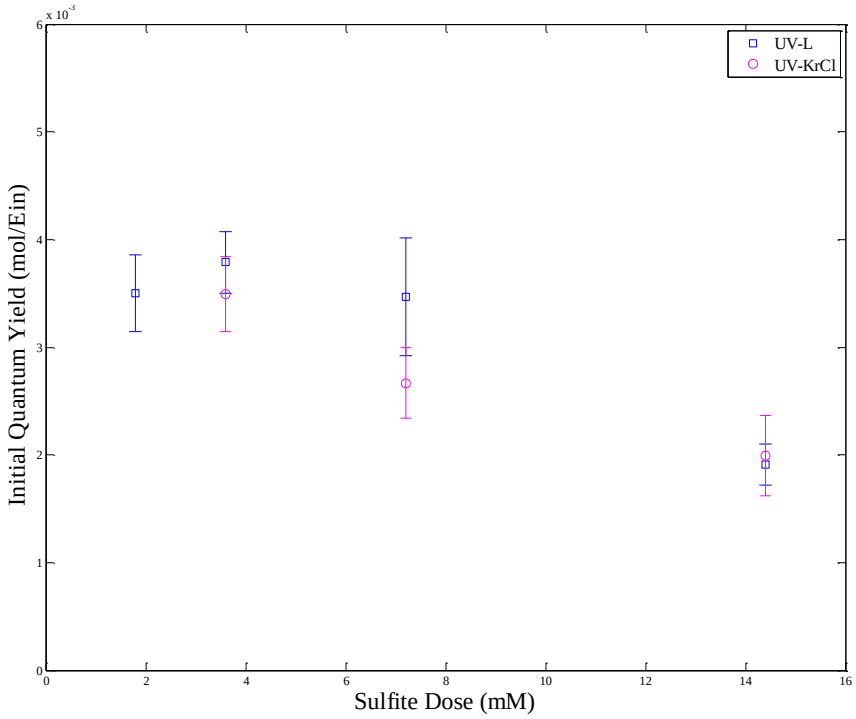

Figure 2-32. Initial quantum yields for PFOA degradation with UV-L and UV-KrCl lamps [PFOA]$_0$ = 0.02 mM, pH = 10.3

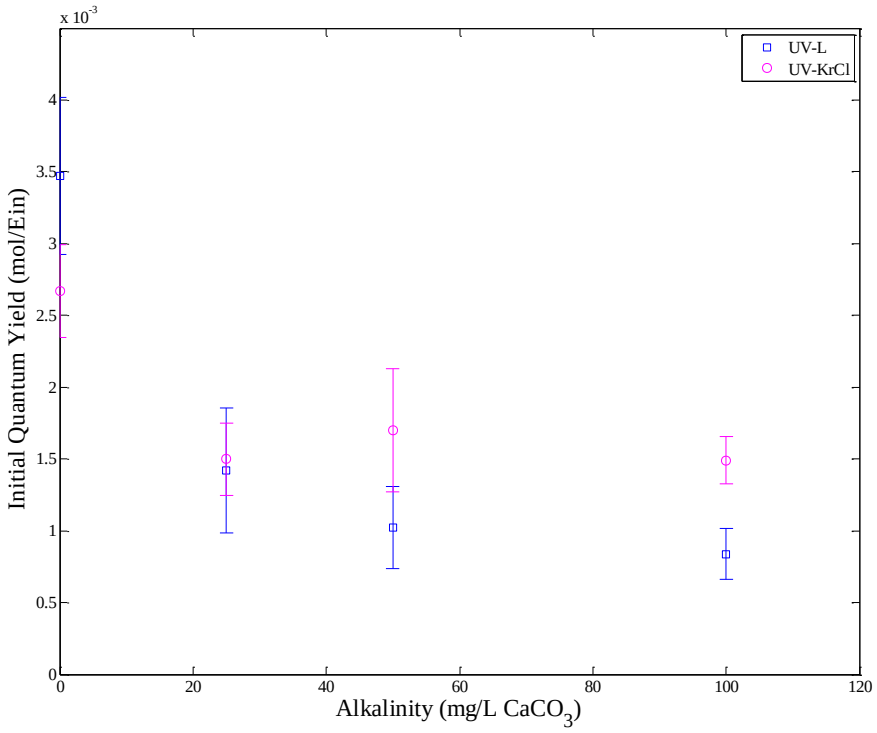

Figure 2-33. Effect of alkalinity on initial quantum yields for PFOA degradation with UV-L and UV-KrCl lamps $[PFOA]_0$ = 0.02 mM, [S(IV)] = 7.2 mM

Effect of UV lamp

A comparison of the two UV lamps can be made by calculating energy requirement using the electrical efficiency per order (E_{EO}), as specified in equation 2-16. Higher values of E_{EO} indicate more energy consumption, i.e. less efficient use of energy. E_{EO} values as a function of sulfite dose, for UV-L and excimer lamps are presented in Tables 2-15 and 2-16, respectively. A comparison is also presented in Fig. 2-34. At all

sulfite doses tested, the UV-L lamp is more energy efficient (lower E_{EO}) than the excimer lamp in defluorination of PFOA. Electrical power required by the excimer lamp is an order of magnitude higher than for the UV-L lamp. Operation of UV/sulfite ARP with a low wavelength UV source increases the fraction of UV absorbed in the reactor. Higher UV absorption leads to higher rate of sulfite photolysis and better kinetics of defluorination, as shown by T_{90} values in Table 2-15 and 2-16. However, this improvement in kinetics, does not translate to lower energy requirements. The very low efficiency (2.27%) associated with generation of UV at 222 nm is the principal inhibitory factor for large scale application of the excimer lamp. Conventional low pressure mercury lamps generate UV at 254 nm with efficiency around 35% and can result in lower E_{EO} compared to the excimer lamp. However, defluorination of PFOA is highly energy intensive relative to treatment processes applied to other water contaminants. Comparative energy requirements for advanced UV based treatment processes are provided in Table 2-17. It should be noted that E_{EO} values calculated in the current study are for 90% defluorination and not 1-log order reduction in parent PFOA concentration.

Alkalinity in the water is a major contributor to increasing energy requirements for the defluorination process. Fig. 2-35 presents the effect of alkalinity on energy requirements of both lamps, which suggests that pretreatment of water for alkalinity removal may be essential for lowering E_{EO}. In order to lower energy requirements and to facilitate large scale application of UV/sulfite ARP, selection of UV source is critical. In this regard, the development of UV-LEDs with higher energy efficiencies is a promising

avenue. Currently, research scale UV-LEDs are available with efficiency around 3% and lifetime of 3000 h.[73, 74] However, UV-LEDs are projected to reach efficiencies around 75% and lifetimes of 100,000 h.[73] Characteristics of current and future UV-LEDs are summarized in Table 2-18.

Operating costs for UV-based treatment processes depend heavily on energy requirements.[75] Cost estimates for energy and chemicals required to achieve 90% defluorination are shown in Tables 2-19 and 2-20. They were obtained by using a unit energy cost of $ 0.071/kWh and sodium sulfite cost of $ 0.97/kg.[76, 77] As the data indicate, energy is the most important factor that will affect design judgement. The optimum value of the combined cost for operating with UV-L is around $4.74/$m^3$. A reduction in costs can only be feasible with selection of UV sources with high electrical to UV conversion efficiency.

Table 2-15. Energy requirement for one-order reduction in organic fluorine of PFOA with UV-L lamp, $[PFOA]_0$ = 0.02 mM, pH = 10.3

Sulfite Dose	T_{90} (h)	Fraction of UV absorbed	P_V (W/m^3)	E_{EO} (kWh/m^3)
1.8	28.8	0.11	3527	102
3.6	9.22	0.21	6655	61
7.2	4.81	0.38	11888	57
14.4	5.46	0.62	19240	105

Table 2-16. Energy requirement for one-order reduction in organic fluorine of PFOA with UV-KrCl lamp, $[PFOA]_0$ = 0.02 mM, pH = 10.3

Sulfite Dose	T_{90} (h)	Fraction of UV absorbed	P_V (W/m^3)	E_{EO} (kWh/m^3)
0.0	6.93	0.01	1171	8.1
3.6	4.52	1.00	220588	997
7.2	3.85	1.00	220588	850
14.4	4.61	1.00	220588	1017

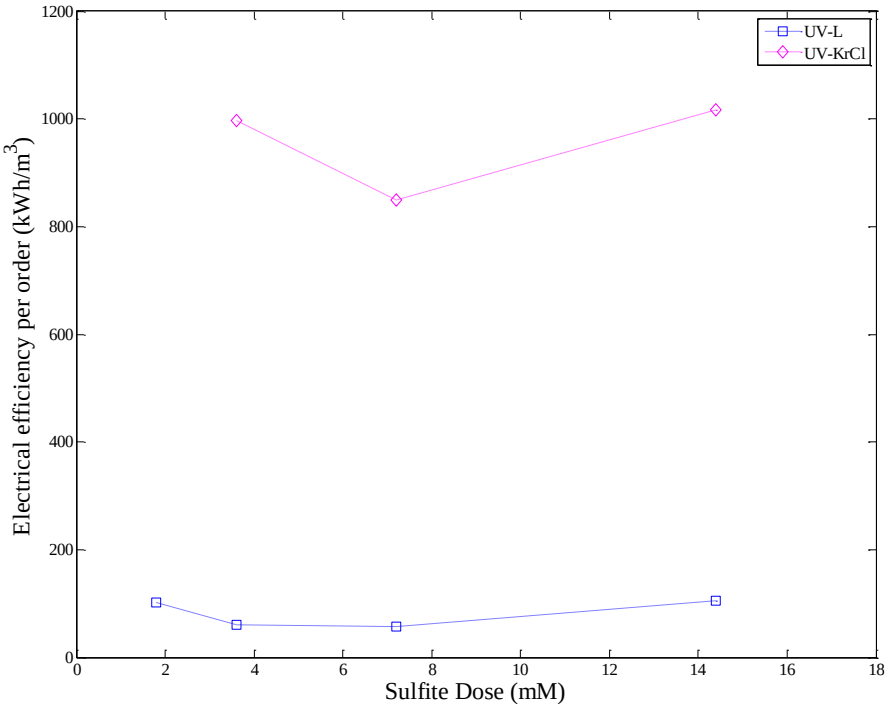

Figure 2-34. Electrical efficiency per order for defluorination of PFOA with UV-L and UV-KrCl lamps, $[PFOA]_0$ = 0.02 mM, pH = 10.3

Table 2-17. Comparative energy requirements for advanced treatment processes

Process	Target Contaminant	Reaction conditions	Typical E_{EO} (kWh/m^3)	Reference
UV/H_2O_2	TCE (trichloroethylene)	pH:7, Alkalinity: 100 mg/L as $CaCO_3$, $[H_2O_2]$: 1 mM	0.05	78
UV/Fe^{2+}-H_2O_2	COD from textile effluent	$[H_2O_2]$: 5 mM, $[Fe^{2+}]$: 72 µM	11.8	79
UV photolysis	NDMA (N-Nitrosodimethylamine)	Drinking water quality and UV-T~90%	0.021-0.34 (UV-L) 1.5 (UV-M)	75, 80
UV/H_2O_2	MTBE (Methyl tertiary butyl ether)	$[H_2O_2]$: 6 mM, ground water Alkalinity: 300 mg/L as $CaCO_3$	0.13-0.27	81
UV/H_2O_2	TCA (1,1,1-trichloroethane)	pH:7, Alkalinity: 100 mg/L, NOM: 1 mg/L, $[H_2O_2]$: 1 mM	10-12	78
UV/H_2O_2	DBCP (dibromochloropropane)	pH:7, Alkalinity: 100 mg/L, NOM: 1 mg/L, $[H_2O_2]$: 1 mM	2.4	78
UV/H_2O_2	TCE, PCE	-	0.53-2.64	78
UV/H_2O_2	Taste and odor compounds	pH: 8, Alkalinity: 110 mg/L as $CaCO_3$	0.05-0.11	81

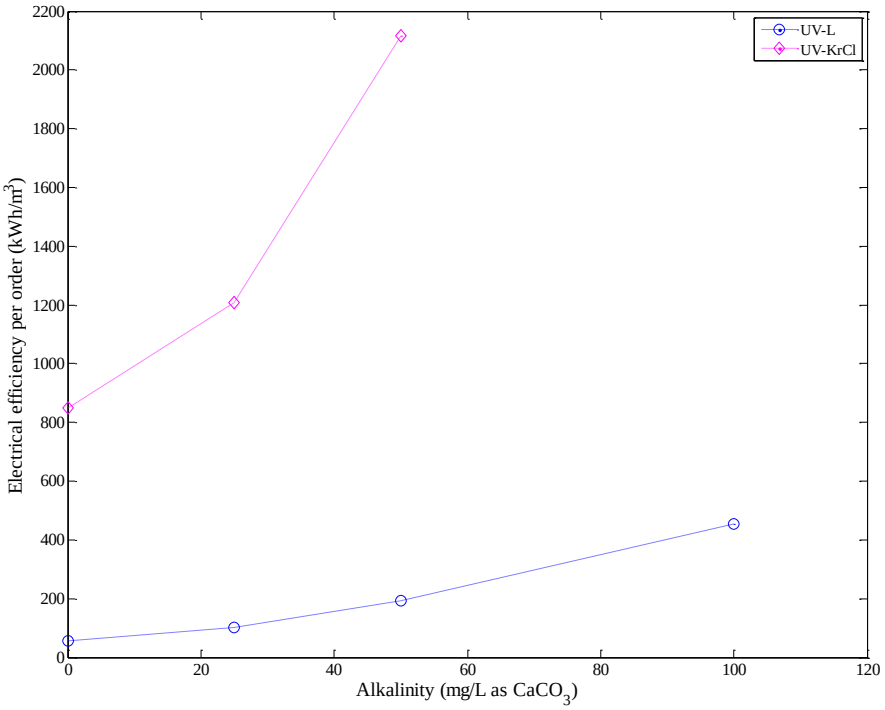

Figure 2-35. Effect of alkalinity on energy requirement to achieve 90% defluorination of PFOA, $[PFOA]_0$ = 0.02 mM, pH = 10.3, [S(IV)] dose = 7.2 mM

Table 2-18. Comparison of present and future UV-LED characteristics with UV lamps used in current study

Characteristic	Present UV-LED [73, 74]	Future UV-LED [73, 74]	UV-L (current study)	Excimer lamp (current study)
Lifetime (h)	3000	100000	9000	8000
Efficiency (%)	3-5	75	33.3	2.27
UV Wavelengths (nm)	240-365	240-365	254	222

Table 2-19. Energy and chemical cost estimates for 90% defluorination of PFOA with UV-Sulfite ARP, $[PFOA]_0$ = 0.02 mM, pH = 10.3

Lamp	Sulfite Dose (mM)	T_{90} (h)	Energy Cost ($/m^3)	Sulfite Cost ($/m^3)	Total Cost ($/m^3)
UV-L	1.8	28.8	7.12	0.22	7.34
UV-L	3.6	9.22	4.30	0.44	4.74
UV-L	7.2	4.81	4.01	0.88	4.89
UV-L	14.4	5.46	7.36	1.76	9.12
UV-KrCl	3.6	4.52	69.9	0.44	70.4
UV-KrCl	7.2	3.85	59.6	0.88	60.4
UV-KrCl	14.4	4.61	71.3	1.76	73.1

Table 2-20. Energy and chemical cost estimates for 90% defluorination of PFOA with UV-Sulfite ARP, $[PFOA]_0$ = 0.02 mM, sulfite dose = 7.2 mM

Lamp	pH	T_{90} (h)	Energy Cost ($/m^3)	Sulfite Cost ($/m^3)	Total Cost ($/m^3)
UV-L	7	9.47	6.25	0.88	7.13
UV-L	9	5.46	4.36	0.88	5.24
UV-L	10	4.81	4.01	0.88	4.89
UV-KrCl	7	5.08	78.6	0.88	79.4
UV-KrCl	9	4.61	71.3	0.88	72.2
UV-KrCl	10	3.85	59.6	0.88	60.4

Conclusions

Application of UV/sulfite ARP for PFOA degradation suggests that reductive defluorination of PFOA is a technically viable treatment process. pH and sulfite dose are the principal process variables that determine rate and efficiency of defluorination. Improvement in kinetics can be achieved under alkaline conditions and increasing sulfite dose. However, at very high concentrations of sulfite, self-scavenging of radicals occurs and this leads to plateauing of defluorination rate and a reduction in quantum yield for the process. Employing a low wavelength excimer UV source for irradiating sulfite, results in higher fraction of UV absorbed and proportional increase in defluorination rate. However, quantum yields for the ARP remains constant between UV-L and

excimer lamps. UV lamp characteristics such as emission spectrum and power requirement determine the electrical efficiency and thereby practical viability of the UV/sulfite ARP. PFOA removal with UV-L lamp is 10 times more energy efficient than with the excimer lamp. This difference can be minimized by selection of low wavelength UV sources that have higher lamp efficiency. Common water constituents such as alkalinity and nitrate scavenge radicals produced during sulfite photolysis and lower the rate of defluorination. The effect of alkalinity on lowering defluorination rate and electrical efficiency is more pronounced than nitrate. The inverse proportionality of defluorination rate on scavenger concentration suggests that pretreatment of wastewater for removal of alkalinity may be necessary to improve the electrical efficiency of the UV/sulfite ARP.

The one-pseudo-component kinetic model provides quantitative estimates for defluorination rate constants and allows evaluation of the effect of process variables on defluorination of PFOA. The ultimate end products of PFOA degradation are formic acid and inorganic fluoride, which are formed through intermediate short chain fluorinated organics. One order reduction in organic fluorine within 4 h, indicates that UV/sulfite ARP is a promising treatment technology to treat perfluorinated compounds. It requires further testing at pilot scale with multiple UV sources. Pilot scale testing of the ARP with energy efficient UV sources can reveal valuable information on the commercial viability of the process. The kinetic, energy requirement and cost data reported for batch reactors in this study serve as initial estimates for designing a pilot scale UV reactor for PFOA removal.

CHAPTER III

PHOTOLYTIC REMOVAL OF AQUEOUS CHLORITE AND MINIMIZING CHLORATE FORMATION

Introduction

Chlorine dioxide (ClO_2) can be used as an alternative or a supplement to chlorine (Cl_2) disinfection of drinking water. ClO_2 has shown similar or superior germicidal efficiency with respect to pathogenic bacteria and viruses. ClO_2 also aids in the removal of taste/odor-causing compounds and oxidizes iron and manganese in water. The principal advantage of ClO_2 disinfection is the reduction in chlorinated organic byproducts such as trihalomethanes and halogenated acetic acids.[82] Approximately 6-8% of water supplies in the U.S use ClO_2 in their drinking water treatment plants.[83] ClO_2 is generated onsite by treating sodium chlorite ($NaClO_2$) with gaseous ($Cl_{2\,(g)}$) or aqueous chlorine (NaOCl). Efficiency of the generation method and feed ratios of the reactants determine the yields of ClO_2 and unwanted byproducts chlorite (ClO_2^-) and chlorate (ClO_3^-) ions.[82] ClO_2, when applied to drinking water, eventually undergoes reduction to chlorite and chloride (Cl^-), as shown in reactions (3-1) and (3-2). Chlorite is the primary end product at neutral pH.[84] Exposure of ClO_2 to sunlight during storage also results in it forming high ClO_2^- concentrations when added to water.

$$ClO_2 + e^- \rightarrow ClO_2^- \qquad (3\text{-}1)$$

$$ClO_2 + 4H^+ + 4e^- \rightarrow Cl^- + H_2O \qquad (3\text{-}2)$$

Industrial sources of chlorite and chlorate include wastewater from pulp and paper mills, textile and dye manufacturing, pesticide production.[85, 86] Chlorite and chlorate in drinking water interfere with hemoglobin content in the bloodstream and are reported to cause neurodevelopmental effects in rats.[87] The Stage 1 DBP rule as part of the SDWA in 1998, determined a maximum contaminant level (MCL) of 1 mg/L for aqueous chlorite.[88]

Chlorite in water can be chemically reduced by addition of reducing agents such as S(IV) and Fe(II). Thiosulfate ($S_2O_3^{2-}$) and forms of S(IV) such as sulfur dioxide (SO_2) and bi/sulfite ion (HSO_3^-, SO_3^{2-}) have been studied as sulfur-based treatment approaches.[89] Sulfite-chlorite reaction in the absence of oxygen, as represented by overall reaction (3) is kinetically feasible with pseudo first-order reaction rates around 0.0166 s^{-1} at neutral pH. Initial chlorite residuals around 1.5 mg/L were completely removed within 30 minutes after sulfite addition in experiments conducted at drinking water plants. The reaction kinetics were better at slightly acidic (pH 6.3) condition than at high pH environment. Depending on pH, S(IV) can exist as $SO_{2(aq)}$, H_2SO_3, HSO_3^- or SO_3^{2-}. In acidic pH environments, where HSO_3^- dominates, the overall reduction of chlorite proceeds through formation of an intermediate species $[O_2Cl\text{-}SO_3H]^{2-}$ as in reaction (4).[90] In the absence of dissolved oxygen (DO), this intermediate species is further reduced to chloride by reacting with S(IV). However, in the presence of DO in water, $[O_2Cl\text{-}SO_3H]^{2-}$ is oxidized to chlorate.[90, 91] Chlorate is extremely resistant to chemical reduction and has similar deleterious health effects as chlorite. As complete de-

oxygenation of water would not be feasible in a treatment process, S(IV) addition for ClO_2^- removal has been limited in application.

$2SO_3^{2-} + ClO_2^- \rightarrow 2SO_4^{2-} + Cl^-$ (3-3)

$ClO_2^- + HSO_3^- \rightarrow [O_2Cl\text{-}SO_3H]^{2-}$ (3-4)

Thiosulfate ($S_2O_3^{2-}$) addition to reduce chlorite residuals does not produce chlorate, but the reaction is kinetically limited and requires longer contact times and higher $S_2O_3^{2-}$ doses to be effective. Careful pH control in the range 4.6 to 6.4 is also required for the thiosulfate reduction process.[90] Ferrous iron is effective in reduction of chlorite over the pH range of 5-10 and does not produce chlorate. Ferrous iron reduction of chlorite also produces ferric solids that aid in coagulation and sedimentation. The only limitation to ferrous iron application is high levels of dissolved organic carbon and DO in the treated water.[92-94]

An alternative to chemical reduction of chlorite is photolytic removal. Aqueous chlorite absorbs UV over the range of 200 to 300 nm with an absorption peak around 260 nm. The molar extinction coefficient of chlorite at 254 nm is reported to be around 130 $M^{-1}cm^{-1}$.[95] UV photolysis of chlorite at 254 nm results in chloride and chlorate as the principal end products, with chlorine dioxide as an intermediate.[96] The photolytic reaction of chlorite can be initiated through the pathways in reactions (3-5) to (3-8), which are summarized from previous research.[97] The products from these reactions

further undergo several photolytic and redox reactions to form stable products Cl^- and ClO_3^-.

$ClO_2^- + hv \rightarrow OCl^- + O(1D)$ (3-5)

$ClO_2^- + hv \rightarrow OCl + O^-$ (3-6)

$ClO_2^- + hv \rightarrow (ClO_2^-)^*$ (3-7)

$(ClO_2^-)^* + ClO_2^- \rightarrow ClO_2 + OCl^- + O^-$ (3-8)

The rate of chlorite photodecomposition is reported to be independent of pH in the range of 4 to 8 and quantum yield for chlorite removal to be around 1.00 ± 0.1 mol/Ein at 254 nm.[95] It is also observed that removing ClO_2 by continuous sparging of the reactor with nitrogen, significantly reduced chlorate yield. Quantum yields for chlorite removal in this modified process were in the range 0.72 to 1.53 mol/Ein.[97]

The current research aims to build on previous studies of chlorite photodecomposition, to better understand the effect of background water constituents on the process. The effects of following process variables on UV photolysis of chlorite is studied: natural organic matter (NOM), alkalinity, nitrate, and sulfite. NOM, alkalinity and nitrate have been selected due to their ubiquitous presence in water supplies and their inhibitory effects on advanced oxidation technologies (AOT).[98] NOM, a heterogeneous mixture of organic compounds absorbs UV in the wavelength range of 200-300 nm, commonly used in water treatment. The specific UV absorbance at 254 nm is used as an indicator for the aromatic fraction of NOM.[99] NOM and nitrate in

photochemical water treatment processes also act as UV filters, reducing the rate of UV absorption by targets.[100] Photolysis of NOM and nitrate can produce oxidizing free radicals, hydroxyl radical (OH·) and nitrite radical (NO_2·).[101] Thus, the effect of NOM on any UV-based treatment process needs careful evaluation. Alkalinity in water also acts as a radical trap by scavenging hydroxyl radicals and forming carbonate radicals ($CO_3^{-\cdot}$).[98] Carbonate radicals have a high oxidation potential (1.78 V) and have been detected in natural water at low concentrations around 10^{-13} M.[98, 102] The synergy of sulfite (SO_3^{2-}) and UV has been tested as an effective reduction process for recalcitrant contaminants in water called advanced reduction processes (ARP).[14, 48] UV irradiation of sulfite generates hydrated electrons (reduction potential -2.77 V) and sulfite anion radicals.[5, 9] UV-sulfite process has been successful in degrading contaminates such as vinyl chloride, bromate and perchlorate to innocuous forms.[14, 48, 103] The objectives of this study are to:

i. Investigate the effect of process variables on kinetics of chlorite photodecomposition
ii. Describe the effect of process variables on chlorate and chloride yields
iii. Identify optimum conditions for minimizing chlorate formation during chlorite photolysis

Methodology

Reagents

Ion chromatography (IC) standard grade potassium chloride, sodium chlorite, potassium chlorate and sodium nitrate (1000 mg/L) were purchased from Inorganic

Ventures (Christiansburg, VA, USA). Sodium sulfite (anhydrous, 98%) was obtained from Sigma-Aldrich (St. Louis, MO, USA). HPLC grade sodium bicarbonate powder was purchased from EMD chemicals, Inc. (Gibbstown, NJ, USA). Fulvic acid isolated from reverse osmosis of Suwannee river water was purchased from International Humic Substances Society (Denver, CO, USA). The acidic functional groups and elemental composition of fulvic acid/NOM powder (Catalog No. 1R101F) are described in the appendix. Potassium phosphate (anhydrous, 97%), potassium hydrogen phosphate (anhydrous, 98%), potassium di-hydrogen phosphate (99%) and phosphoric acid (85%) were purchased from Alfa Aesar (Ward Hill, MA, USA).

Experimental procedure

For experiments requiring low levels of dissolved oxygen, all chemical solutions were prepared and experiments conducted inside an anaerobic chamber (Coy Laboratory Products Inc.). The chamber atmosphere was maintained at 95% nitrogen (N_2) and 5% hydrogen (H_2). A palladium catalyst connected to a recirculating fan removed trace oxygen in the chamber. Oxygen and hydrogen levels in the chamber were monitored with an Oxygen and Hydrogen Analyzer (Coy Laboratory Products Inc.). Deionized water (DI) (ultra-pure 18 MΩ•cm) was deoxygenated by purging 1 gal of water with 99.99% N_2 for 2 h. This deoxygenated deionized water was allowed to equilibrate with the atmosphere in the anaerobic chamber for 12 h. For experiments with dissolved oxygen, water was prepared by bubbling natural air through 1 gal of DI water for 1 h. For all experiments, initial chlorite concentration of 10 mg/L and buffer concentrations of 10 mM were used.

UV reactor

Two identical bench scale UV reactors were setup, inside and out of the anaerobic chamber. UVS-236 DS surface disinfectors purchased from Lumalier (Memphis, TN, USA) were equipped with Phillips TUV PL-L36W/4P lamps. The germicidal UV lamps which emit monochromatic UV at 254 nm, have less than 4.5 mg mercury and do not produce ozone. A UV reactor enclosure was built with the UV lamp positioned directly above the petri dish with the experimental solution. A water sample of 100 mL was placed in a petri dish on a magnetic stirrer to ensure completely mixed condition. UV intensities at surface of the petri dish were measured with a UVC 512 light meter calibrated at 254 nm (Professional Equipment, Janesville, WI, USA). An Agilent 8453 UV-visible spectroscopy system was used for measuring the absorption spectrum and calculating molar extinction coefficients of chlorite and NOM.

Analytical methods

Analysis for anions, chloride, chlorite and chlorate was conducted on a Dionex DX-500 ion chromatography system. IonPac AS19 hydroxide selective anion exchange column (4 x 250 mm) and an AG19 guard column (4 x 50 mm) were used to separate the ions. A 20-mM sodium hydroxide solution at a flow rate of 1 mL/min was used as the eluent. Sample vials (0.5 mL) were used in the AS-40 auto sampler with a sample injection loop of 200 µL. The DX-500 was equipped with a GP 40 gradient pump, CD 20 conductivity detector and AERS 500 (4 mm) suppressor.

Data analysis

In order to explain the effect of process variables on chlorite removal, quantitative parameters that describe rate and efficiency of the reaction need to be developed. First order exponential decay model was fit to observed experimental data by conducting non-linear, least squares regression. Levenberg–Marquardt algorithm in MATLAB was used to obtain estimates for pseudo first order rate constant (k_{obs}). Product yields (mol/mol) were calculated as the ratio of final chloride and chlorate concentrations observed with total concentration of chlorite removed. For experiments without NOM, quantum yield (ϕ) for chlorite photolysis was estimated by solving equation 3-1 with experimental data obtained for concentrations of chlorite with time. Non-linear least squares regression was conducted to obtain the estimate for ϕ. For experiments with NOM, the initial quantum yield (ϕ_0) for chlorite photolysis was estimated by equation 3-2.

$$\frac{d\left[ClO_2^-\right]}{dt} = -\Phi \frac{I_0}{L}\left(1 - e^{-\left(\varepsilon_{clO_2^-} C_{clO_2^-} L\right)}\right) \qquad 3\text{-}1$$

$$\Phi_0 = \frac{\alpha}{\varepsilon_{ClO_2^-} C_{ClO_2^-}} \left(\frac{k_{obs} C_{0,ClO_2^-}}{\frac{I_0}{L}\left(1 - e^{-\alpha L}\right)} \right) \qquad 3\text{-}2$$

I_0 is the flux of incident UV photons,

L is the depth of the reactor,

ϵ_{ClO2-} is the $\log_e$ base based molar extinction coefficient of chlorite at 254 nm,

C_{ClO2^-} is the concentration of ClO_2^-,

$C_{0, ClO2^-}$ is the initial concentration of ClO_2^-,

k_{obs} is the pseudo first-order rate constant for chlorite removal,

$$\alpha = \varepsilon_{ClO_2^-} C_{ClO_2^-} + \varepsilon_{NOM} C_{NOM}$$

ε_{NOM} is the $\log_e$ based molar extinction coefficient of NOM at 254 nm,

C_{NOM} is the concentration of NOM as carbon.

Electric energy per order (E_{EO})

E_{EO} is the electrical energy required to degrade a target contaminant by one order of magnitude in a unit volume of contaminated water. For a batch reactor, E_{EO} can be calculated as follows.

$$E_{EO} = \frac{P.t}{\log(\frac{C_0}{C_f})V} \qquad 3\text{-}3$$

P is input power of the UV lamp needed to produce light energy absorbed in the reactor,

t is the time of UV lamp operation,

V is the volume of the water treated,

C_0 and C_f are the initial and final concentrations of the contaminant,

This relationship can be simplified by assuming first-order kinetics so that the substitution $\log(C_0/C_f) = k.t/2.303$ can be made. It can be further simplified by defining the power input per unit volume (P_v).

$$E_{EO} = \frac{2.303 P_V}{k} \qquad 3\text{-}4$$

k is the first order-rate constant

The power per unit volume of the UV lamp needed to produce light energy absorbed in the reactor, $I'_{V,absorbed}$ can be calculated as,

$I'_{V,absorbed} = I'_{V,applied}$ * fraction of UV absorbed

$$I'_{V,absorbed} = \frac{I'_0}{L}(1 - e^{-\sum \varepsilon_i C_i L}) \qquad 3\text{-}5$$

I'_0 is the incident UV irradiance,

L is the depth of the reactor,

ϵ_i is the $\log_e$ base based molar extinction coefficient of UV absorbing species i,

C_i is the concentration of species i,

The electrical power consumed per unit volume can be determined from the light power absorbed using the electrical efficiency of the UV lamps and these are specified in Table 3-2.

$P_V = I_{V,\,absorbed} / (\eta)$

η is efficiency of the UV lamp

Results and discussion

UV absorbance

The UV absorbance spectrum of ClO_2^- in the range of 190 to 300 nm is presented in Fig. 3-1. It indicates presence of a local absorbance peak around 260 nm, which is very close the wavelength of UV-L lamps, commonly used in water/wastewater disinfection. The molar extinction coefficient of ClO_2^- ($\log_{10}$ base) at 254 nm, calculated

from data in Fig. 3-1 is 136.4 M^{-1} cm^{-1}. The UV absorbance spectrum of fulvic acid used in the study in the range of 190 to 300 nm is presented in Fig. 3-2. The molar extinction coefficient of NOM (common log) at 254 nm, calculated from data in Fig. 3-2 is 926 M^{-1} cm^{-1}.

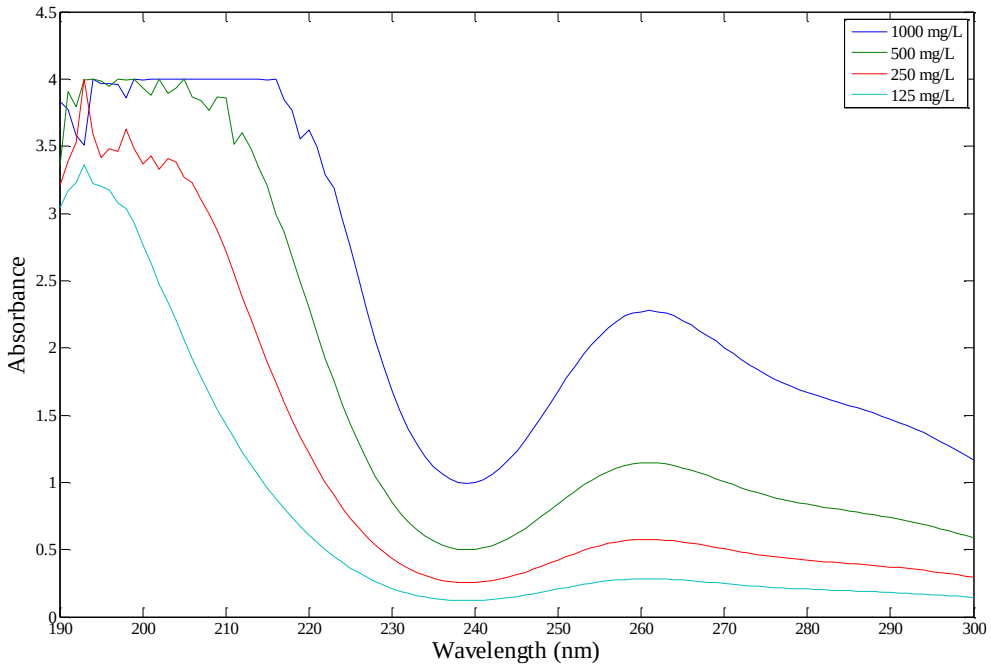

Figure 3-1. UV absorbance spectrum of aqueous chlorite at varying concentrations; pH 7

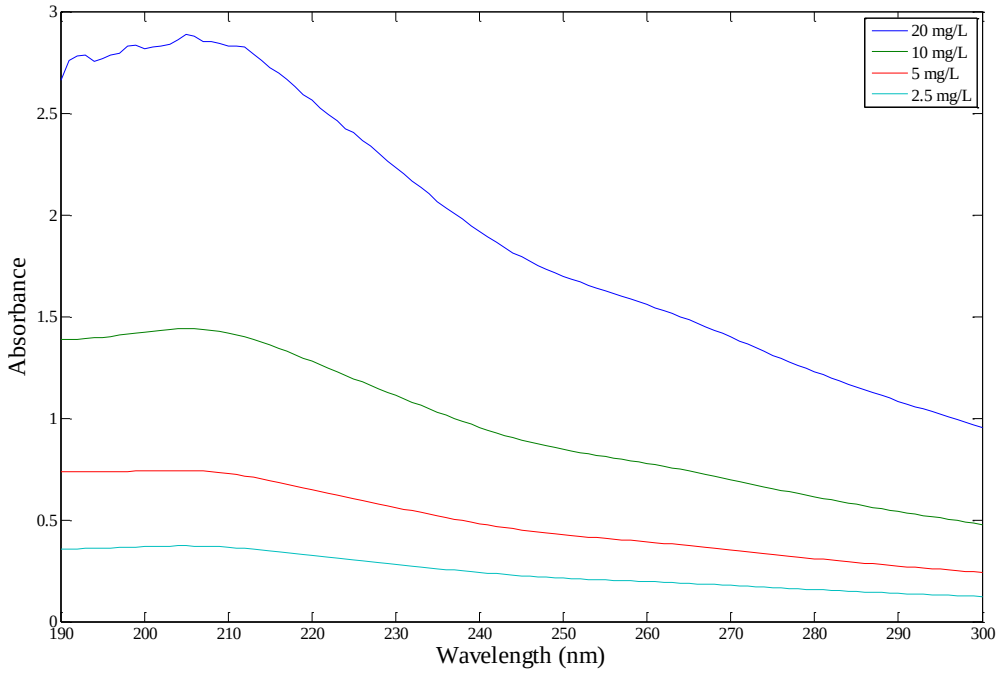

Figure 3-2. UV absorbance spectrum of NOM (fulvic acid) at different concentrations as mg/L carbon, pH=7

Effect of NOM on chlorite photolysis

The effect of NOM on the rate of chlorite photodecomposition and yields of chloride and chlorate is presented in Table 3-1 and Table 3-2. Presence of NOM in water significantly reduced the rate of chlorite photodecomposition. This effect is illustrated in Fig. 3-3. NOM (fulvic acid) used in the current study absorbs UV significantly with a molar extinction coefficient (based on concentration of carbon content) of 926 M^{-1} cm^{-1} at 254 nm. This strong UV-254 absorption leads to a breakdown of parent NOM

molecules to low molecular weight intermediates. The average UV irradiance (I_{avg}) in the reactor decreases with increasing NOM concentrations, according to equation 3-6.[104] An increase in NOM concentration, elevates α and lowers I_{avg}. This reduces the rate of UV absorbed by ClO_2^- as in equation 3-7. A reduction in the rate of UV absorption by ClO_2^-, lowers the rate of photodecomposition (Fig. 3-3), which manifests as lowered first order rate constant k_{obs} (Tables 3-1 and 3-2). Data in Fig. 3 also suggest that DO by itself had limited impact on the rate constant for chlorite reduction, reducing rate constant by 20%. However, presence of NOM and DO together had a major effect, lowering rate constant by 45%, at high NOM concentrations. This is due to the difference in photolytic transformation of NOM at high DO levels. Photons are absorbed by certain functional groups (chromophores) in NOM and the excited chromophores transfer energy to DO to form singlet oxygen.[105] Oxygen in excited state has greater reactivity towards NOM and forms intermediate organic radical species that are further oxidized. Photo-oxidation of NOM, is different from direct photolysis and proceeds through species such as aromatic carboxylic acids, with greater chlorine reactivity, thereby causing slower kinetics of ClO_2^- reduction. Additionally, as shown in Tables 3-1 and 3-2, yield for other chlorinated byproducts (other Cl), in presence of DO and NOM are higher than those for NOM without DO.[101, 105-107]

$$I_{avg} = \frac{I_0\left(1-\exp\left(-\alpha L\right)\right)}{\alpha L} \qquad 3\text{-}6$$

$$r_{UV,ClO_2^-} = \varepsilon_{ClO_2^-} C_{ClO_2^-} I_{avg} \qquad 3\text{-}7$$

$r_{UV,ClO2^-}$ is he average rate of UV absorption by chlorite

Combining equations 3-1, 3-6 and 3-7, the first order rate constant for chlorite loss could be expressed as,

$$k = \phi \varepsilon_{ClO_2^-} I_0 \left[\frac{1 - \exp(-\alpha L)}{\alpha L} \right] \qquad 3\text{-}8$$

Under current experimental conditions, increasing NOM would only alter α, as in Table 3-3. The validation of model in equation 3-8, is presented in Fig. 3-4.

Table 3-1. Effect of NOM on UV photolysis of chlorite in absence of dissolved oxygen; $[ClO_2^-]_0$=10 mg/L pH = 7.2, UV irradiance = 9.45 mW/cm^2

NOM as Carbon, (mg/L)	k_{obs} (min^{-1})	Yield, Cl^- (mol/mol)	Yield, ClO_3^- (mol/mol)	Yield, Other Cl (mol/mol)
0.00	0.312 ± 0.014	0.544	0.236	0.220
2.50	0.203 ± 0.008	0.745	0.096	0.159
5.00	0.152 ± 0.004	0.874	0.013	0.113
10.0	0.106 ± 0.002	0.913	0.005	0.082

Table 3-2. Effect of NOM on UV photolysis of chlorite in presence of dissolved oxygen; [DO] = 8.3 mg/L, $[ClO_2^-]_0$=10 mg/L, pH = 7.2, UV irradiance = 9.45 mW/cm^2

NOM as Carbon, (mg/L)	k_{obs} (min^{-1})	Yield, Cl^- (mol/mol)	Yield, ClO_3^- (mol/mol)	Yield, Other Cl (mol/mol)
0.00	0.254 ± 0.016	0.432	0.235	0.333
2.50	0.180 ± 0.008	0.674	0.130	0.196
5.00	0.096 ± 0.004	0.745	0.031	0.224
10.0	0.059 ± 0.001	0.821	-	0.179

Table 3-3. Change in α with NOM concentration

NOM as Carbon, (mg/L)	α (cm^{-1})
0.00	0.047
2.50	0.491
5.00	0.935
10.0	1.824

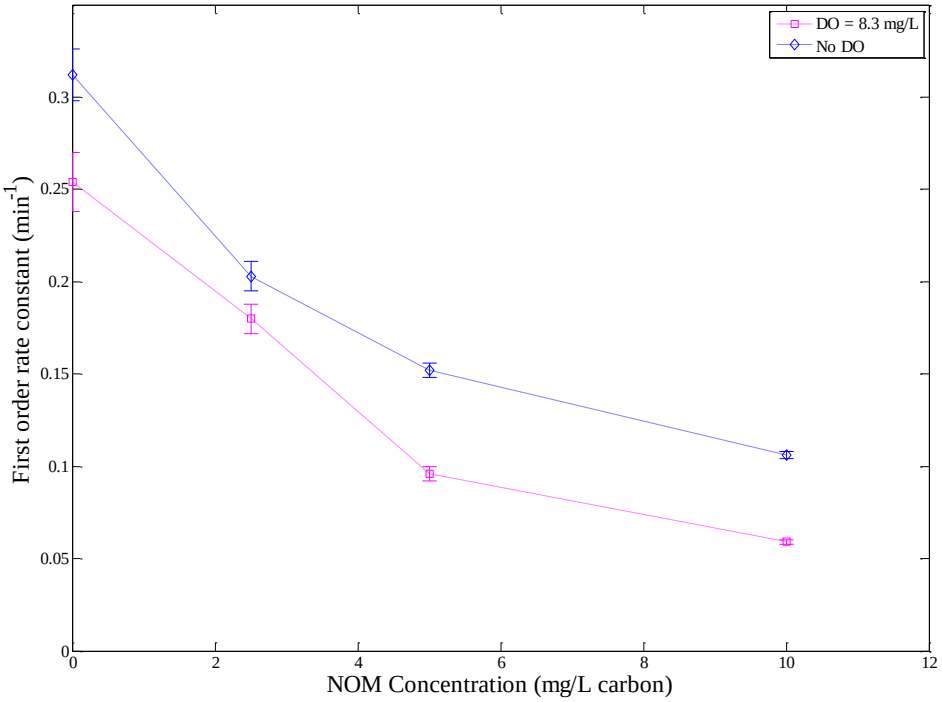

Figure 3-3. First-order rate constant (min^{-1}) of chlorite photolysis as affected by NOM concentration with and without the presence of dissolved oxygen; $[ClO_2^-]_0$=10 mg/L, pH=7.2, UV_{254}=9.45 mW/cm^2

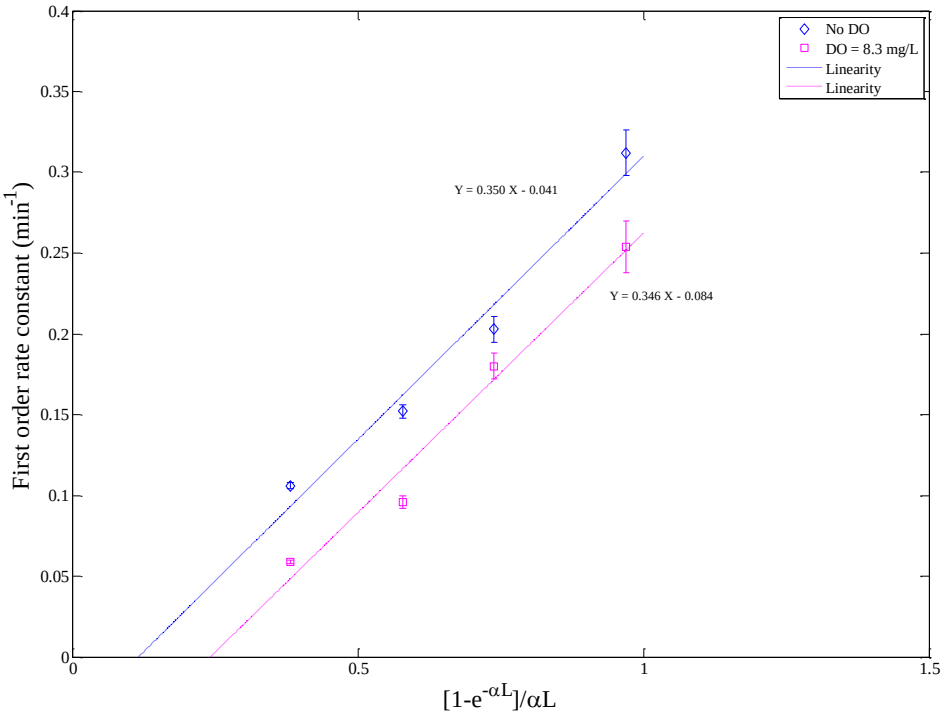

Figure 3-4. Validation of model dependence of rate constant on average UV irradiance in the reactor, $[ClO_2^-]_0$=10 mg/L, pH=7.2

Addition of NOM increased the yield of chloride and reduced that of chlorate as shown in Fig. 3-5 and 3-6. This trend is consistent at both levels of DO concentration. In absence of DO, addition of NOM at concentration of 10 mg/L, resulted in more than 90% of chlorite being reduced to chloride. Chlorate formation, even at a high DO level of 8.3 mg/L, could be eliminated with sufficiently high NOM concentrations. The material balances on total chlorine in the reactor showed that around 10-20% of total chlorine did not exist as Cl^-, ClO_2^- or ClO_3^-. This missing chlorine could be caused by

loss of chlorine from the solution due to volatilization or by failing to measure chlorine in all species that were present. Since the reactor had an open surface exposed to nitrogen or air, volatile intermediates of chlorite photolysis, such as ClO_2 and Cl_2, could be stripped from water. One type of chlorinated species that was not measured could be chlorinated organic byproducts formed by reaction of hypochlorite with NOM. In the absence of DO, increasing concentration of NOM reduced the yield of missing chlorine, indicating that volatile inorganics constitute a major fraction of missing chlorine in absence of DO. Effect of NOM on product yields can also be explained by the scavenging of oxygen and oxidizing radicals produced during chlorite photolysis. Reactions 3-5 to 3-8 identify the generation of oxidizing species during chlorite photolysis. The products from these reactions further react according to 3-9 to 3-12.[97, 108-110] Scavenging of oxidizing radicals, such as the hydroxyl radical, by NOM has been well reported in AOTs.[111] In the current system, NOM could scavenge OH· produced in reaction 3-9 and O (1D) produced in reaction 3-5, preventing ClO_2 formation in reaction 3-10. Cosson et al. report that chlorate formation does not occur due to direct chlorite photolysis, but by production and decomposition of chlorine dioxide as an intermediate compound, as in the overall stoichiometric reaction 3-11.[97] Higher NOM concentrations would restrict ClO_2 formation, thereby ensuring lower chlorate yield. The primary reaction pathway for chlorite in the presence of NOM would be through reactions 3-5 and 3-12.[110]

$$O^- + H_2O \rightarrow OH^- + OH^{\cdot} \qquad (3\text{-}9)$$

$OH\cdot + ClO_2^- \rightarrow ClO_2 + OH^-$ (3-10)

$10\ ClO_2 + 5H_2O + hv \rightarrow 4\ Cl^- + 6ClO_3^- + 3.5O_2 + 10\ H^+$ (3-11)

$OCl^- + hv \rightarrow Cl- + O\ (1D)$ (3-12)

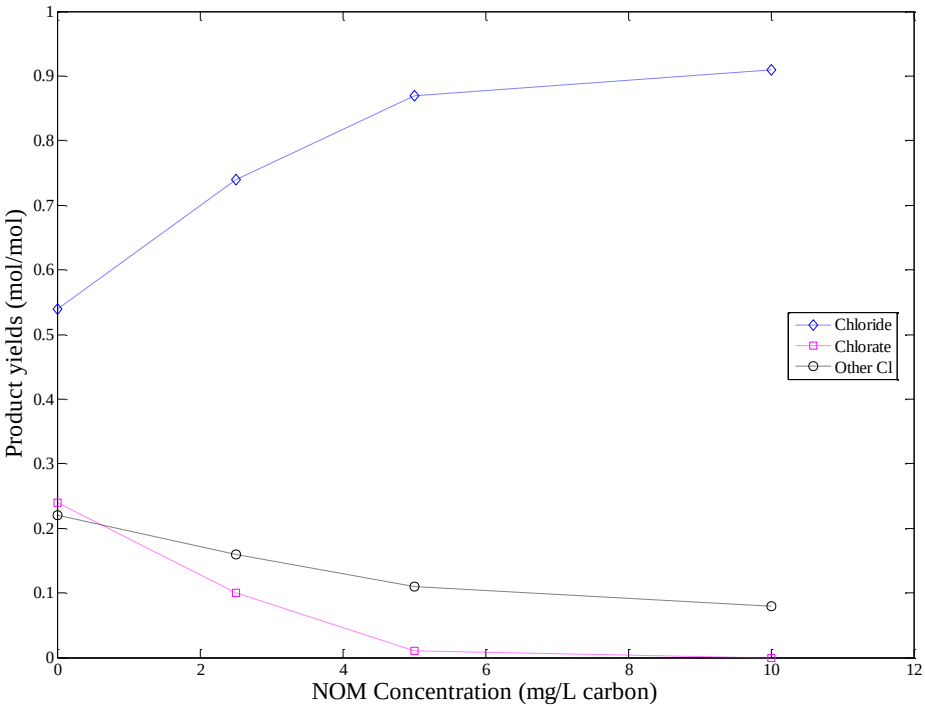

Figure 3-5. Product yields of chloride, chlorate and other chlorine species (mol/mol) from chlorite photolysis as affected by NOM in the absence of dissolved oxygen; $[ClO_2^-]_0$=10 mg/L, pH=7.2, UV_{254}=9.45 mW/cm^2

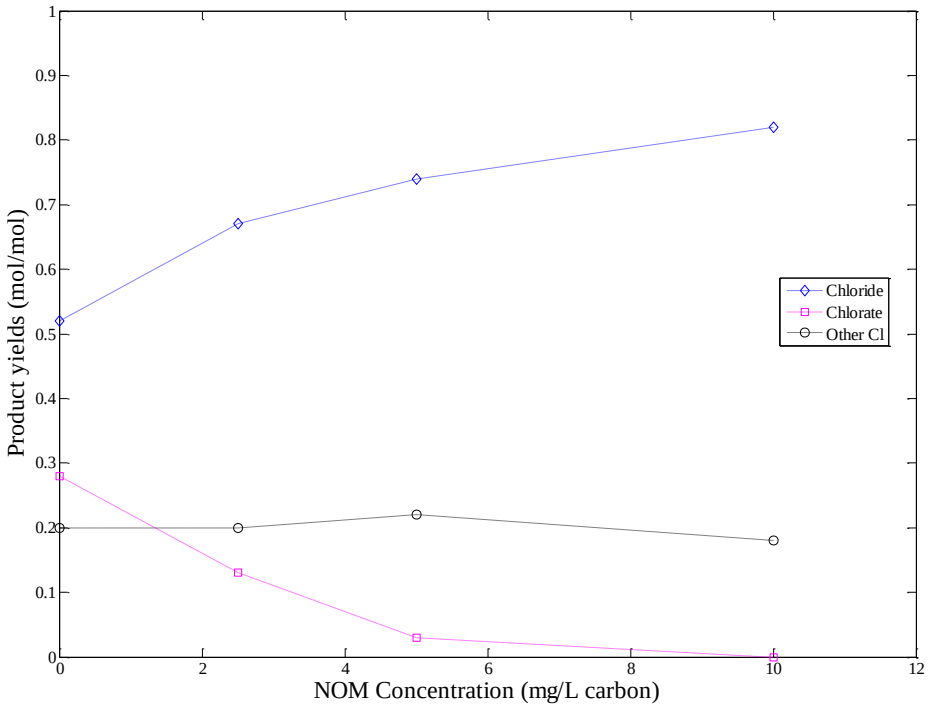

Figure 3-6. Product yields of chloride, chlorate, and other chlorine species (mol/mol) from chlorite photolysis as affected by NOM in the presence of dissolved oxygen: [DO]=8.3 mg/L, $[ClO_2^-]_0$=10 mg/L, pH=7.2, UV_{254}=9.45 mW/cm^2

Effect of sulfite

Effect of sulfite addition on chlorite photolysis was tested at three pH levels (5.4, 7.2 and 10.3) and at three DO levels. The data in Fig. 3-7 and 3-8, describe the influence of pH and DO on chlorite reduction by the sulfite-UV method. In absence of DO, no chlorate was detected, and greater than 90% of chlorite was reduced to chloride. At DO levels of 6.8 and 8.3 mg/L, high chlorate yields (0.47 mol/mol) were observed at pH 10.3. Negligible chlorate formation was observed at neutral pH. Acidic and neutral pH favored chlorite reduction to chloride. The effect of DO on chlorate formation is in accordance with trends previously reported.[89-91]

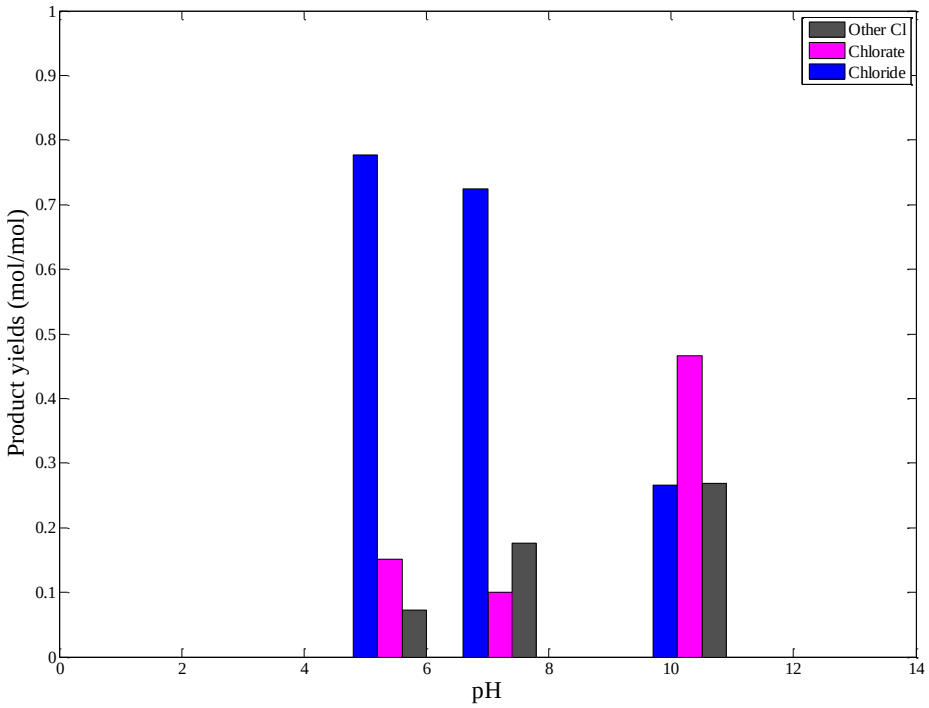

Figure 3-7. Effect of pH on product yields of chloride, chlorate, and other chlorine species (mol/mol) from UV-Sulfite reduction of chlorite as affected by pH in presence of dissolved oxygen; $[ClO_2^-]_0$=10 mg/L, [DO] = 8.3 mg/L, $[S(IV)]_0$ = 1.5 mM, UV irradiance = 9.45 mW/cm^2, Irradiation time = 10 min

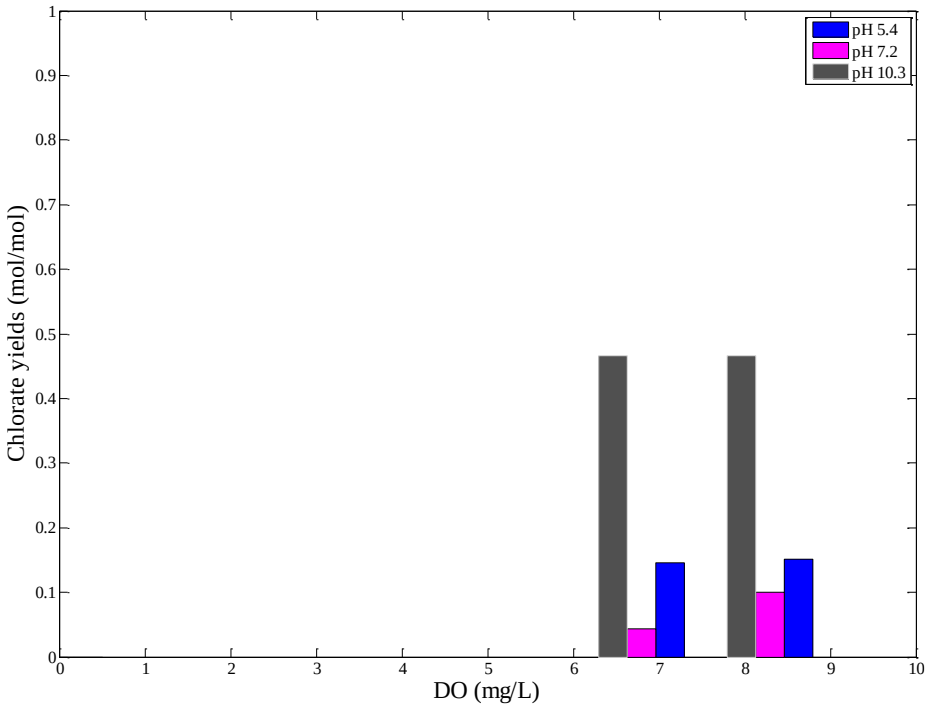

Figure 3-8. Effect of DO on chlorate formation from UV-Sulfite reduction of chlorate (mol/mol), [S(IV)] = 1.5 mM, $[ClO_2^-]_0$=10 mg/L, UV irradiance = 9.45 mW/cm^2, Irradiation time = 10 min

The mechanism of UV-sulfite process on chlorite removal proceeds through three major pathways: direct redox reaction between S(IV) species and ClO_2^-, mediation of hydrated electrons produced by photolysis of S(IV) and direct photolysis of ClO_2^-. The first pathway in absence of DO, has been summarized by the overall reaction 3-13.[91]

$$2SO_3^{2-} + ClO_2^- \rightarrow 2SO_4^{2-} + Cl^- \qquad (3\text{-}13)$$

At high DO levels, ClO_2 is formed as an intermediate that decays into an oxidized product (ClO_3^-) and a reduced product, Cl^-, as shown in reaction 3-14.[90]

$$2\ ClO_2 + 2\ S(IV) + H_2O \rightarrow Cl^- + ClO_3^- + 2SO_4^{2-} + 2H^+ \quad (3\text{-}14)$$

The second pathway involves generation of hydrated electrons that reduce chlorite according to reactions 3-15 to 3-17.[110]

$$SO_3^{2-} + hv \rightarrow SO_3^{-}\cdot + e_{aq}^- \quad (3\text{-}15)$$

$$e_{aq}^- + ClO_2^- \rightarrow OCl^- + O^- \quad (3\text{-}16) \qquad k_{16} = (4.5 \pm 0.5) \times 10^{10}$$

$$e_{aq}^- + OCl^- \rightarrow Cl^- + O^- \quad (3\text{-}17) \qquad k_{17} = (5.3 \pm 1.0) \times 10^{10}$$

For the overall reduction of chlorite to proceed through reactions (3-16) and (3-17), the key factor is the rate of formation of hydrated electrons. UV irradiation of sulfite solutions produces hydrated electron and sulfite anion radical, as shown in reaction (3-15). At a fixed pH and UV irradiance, the rate of formation of hydrated electrons is directly dependent on sulfite ion concentration, unless the concentration of S(IV) is so high that all of the light is absorbed. Higher S(IV) doses would lead to greater rate of production of hydrated electrons, facilitating chlorite reduction to proceed through reactions (3-16) and (3-17). Even in presence of high DO, ClO_2 formation could be minimized by maintaining high S(IV) doses as shown in Fig. 3-9 ad 3-10.

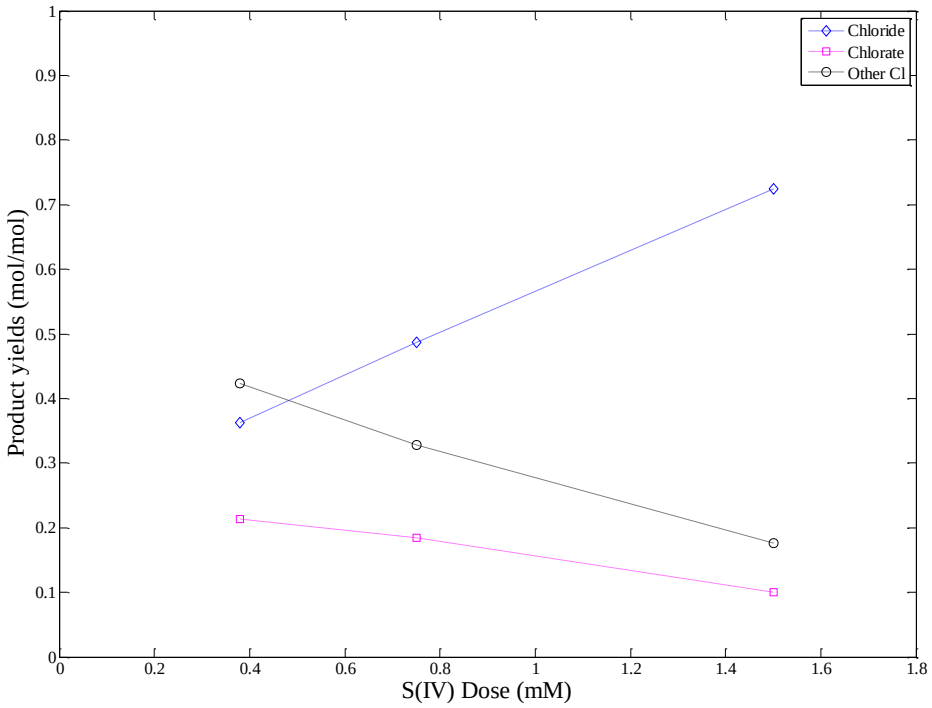

Figure 3-9. Product yields of chloride, chlorate, and other chlorine species (mol/mol) from UV-Sulfite reduction of chlorite as affected by S(IV) dose in the presences of dissolved oxygen; $[ClO_2^-]_0$=10 mg/L, [DO] = 8.3 mg/L, pH 7.2, UV irradiance = 9.45 mW/cm^2, Irradiation time = 10 min

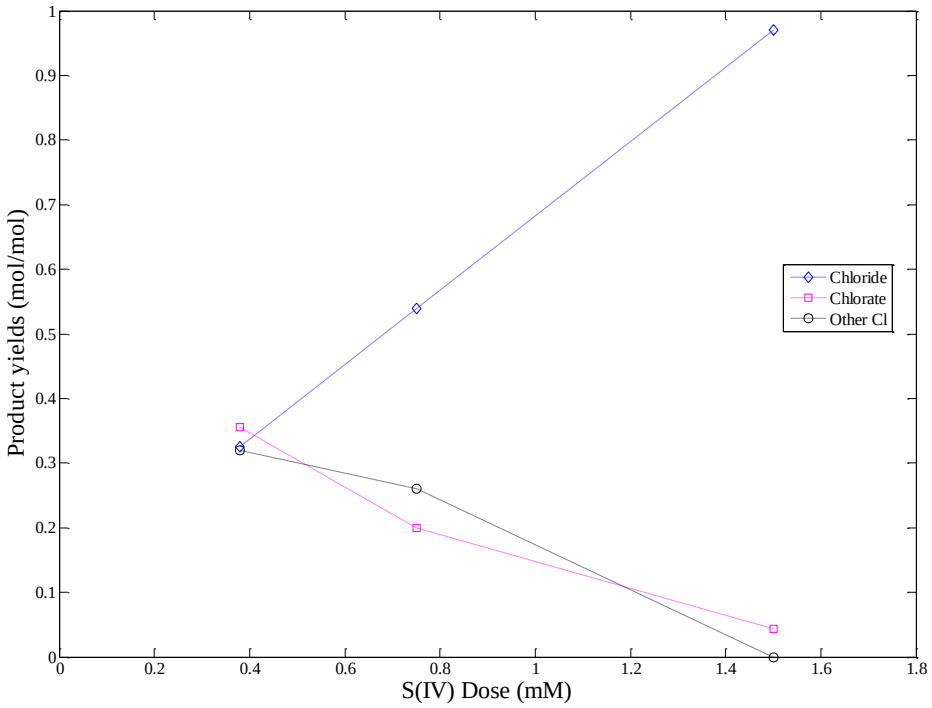

Figure 3-10. Product yields of chloride, chlorate, and other chlorine species (mol/mol) from UV-Sulfite reduction of chlorite as affected by S(IV) dose in presence of dissolved oxygen; $[ClO_2^-]_0$=10 mg/L, [DO] = 6.8 mg/L, pH 7.2, UV irradiance = 9.45 mW/cm^2, Irradiation time = 10 min

Data shown in Fig. 3-9 and 3-10, at DO levels of 6.8 and 8.3 mg/L show rising chloride yields accompanied by declining chlorate formation, as S(IV) doses increase. This trend is due to the predominance of the hydrated electron mechanism instead of S(IV) reduction mechanism. At low sulfite concentrations, the UV absorption rate of sulfite would be lower. Additionally, the molar extinction coefficient (254 nm) of sulfite

solutions at pH 7 is 16.7 L/mol-cm, which is significantly lower than that of chlorite (136.36 L/mol-cm).[48] So, considering the concentrations of chlorite and S(IV), the rate of UV absorption due to chlorite will be dominant at low sulfite doses, promoting ClO_2 formation and oxidation to chlorate. DO competes with chlorite for sulfite oxidation, which favors chlorate formation.[90] However, even at a high DO level of 8.3 mg/L, a stoichiometric excess of sulfite (5 times) ensured that less than 10% chlorite is oxidized to chlorate. At DO level of 6.8 mg/L, chlorate yield was as low as 0.05 mol/mol. Presence of sulfite also reduced the total loss of other Cl byproducts as observed in Fig. 3-9 and 3-10.

Effect of alkalinity

The effect of alkalinity on the rate of chlorite photodecomposition and yields of chloride and chlorate is presented in Tables 3-4 and 3-5. Fig. 3-11 shows the effect of alkalinity on first-order rate constants for chlorite removal at neutral pH. A consistent decline in the rate constant was observed at both DO levels. Fig. **3-**12 and Fig. 3-13 show the effect of alkalinity on product yields at neutral pH. In absence of DO, chloride yield increased by 16% with the addition of 50 mg/L of alkalinity as $CaCO_3$. An increase of 30% in chloride yield was observed at a DO of 8.3 mg/L. Chlorate yields at both DO levels were reduced to around 0.2 mol/mol with alkalinity at 50 mg/L as $CaCO_3$. Due to the low levels of alkalinity tested, the scavenging effect of oxygen produced during chlorite photolysis was limited. But the trend of increasing chloride yields was consistent. In natural water, total alkalinity could be around several hundred mg/L as

$CaCO_3$, which would greatly enhance the scavenging effect and inhabit ClO_2 formation, thereby preventing ClO_3^- formation. Under UV irradiation of high alkalinity natural water, bi/carbonate ion could also form carbonate radical, by reacting with hydroxyl radical. Carbonate radical has been detected in natural waters at low concentrations of 10^{-13} to 10^{-15} M and it is a strong oxidizing agent.[98, 112] In the current system, formation of carbonate radical is negligible due to lack of a strong source of hydroxyl radicals. The principal effects observed from alkalinity addition seems to increase yield of chlorite and lower the removal rate constants.

Table 3-4. Effect of alkalinity on UV photolysis of chlorite, in absence of dissolved oxygen; pH = 7.2, UV irradiance = 9.45 mW/cm^2

Alkalinity as $CaCO_3$, (mg/L)	k_{obs} (min^{-1})	Yield, Cl^- (mol/mol)	Yield, ClO_3^- (mol/mol)	Yield, Other Cl (mol/mol)
0.00	0.312 $\pm$ 0.014	0.544	0.236	0.220
12.5	0.306 $\pm$ 0.020	0.598	0.250	0.152
25.0	0.291 $\pm$ 0.024	0.630	0.227	0.143
50.0	0.258 $\pm$ 0.026	0.633	0.219	0.148

Table 3-5. Effect of alkalinity on UV photolysis of chlorite in presence of dissolved oxygen; [DO] = 8.3 mg/L, pH = 7.2, UV irradiance = 9.45 mW/cm^2

Alkalinity as $CaCO_3$, (mg/L)	k_{obs} (min^{-1})	Yield, Cl^- (mol/mol)	Yield, ClO_3^- (mol/mol)	Yield, Other Cl (mol/mol)
0.00	0.254 + 0.016	0.432	0.235	0.333
12.5	0.192 $\pm$ 0.028	0.479	0.240	0.281
25.0	0.165 $\pm$ 0.025	0.536	0.217	0.247
50.0	0.162 $\pm$ 0.013	0.545	0.187	0.268

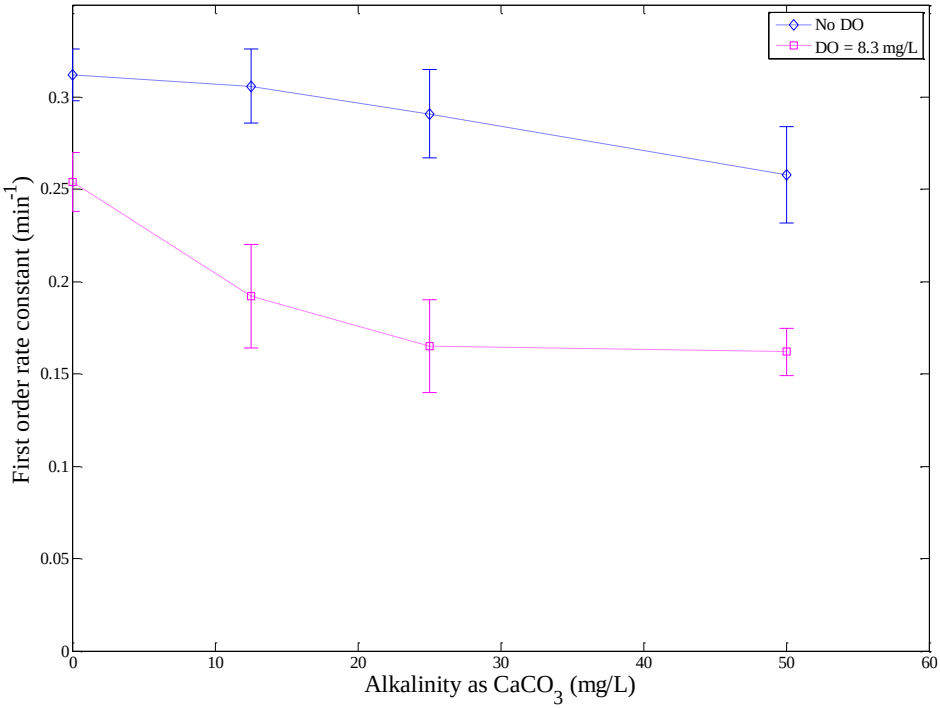

Figure 3-11. First order rate constants (min^{-1}) of chlorite photolysis as affected by alkalinity in presence and absence of dissolved oxygen; $[ClO_2^-]_0$=10 mg/L, pH=7.2, UV_{254}= 9.45 mW/cm^2

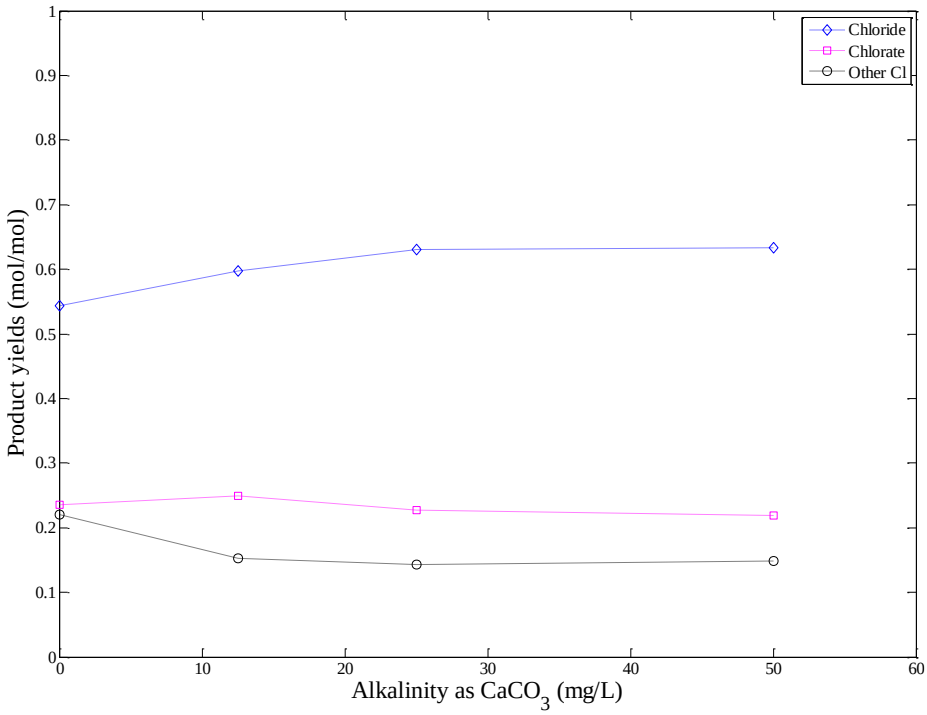

Figure 3-12. Product yields of chloride, chlorate, and other chlorine species (mol/mol) from chlorite photolysis as affected by alkalinity in absence of dissolved oxygen; $[ClO_2^-]_0$=10 mg/L, pH = 7.2, UV_{254}= 9.45 mW/cm^2

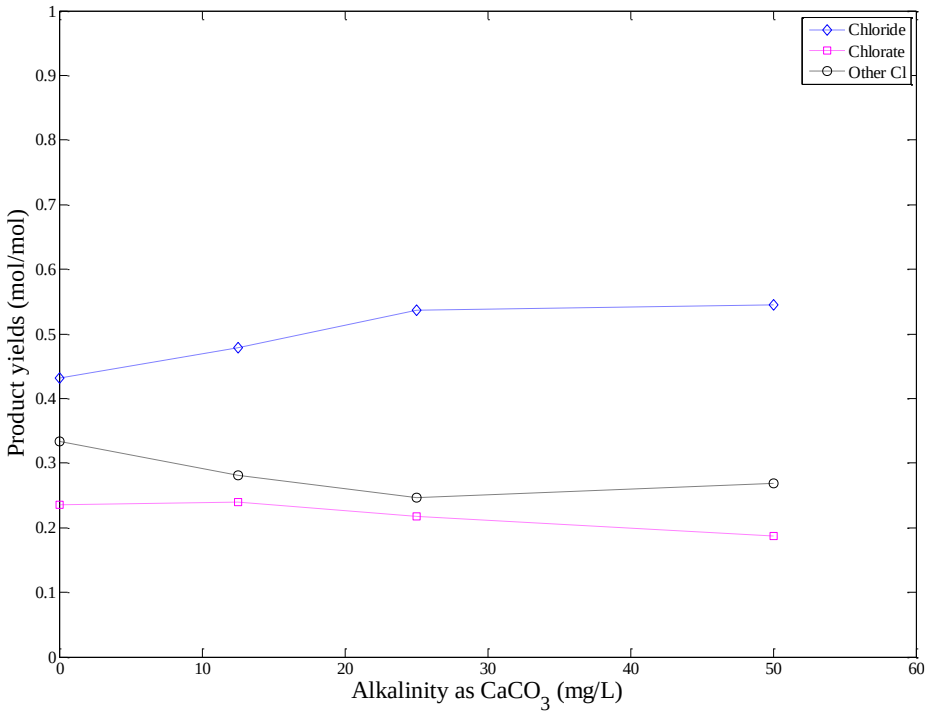

Figure 3-13. Product yields of chloride, chlorate, and other chlorine species (mol/mol) from chlorite photolysis as affected by alkalinity in presence of dissolved oxygen; $[ClO_2^-]_0$=10 mg/L, [DO] = 8.3 mg/L, pH = 7.2, UV_{254}= 9.45 mW/cm^2

Effect of nitrate

Data presented in Fig. 3-14, Tables 3-6 and 3-7, show that addition of nitrate did not influence chlorite removal rates during photolysis by UV at 254 nm. This behavior is consistent in the presence and absence of DO. This lack of effect could be due to the monochromatic (254 nm) emission spectrum of the UV source applied in the current study. Nitrate does not absorb UV at 254 significantly. NO_3^- has strong UV absorption

peak at 201 nm and weak absorption peak around 302 nm. The molar absorptivity of NO_3^- at 290 nm is reported to be around 5.6 $M^{-1}cm^{-1}$.[113] At the nitrate concentration tested, absorbance at 254 nm due to nitrate would be significantly lower than that due to chlorite. Thus, the rate of UV absorption by nitrate is negligible in comparison to that by chlorite. Addition of nitrate would not significantly alter the average UV irradiance (I_{avg}) in the reactor, thereby minimizing any effect of nitrate on direct photolysis rate of chlorite. However, UV photolysis of nitrate could lead to the following reactions (3-18 to 3-20) that could interfere with intermediates in chlorite photolysis.[72, 114]

$$NO_3^- + hv \rightarrow NO_2^- + O \qquad (3\text{-}18)$$

$$NO_3^- + hv \rightarrow ONO_2^- \qquad (3\text{-}19)$$

$$NO_3^- + hv + H^+ \rightarrow NO_2\cdot + OH\cdot \qquad (3\text{-}20)$$

UV wavelength and pH determine the dominant pathway in reactions (3-18 to 3-20). At conditions tested in current study (ƛ 254 nm and pH 7), reaction (3-19) that produces peroxynitrite is dominant.[72, 115] Peroxynitrite is an oxidizing agent and could cause chlorate formation. However, as described in Fig. 3-14 and 3-15, addition of nitrate at concentrations less than 20 mg/L, had no effect on product yields. Low nitrate concentrations tested in the study may lower rates of peroxynitrite formation. This slow kinetics would further reduce any scavenging of intermediates in chlorite photolysis. Thus, chloride and chlorate yields were constant at low nitrate concentrations, 0 to 10 mg/L. However, when 20 mg/L nitrate was added, 18% decrease in chloride and a

proportional increase in chlorate yield was observed in absence of DO, as documented in Table 3-5. Increased chlorate could be due to peroxynitrite oxidation of ClO_2^- leading to ClO_2 formation. Depending on DO and chlorite residuals, there can be a threshold level of nitrate required for effecting chlorite photolysis. As, chlorate formation is promoted at higher nitrate concentrations, pretreatment of water for nitrate removal may be necessary in photolytic treatment of ClO_2^-.

Table 3-6. Effect of nitrate on UV photolysis of chlorite in absence of dissolved oxygen; pH = 7.2, UV irradiance = 9.45 mW/cm^2

Nitrate (mg/L)	k_{obs} (min^{-1})	Yield, Cl^- (mol/mol)	Yield, ClO_3^- (mol/mol)	Yield, Other Cl (mol/mol)
0.00	0.312 $\pm$ 0.014	0.544	0.236	0.220
5.00	0.316 $\pm$ 0.014	0.540	0.269	0.191
10.0	0.357 $\pm$ 0.057	0.573	0.265	0.161
20.0	0.329 $\pm$ 0.015	0.471	0.296	0.233

Table 3-7. Effect of nitrate on UV photolysis of chlorite in presence of dissolved oxygen; [DO] = 8.3 mg/L, pH = 7.2, UV irradiance = 9.45 mW/cm^2

Nitrate (mg/L)	k_{obs} (min^{-1})	Yield, Cl^- (mol/mol)	Yield, ClO_3^- (mol/mol)	Yield, Other Cl (mol/mol)
0.00	0.254 + 0.016	0.432	0.235	0.333
5.00	0.229 $\pm$ 0.010	0.445	0.335	0.220
10.0	0.237 $\pm$ 0.012	0.461	0.280	0.259
20.0	0.225 $\pm$ 0.009	0.441	0.289	0.270

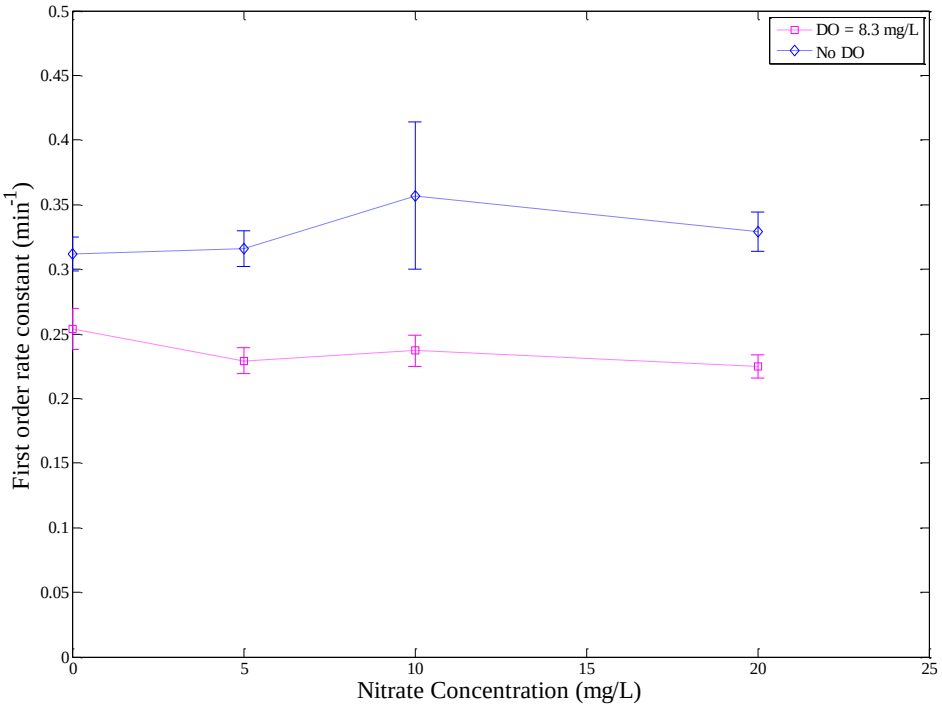

Figure 3-14. First-order rate constants (min^{-1}) of chlorite photolysis as affected by nitrate in presence and absence of dissolved oxygen; $[ClO_2^-]_0$=10 mg/L, pH=7.2, UV_{254}= 9.45 mW/cm^2

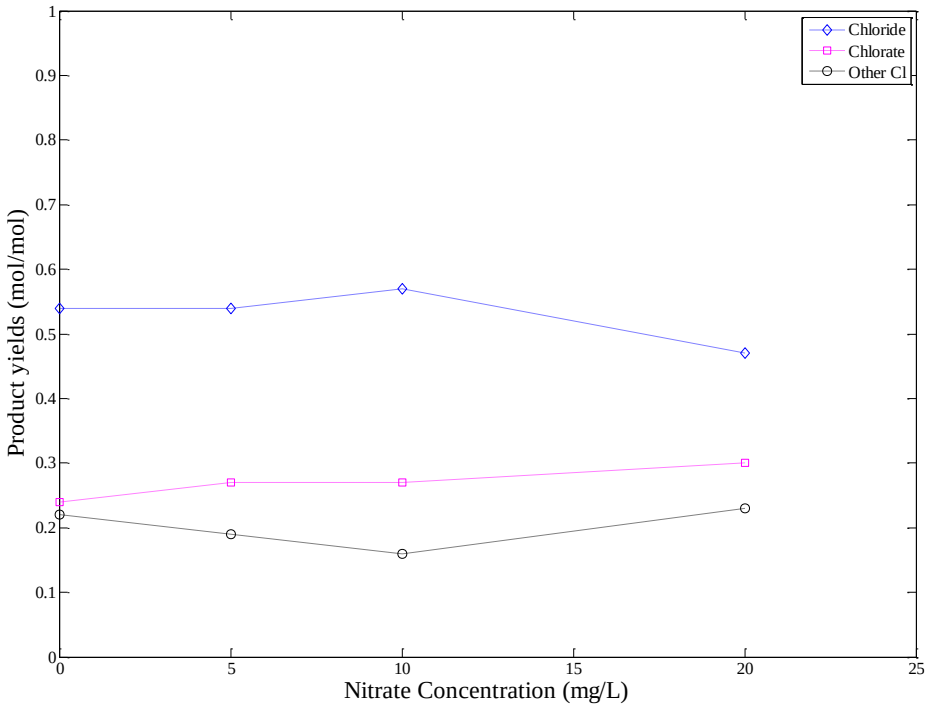

Figure 3-15. Product yields of chloride, chlorate, and other chlorine species (mol/mol) from chlorite photolysis as affected by nitrate in absence of dissolved oxygen; $[ClO_2^-]_0$=10 mg/L, pH=7.2, UV_{254}= 9.45 mW/cm^2

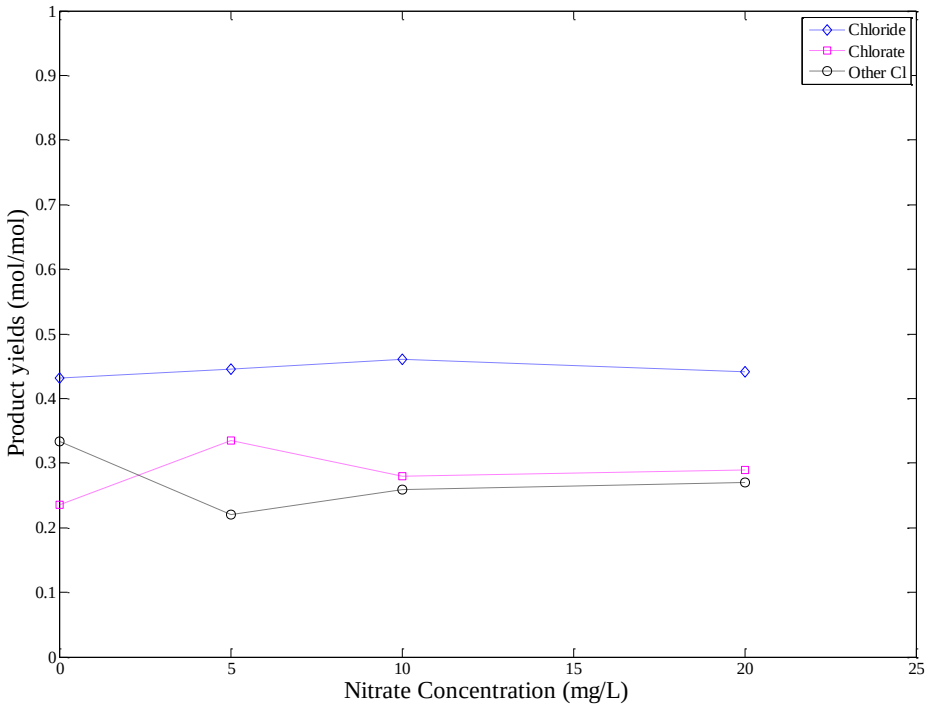

Figure 3-16. Product yields of chloride, chlorate, and other chlorine species (mol/mol) from chlorite photolysis as affected by nitrate in presence of dissolved oxygen; $[ClO_2^-]_0$=10 mg/L, [DO] = 8.3 mg/L, pH=7.2, UV_{254}=9.45 mW/cm^2

Quantum yield and energy requirement

Table 3-8 and 3-9 show the quantum yields and energy requirements for chlorite photodecomposition at 254 nm. Quantum yields are comparable to previously reported values around 0.9 to 1 mol/Ein at neutral pH.[96, 97, 110] Addition of NOM lowered quantum yields by reducing the average UV irradiance in the reactor. Addition of DO and alkalinity also lowered the quantum yield by scavenging intermediate radicals in chlorite photolysis. Nitrate had negligible effect on quantum yield of chlorite photolysis. Evaluation of the UV process for practical application can be made by calculating energy requirement using the electrical efficiency per order (E_{EO}). E_{EO} values as a function of background water constituents are presented in Tables 3-8 and 3-9. E_{EO} requirements were higher in the presence of NOM and DO, suggesting that even though NOM decreases the yield of chlorate, higher energy consumption would be necessary to operate the process. Alkalinity and nitrate did not increase E_{EO}.

Table 3-8. Quantum yield of chlorite photodecomposition at 254 nm as affected by NOM, alkalinity and nitrate in absence of dissolved oxygen; $[ClO_2^-]_0$ = 10mg/L, pH = 7

NOM (mg/L as C)	Alkalinity (mg/L as CaCO3)	Nitrate (mg/L)	Quantum yield (mol/Ein)	E_{EO} (kWh/m^3)
-	-	-	0.852	0.158
2.5	-	-	0.722	0.184
5.0	-	-	0.688	0.192
10.0	-	-	0.714	0.184
-	12.5	-	0.926	0.140
-	25.0	-	0.836	0.159
-	50.0	-	0.757	0.174
		5.0	0.915	0.156
		10.0	0.836	0.138
		20.0	0.918	0.149

Table 3-9. Quantum yield of chlorite photodecomposition at 254 nm as affected by NOM, alkalinity and nitrate in presence of dissolved oxygen; $[ClO_2^-]_0$ = 10mg/L, pH = 7, DO = 8.3 mg/L.

NOM (mg/L as C)	Alkalinity (mg/L as $CaCO_3$)	Nitrate (mg/L)	Quantum yield (mol/Ein)	E_{EO} (kWh/m^3)
-	-	-	0.692	0.193
2.5	-	-	0.633	0.211
5.0	-	-	0.421	0.315
10.0	-	-	0.395	0.336
-	12.5	-	0.542	0.256
-	25.0	-	0.429	0.297
-	50.0	-	0.481	0.303
-	-	5.0	0.624	0.214
-	-	10.0	0.641	0.207
-	-	20.0	0.609	0.218

Conclusions

Background water constituents significantly impact UV photodecomposition of chlorite. In the absence of DO, NOM and alkalinity reduce rate of chlorite removal but promote chloride yields by scavenging oxidizing intermediates. In the absence of DO, high concentrations of NOM could eliminate the problem of chlorate formation during chlorite photolysis. NOM in combination with DO could increase the formation of unwanted byproducts during UV photolysis. Sulfite under UV irradiation produces hydrated electrons that improve reduction rate of chlorite. Even at high DO levels, UV-Sulfite process could ensure high chloride yields and minimal chlorate formation. Nitrate levels in the range tested do not have any impact on chlorite reduction rates and product yields. In contrast to AOT, background NOM and alkalinity can improve performance of a UV-based reduction process.

CHAPTER IV

APPLICATION OF UV/SULFITE ADVANCED REDUCTION PROCESS TO BROMATE REMOVAL*

Introduction

Bromate is a disinfection byproduct considered a possible human carcinogen by the International Agency for Research on Cancer (IARC).[116] Bromate is regulated by US EPA under the disinfectants/disinfection byproducts rule of the Safe Drinking Water Act (SDWA). EPA has set the maximum contaminant level (MCL) for bromate in drinking water at 10 μg/L.[117] Occurrence of bromate in drinking water is primarily due to the ozonation of source water containing bromide.[118] Depending on pH, organic content, ozone concentration and other source water characteristics, bromide can either undergo direct sequential oxidation with ozone to form hypobromite, bromite and bromate or it can react with hydroxyl radical to from bromine radical, bromine oxide radical, bromite and bromate.[119] Typical concentrations of bromide in natural waters of the United States are around 100 μg/L.[120] Seawater contains very high concentrations of bromide (around 67 mg/L), which results in elevated levels of bromide in the groundwater of areas with saltwater intrusion[121] and in desalinated seawater. Increasing global water demand and dwindling freshwater reserves have driven many communities to be dependent on desalination of seawater for daily water needs. The international desalination association

---

* Reprinted from Journal of Water Process Engineering, 5, Venkata Sai Vamsi Botlaguduru, Bill Batchelor, Ahmed Abdel-Wahab, Application of UV–sulfite advanced reduction process to bromate removal, 76-82, Copyright (2015), with permission from Elsevier

(IDA) estimates around 300 million people worldwide depend on desalinated water for various purposes.[122] The use of desalinated seawater as the source for drinking water further intensifies the issue of bromate formation in water treatment processes.

Bromate problems in drinking water can be addressed in two ways, either by minimizing bromate formation during ozonation or by using an additional treatment process to remove bromate. Ozonation process control approaches include maintaining acidic pH, addition of ammonia and hydroxyl radical scavengers. These approaches resulted in partially minimizing bromate formation, but are limited by factors such as reduction in disinfection efficiency, costs involved with pH control and the necessity for removal of radical scavengers.[123] An alternate approach to tackle the bromate issue is to treat the disinfected water with an additional treatment process. Several conventional and innovative treatment technologies have been tested for bromate removal. Coagulation with alum and ferric chloride was ineffective, with highest removal only around 20%.[118] Adsorption of bromate onto granular activated carbon is specific to the type of carbon used and is reported to be dependent on pH, dissolved organic carbon and presence of competing anions such as sulfate.[124] Complete reduction of bromate to bromide is achieved by addition of chemical reducing agents such as ferrous iron and sulfite.[125] However, the time required to reduce 0.1 mg/L of bromate with sulfite was estimated to be around 4 days, which is too long to be efficiently used in a treatment process.[126] Under the same conditions, ferrous iron could completely reduce bromate within time periods as low as 18.7 min. The efficiency of ferrous iron reduction is subject to pH and dissolved oxygen level. After ozonation, a water typically contains

high concentrations of DO, requiring higher ferrous iron doses.[123] Ferrous iron also forms turbidity at high doses, if it is not completely oxidized to ferric iron. Photolysis of bromate with UV irradiation is an alternative treatment method to chemical reduction that is reported to be feasible at most pH levels.[118, 123, 127] UV wavelength and dose are the two principal factors that affect performance of this photolytic conversion of bromate to bromide. Bromate removal of 50% with a low pressure UV lamp (UV-L) required high UV doses of around 630 mJ/cm^2. If typical UV doses used for disinfection (40 mJ/cm^2) are applied, it is estimated that negligible removal of bromate would occur.[128] Common water constituents such as NOM, carbonate, nitrate and suspended particles are also reported to interfere with bromate photodecomposition by absorbing UV light. UV irradiation of bromate is also limited by the fact that bromate has very low UV molar absorptivity (around 11.5 L/mol-cm) at the range of wavelengths commonly used in water disinfection.[123, 129]

Advanced Reduction Processes (ARPs) are effective for treatment of oxidized contaminants in water/wastewater.[47] The principal operating mechanism of ARPs is to generate highly reactive free radicals that completely reduce oxidized target compounds to innocuous forms. The formation of free radicals is accomplished by activating reducing agents in solution. UV light is highly effective at generating hydrated electrons (e_{aq}^-) by activating sulfite solutions (4-1) although the reaction is reversible (4-1) and sulfite radicals consume themselves (4-2).[9] The hydrated electron is a strong reductant with a standard reduction potential of -2.9 V. In the current study the combination of UV-Sulfite is tested as an ARP for bromate reduction.

$SO_3^{2-} + hv \rightarrow {}^{\bullet}SO_3^{-} + e_{aq}^{-}$ (4-1)

${}^{\bullet}SO_3^{-} + e_{aq}^{-} \rightarrow SO_3^{2-}$ (4-2)

${}^{\bullet}SO_3^{-} + {}^{\bullet}SO_3^{-} + H_2O \rightarrow SO_4^{2-} + SO_3^{2-} + 2H^{+}$ (4-3)

The objectives of the current study are:

i. Investigate the effect of process variables (pH, sulfite dose, UV irradiance, UV wavelength) on bromate removal kinetics and process efficiency

ii. Estimate the energy requirements of the UV/sulfite ARP for bromate removal

iii. Study the effect of natural organic matter on the UV/Sulfite ARP for bromate removal

Methodology

Chemical reagents

Potassium bromate (1000 mg/L) and potassium bromide (1000 mg/L) of Ion Chromatography (IC) standard grade were purchased from Inorganic Ventures (Christiansburg, VA, USA). Sodium sulfite (anhydrous, 98.6%) was obtained from Avantor Performance Materials (Center Valley, PA, USA). Potassium phosphate (anhydrous, 97%), potassium hydrogen phosphate (anhydrous, 98%), potassium di-hydrogen phosphate (99%) and phosphoric acid (85%) were purchased from Alfa Aesar (Ward Hill, MA, USA).

Experimental procedure

All chemical solutions were prepared and experiments were conducted inside an anaerobic chamber (Coy Laboratory Products Inc.). The chamber atmosphere was maintained at 95% nitrogen (N_2) and 5% hydrogen (H_2). Trace levels of oxygen in the chamber were removed by a palladium catalyst connected to a recirculating fan. The catalyst reacted with H_2 in the chamber atmosphere and converted trace oxygen to water vapor. Oxygen levels were monitored with an Oxygen and Hydrogen Analyzer (Coy Laboratory Products Inc.) and a resazurin indicator. Deionized water (ultra-pure 18 MΩ·cm) was deoxygenated by purging with 99.99% N_2 for 2 h. This deoxygenated deionized water was allowed to equilibrate with the atmosphere in the anaerobic chamber for 12 h. All chemicals sensitive to oxidation were stored in the chamber throughout the time period of the experiments.

Reactor system

Two monochromatic sources of UV radiation were used for activating sulfite. A low pressure UV lamp (TUV PL-L36W/4P) emitting light with a wavelength of 253.7 nm was obtained from Phillips. UV light at lower wavelength of 222 nm was obtained from a KrCl excimer lamp purchased from the Institute of High-Current Electronics, Russian Academy of Sciences, Tomsk, Russia. The lamps were fixed in separate enclosures and positioned directly above the reactor, which was a petri dish that contained the experimental solution. The reactor was placed on a magnetic stirrer to ensure a completely mixed condition. The solution volume in the petri dish was 100 mL

with a depth of 1.3 cm. UV irradiance at the top surface of the petri dish could be varied by changing the distance between the lamp and the dish. UV irradiance measurements were made with a UVC 512 light meter (Professional Equipment, Janesville, WI, USA). The spectrum range for the light meter was between 220 and 280 nm. Agilent 8453 UV-visible spectroscopy system was used for the absorbance measurements.

Analytical method

Bromate and bromide were analyzed by ion chromatography on a Dionex DX-500 system. A 4-mm IonPac AS19 column was used with a 20-mM sodium hydroxide solution as the eluent. An eluent flow rate of 1 mL/min was maintained throughout the 30-min analysis time. 5-mL sample vials were used in the AS-40 auto sampler with a sample injection loop of 1000 µL.

Data analysis

In order to explain the effect of process variables on bromate removal, quantitative parameters that describe rate and efficiency of the reaction needed to be developed. First-order exponential decay model was fit to observed experimental data by conducting non-linear, least squares regression using the Levenberg–Marquardt algorithm in MATLAB to obtain estimates for pseudo-first-order rate constant (k_{obs}). To evaluate the effect of process variables on k_{obs}, a generic model for the working of UV/sulfite ARP was applied.

Generic ARP model

Degradation of contaminants to intermediate products and complete reduction to innocuous end products by UV/Sulfite ARP is complex and involves multiple photolytic and chemical steps. The overall kinetics (rate of removal) of a specific target can be described by identifying the major reactions occurring in an ARP and developing rate equations for each reaction. This generic ARP model is useful in describing the effect of process variables on rate constants (k_{obs}) obtained from experimental data. The major reactions assumed to occur in an ARP and their respective rate equations are specified in Table 4-1.

Table 4-1. Basic reaction/steps involved in a UV/Sulfite ARP

Steps	Reaction	Reactions	Rate equations
A.	Photolysis of target	Target + hν → Products	$r_A = \phi_T I_{avg} \epsilon_T C_T$
B.	Photolysis of sulfite	Sulfite + hν → R	$r_B = \phi_S I_{avg} \epsilon_S C_S$
C.	Target radical reaction	Target + R → Products	$r_C = k_{TR} C_T C_R$
D.	Scavenging of radicals	Scavengers + R → Products	$r_D = k_{ScR} C_{SC} C_R$

r_1, r_2, r_3 and r_4 are rates of individual reactions in the ARP model,

ϕ_T and ϕ_S are quantum yields for photolysis of target and sulfite,

$\varepsilon_{,T}$ and ε_S are molar extinction coefficients for target and sulfite ($\log_e$ base),

$C_{,T}$, C_S, C_R and C_{SC} are concentrations of target, sulfite, radicals and scavengers

K_{TR} and K_{SCR} are pseudo-first-order rate constants for target-radical and scavenger-radical reactions, I_{avg} is the average UV irradiance in the reactor, which can be calculated as in equation 4-1

$$I_{avg} = \frac{I_0\left(1-e^{(-\alpha L)}\right)}{\alpha L} \qquad 4\text{-}1$$

$$\alpha = \sum_{1}^{n} \varepsilon_i C_i \qquad 4\text{-}2$$

$\varepsilon_{,i}$ is the $\log_e$ based molar extinction coefficient

C_i is concentration of UV absorbing species i,

I_0 is the incident UV photon flux at the top of the reactor, converted from measured UV irradiance at that point,

L is the depth of the reactor.

Step A describes direct photolysis of target compound by UV absorption.

Step B describes photolysis of sulfite to produce reducing radicals i.e. hydrated electrons, according to reaction (1).

Step C accounts for reduction of target by reaction with reducing radicals.

Step D accounts for all of the scavengers such as carbonate, nitrate or dissolved organic matter that may consume reducing radicals in solution.

Assuming a quasi-stationary state for radicals, and conducting a material balance for radicals in the reactor,

$r_B - (r_C + r_D) = 0$

$\phi_S I_{avg} \epsilon_S C_S = k_{TR} C_T C_R + k_{ScR} C_{SC} C_R$

Thus, concentration of radicals is

$$C_R = \left\{ \frac{\phi_S I_{avg} \varepsilon_S C_S}{k_{TR} C_T + k_{SCR} C_{SC}} \right\} \qquad 4\text{-}3$$

As target compound is removed by steps 1 and 3, the overall removal rate of target can be related to the derivatives of concentration using a material balance as

$dC_T/dt = - (r_A + r_C)$

$dC_T/dt = - (\phi_T I_{avg} \epsilon_T C_T + k_{TR} C_T C_R)$

Substituting the expression for C_R from equation 4-3, a generic equation for change in target concentration by the UV/Sulfite ARP in a batch reactor can be expressed as,

$$\frac{dC_T}{dt} = -\left\{ \phi_T I_{avg} \varepsilon_T C_T + k_{TR} C_T \left[\frac{\phi_S I_{avg} \varepsilon_S C_S}{k_{TR} C_T + k_{SCR} C_{SC}} \right] \right\} \qquad 4\text{-}4$$

If target removal is assumed to follow first-order kinetics as,

$$\frac{dC_T}{dt} = -k_{obs} C_T$$

The observed first-order rate constant (k) can be expressed as

$$k_{obs} = \left\{ \phi_T I_{avg} \varepsilon_T + \left[\frac{k_{TR} \phi_S I_{avg} \varepsilon_S C_S}{k_{TR} C_T + k_{SCR} C_{SC}} \right] \right\} \quad 4\text{-}5$$

Equation 4-5 represents the dependence of observed first-order rate constant for target removal on various process variables. The most important variables being the concentration of sulfite (C_S), average UV irradiance (I_{avg}) and concentration of scavengers (C_{SC}).

Quantum yield (ϕ_P and ϕ_0)

The quantum yield for a photochemical reaction is defined as the ratio of the rate of the reaction to the rate of photon absorption, as in equation 4-6 for a batch reactor. In a case where a single target compound absorbs UV and is removed by photolysis, the quantum yield can be determined from equation 4-8.

$$\phi_T = \frac{r_{rxn}}{r_{photon}} \quad 4\text{-}6$$

$$\phi_T = \frac{-\left(\frac{dc_T}{dt} \right)}{\left(I_{avg} \varepsilon_T C_T \right)} \quad 4\text{-}7$$

$$\frac{dC_T}{dt} = -\phi_T I_{avg} \varepsilon_T C_T \quad 4\text{-}8$$

Substituting equation 4-1 for I_{avg},

$$\frac{dC_T}{dt} = -\phi_T \frac{I_0}{L} (1 - e^{\varepsilon_T C_T L}) \quad 4\text{-}9$$

Quantum yields for direct bromate photolysis (ϕ_P) were estimated from solving the differential equation 4-8 to obtain an equation of C_T as a function of time. The solution

for C_T was used to determine the quantum yield by conducting a non-linear regression analysis with experimental observations of C_T. Appendix C contains description of the procedure.

In addition to direct photolysis, photons are absorbed by sulfite in the UV/Sulfite ARP to produce hydrated electrons, which further reduce the target. The efficiency of the UV/Sulfite ARP was characterized using the initial quantum yield for removal of bromate (ϕ_0), which was calculated with the following equation. This approach uses initial conditions, which are better defined.

$$\phi_{ARP,0} = \frac{k_{ARP} C_{T,0}}{\frac{I_0}{L}(1-e^{-\alpha L})\varepsilon_S \, C_S} \qquad 4\text{-}10$$

$C_{T,0}$ is the initial target concentration,

k_{ARP} is the rate constant for the ARP mechanism and is calculated as the difference between the observed (k_{obs}) rate constant and direct photolysis rate constant.

Energy requirement

The key factor determining the effectiveness of ARPs is the ability to generate hydrated electrons (e_{aq}^-). Despite the fact that many combinations of ARPs have been tested to be very successful at the lab scale, their development and full scale commercialization depends on the cost of hydrated electron generation. Since most ARPs involve UV lamps to activate reagents, they intensively use electric energy and this could be a major fraction of their operating costs. Thus, estimates for energy requirements are necessary to compare different ARPs and provide the necessary data for scaling them up. Although, a number of factors such as environmental regulations,

effluent quality goals and operational ease are considered in selecting a treatment technology, economics plays a decisive role. The following equations describe the procedure for estimating energy requirement for bromate removal using the UV/Sulfite ARP.

Electric efficiency per order (E_{EO})

E_{EO} is the electrical energy required to degrade a target contaminant by one order of magnitude in a unit volume of contaminated water. For a laboratory batch reactor, E_{EO} can be calculated as follows.

$$E_{EO} = \frac{P.t}{\log(\frac{C_0}{C_f})V} \qquad 4\text{-}11$$

P is input power of the UV lamp needed to produce light energy absorbed in the reactor,

t is the time of UV lamp operation,

V is the volume of the water treated,

C_0 and C_f are the initial and final concentrations of the contaminant,

If the target is assumed to follow first-order kinetics, $\log(C_0/C_f) = k.t/2.303$,

The power variable P, normalized by volume can be expressed as P_v and E_{EO} can be expressed as

$$E_{EO} = \frac{2.303P_V}{k} \qquad 4\text{-}12$$

k is the first-order rate constant

The power of light energy per volume that is actually absorbed in the reactor ($P_{V,absorbed}$) can be calculated as,

$P_{V,absorbed}$ = $P_{V,applied}$ * fraction of UV absorbed

$$P_{V,absorbed} = \frac{I_0^{'}}{L}(1-e^{-\sum \varepsilon_i C_i L}) \qquad 4\text{-}13$$

In the current UV setup most of the energy consumed to produce UV is not used for the producing radicals, because much of the light leaves the bottom of the reactor. This mode of operation was chosen to maintain more constant irradiance in the reactor, because measurement of kinetics is the primary objective, not energy efficiency. However, in a full-scale application, all of the UV energy would be absorbed in solution to facilitate energy efficiency and faster target removal. Thus, it is necessary to calculate the power per volume of light energy that is actually absorbed in the reactor. The power per volume consumed by the lamp to produce the light energy that was absorbed can be calculated using the energy efficiencies of the UV lamps, which are specified in Table 4-2.

$P_V = P_{V,\ absorbed} / (\eta)$

η is efficiency of the UV lamp

Table 4-2. Power ratings and UV output of UV Lamps

Lamp Type	Input Power (W)	UV output (W)	Energy of photon (kJ/Ein)	Efficiency (η)
UV-KrCl	45	1.02	539.3	0.023
UV-L	36	12.0	471.4	0.333

Results and discussion

Photolysis

Direct UV photolysis of bromate in absence of sulfite resulted in removal patterns as presented in Fig. 4-1. A first-order decay model was fit to the degradation data at both wavelengths and is shown as the line in Fig. 4-1. UV irradiance at the surface of the reactor was measured at 9.00 mW/cm^2 for the UV-L lamp and 7.5 mW/cm^2 for the excimer lamp. The rate constants and model goodness of fit parameters are presented in Table 4-3. As presented in Fig. 4-2, k_{obs} for bromate photolysis with excimer lamp was significantly higher than the k_{obs} value for UV-L photolysis. This difference in kinetics could be attributed to the UV absorbance of bromate being different at the two wavelengths. According to equation 4-7, the rate of bromate photolysis is proportional to the average UV irradiance in the reactor and the molar extinction coefficient of bromate (ε_B), which is dependent on UV wavelength. The absorbance spectrum of bromate at five different concentrations in the range 6.25 to 100 mg/L was measured and the results are shown in Fig. 4-3. It is evident from the spectrum in Fig. 4-3 that bromate absorbs a greater proportion of UV at 222 nm than at 254 nm.

From the absorbance values for the five bromate concentrations, the molar extinction coefficients (log_{10} base) were calculated according to Beer-Lamberts law to be 524 M^{-1} cm^{-1} at 222 nm and 13.8 M^{-1} cm^{-1} for 254 nm. Only data for high concentrations of bromate (300 - 5000 mg/L) were used for 254 nm. The difference in ε_B is directly translated into higher kinetics under the excimer lamp. Significantly faster kinetics with excimer lamp indicate potential for using low wavelength UV lamps for direct photolytic removal of UV absorbing recalcitrant contaminants. However, the degradation of bromate under the UV-L lamp is comparable in terms of efficiency. The quantum yields presented in Table 4-4, show no difference between the two UV lamps in terms of photochemical efficiency. However, the energy requirement estimated for the UV-L lamp is an order of magnitude lower than the E_{EO} for the excimer lamp. The difference in E_{EO} for bromate reduction is a result of energy efficiencies of the two lamps in producing UV light. The UV-L lamp is more efficient (33%) in converting electrical energy to UV output, whereas the excimer lamp is extremely inefficient (2.26%). This inefficiency in producing 222 nm UV radiation offsets the advantage the excimer lamp offers in greater kinetics of bromate removal. The kinetic and energy data for bromate photolysis suggests that the excimer lamp offers faster kinetics with higher energy requirements, whereas the UV-L lamp offers greater energy efficiency with slower kinetics. Design of a UV photolytic treatment process for bromate removal would thus require a tradeoff between process kinetics and efficiency. Another design parameter that influences choice of lamps is the interference caused by UV absorbing compounds in water/wastewater. Water/wastewater constituents such as NOM, nitrate,

nitrite and iron absorb UV and attenuate the UV irradiance available for photolytic treatment. UV absorbance of these compounds is different at 254 and 222 nm. As NOM, nitrate, nitrite and iron have greater absorbance at low wavelength UV, attenuation of UV at high concentration of interfering compounds would be a greater problem with the excimer lamp.[130-132]

Direct photolysis of bromate under UV irradiation would lead to the formation of hypobromite and oxygen. Hypobromite further photolyzes to bromide. This process has been summarized in the following reactions.[123]

$BrO_3^- + UV \rightarrow OBr^- + O_2$ (4-4)

$OBr^- + UV \rightarrow Br^- + 0.5O_2$ (4-5)

The formation of hypobromite or hypobromous acid in the open reactor used in the current study could account for the loss of 5-10% of bromine in the system that caused less than complete conversion of bromate to bromide.

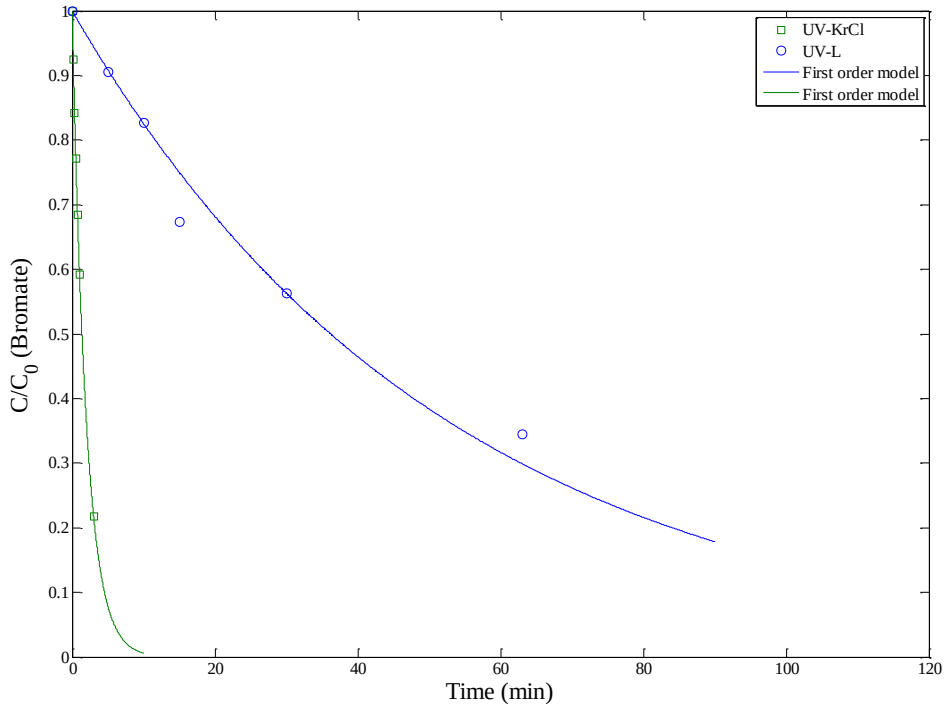

Figure 4-1. Photolysis of bromate with UV-L and UV-KrCl lamps, $[BrO_3^-]_0$=250 µg/L, pH=7, $I'_{0,uv-l}$=9 mW/cm^2, $I'_{0,uv-krcl}$=7.5 mW/cm^2

Table 4-3. Rate constants for bromate photolysis with UV-L and UV-KrCl lamps, $[BrO_3^-]_0$=250 µg/L, pH=7, $I'_{0,uv-l}$=9 mW/cm^2, $I'_{0,uv-krcl}$=7.5 mW/cm^2

UV Lamp	Wavelength (nm)	k_{obs} (min^{-1})	95% CI	R^2	SSE	RMSE
UV-KrCl	222	0.510	0.074	0.988	73	4.28
UV-L	254	0.018	0.005	0.977	457	10.69

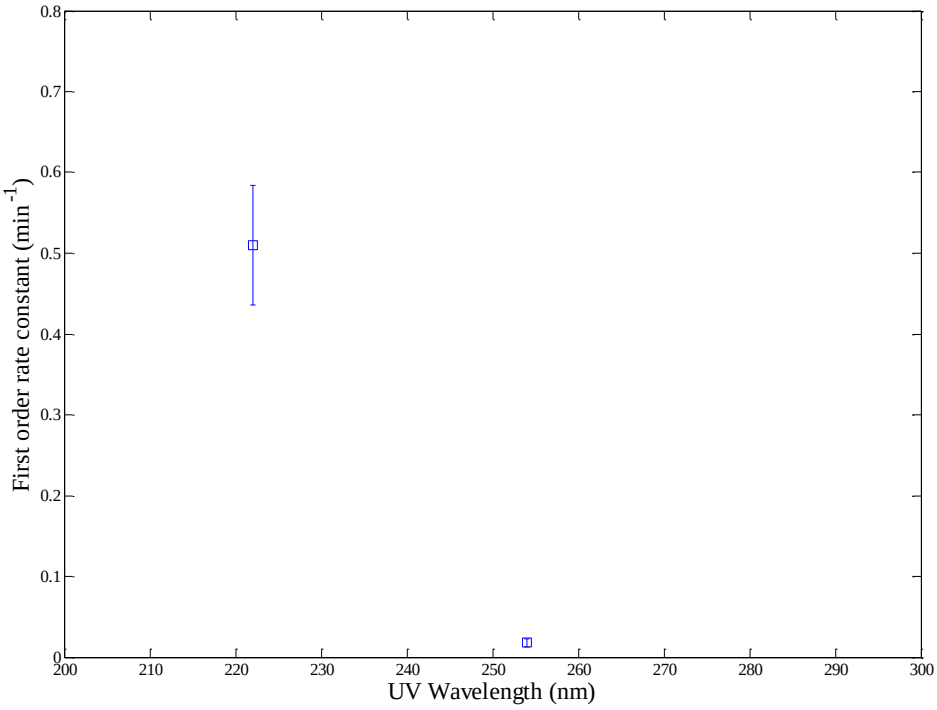

Figure 4-2. Effect of UV wavelength on first-order rate constant for bromate photolysis, $[BrO_3^-]_0$=250 µg/L, pH=7, $I'_{0,uv-l}$=9 mW/cm^2, $I'_{0,uv-krcl}$ =7.5 mW/cm^2

Table 4-4. Quantum yields and energy estimates for bromate photolysis with UV-L and UV-KrCl lamps, $[BrO_3^-]_0$=250 µg/L, pH=7, $I'_{0,uv-l}$=9 mW/cm^2, $I'_{0,uv-krcl}$=7.5 mW/cm^2

UV Lamp	Quantum Yield (mol/Ein)	95% CI	Fraction of UV absorbed	E_{EO} (kWh/m^3)
UV-KrCl	0.512	0.002	3.094E-03	0.059
UV-L	0.526	0.002	8.319E-05	0.004

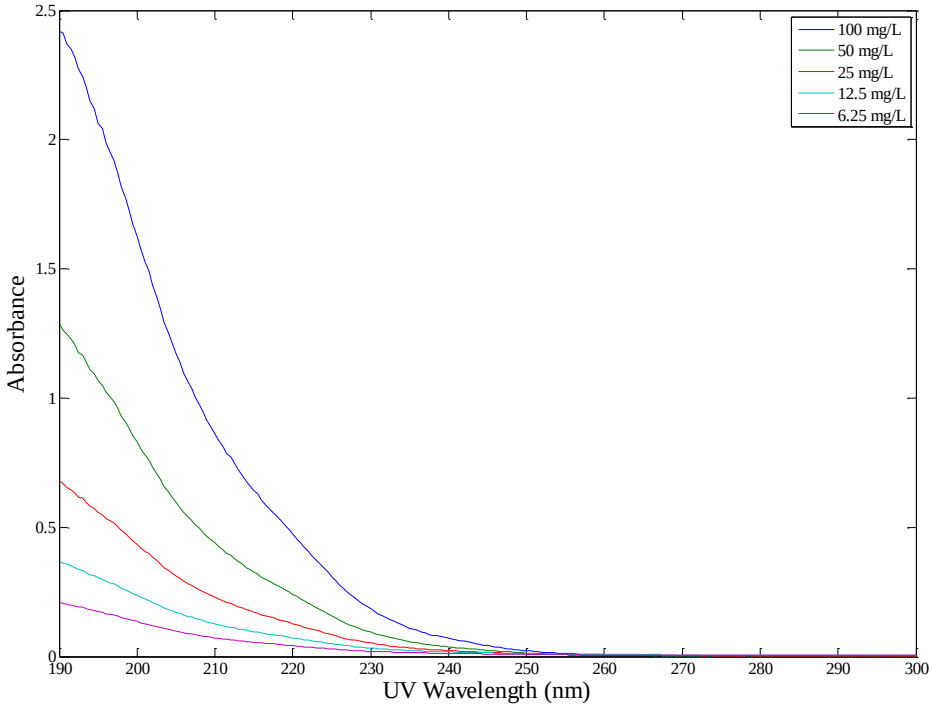

Figure 4-3. UV Absorbance spectra for varying concentrations of bromate

Effect of pH

Removal of bromate under four different pH conditions with the UV-L lamp is shown in Fig. 4-4. The values of rate constants in Table 4-5 indicate that alkaline pH results in significant improvement in kinetics over neutral and acidic pH. There is little difference between the rate constants for pH 7 and 9, with pH 5 having a slightly lower observed rate constant. pH affects the relative concentrations of sulfurous acid (H_2SO_3), bisulfite (HSO_3^-) and sulfite (SO_3^{2-}) in solution. The two acid dissociation constants of sulfurous acid are 1.9 and 7.2. Under moderately acidic conditions, HSO_3^- is dominant and at higher pH, SO_3^{2-} is the major species. Therefore, UV absorbance of sulfite solutions is also pH dependent, as shown in Table 4-6. Bisulfite and sulfite absorb UV at different wavelengths, and it is reported that bisulfite does not absorb considerable amounts of UV in the range of 225-300 nm.[17, 133] The data in Table 4-6 also is in accordance with the reported studies. This absorbance behavior also suggests that acidic pH conditions are not favorable to e_{aq}^- production. According to equation 4-5, the observed first order rate constant can be expressed as the sum of a direct photolysis rate constant and an aqueous electron reduction rate constant. Thus, the rate constant for bromate reduction with aqueous electron can be isolated as the difference between observed and direct photolysis rate constants and expressed as k_{ARP} in Table 4-5. the low k_{ARP} values relative to k_{obs} values shows that the kinetics of ARP reactions are very slow at acidic pH,, resulting in direct photolysis being the dominant removal mechanism for bromate under those conditions.

It is reported that the aqueous electron reacts instantaneously with bromate to abstract oxygen and sequentially reduce bromate to bromite, hypobromite and finally bromide. The following equations occurring at neutral and alkaline pH can be used to explain bromate reduction.[123]

$e_{aq}^- + BrO_3^- + 2\ H^+ \rightarrow BrO_2^{-\bullet} + H_2O$ (4-6) $k_8 = 3 \times 10^9\ M^{-1}\ s^{-1}$

$e_{aq}^- + BrO_2^{-\bullet} \rightarrow BrO_2^-$ (4-7)

$e_{aq}^- + BrO_2^- \rightarrow BrO^\bullet + 0.5O_2^-$ (4-8) $k_9 = 10^{10}\ M^{-1}\ s^{-1}$

$e_{aq}^- + BrO^\bullet \rightarrow BrO^-$ (4-9) $k_{10} = 10^{10}\ M^{-1}\ s^{-1}$

$e_{aq}^- + BrO^- \rightarrow Br^- + O^{-\bullet}$ (4-10) $k_{11} = 1.5 \times 10^{10}\ M^{-1}\ s^{-1}$

The rates of the above reported reactions suggest that a process that could generate aqueous electrons could be very well suited for application in in drinking water treatment. Thus, generation of aqueous electrons and their rate of formation is the key to achieving bromate reduction.

In acidic pH environment, bromate also reacts with hydrogen atom to form bromate radical. Hydrogen atom is the conjugate acid of aqueous electron and exists in acidic conditions. It is a strong reducing species in acidic solutions with a reduction potential of -2.3 V.[5] These reactions could be occurring at low pH conditions.

$e_{aq}^- + H^+ \rightarrow H^\bullet$ (4-11)

$BrO_3^- + H^\bullet \rightarrow BrO3^{-\bullet} + H^+$ (4-12)

Bromate radical is highly reactive and under irradiation could reduce to bromite radical and ultimately to stable bromide in solution. The low rate constant reported as k_{ARP} in Table 4-5 for pH 5, can also be attributed to reactions (11) and (12). Initial quantum yields ($\phi_{ARP,0}$) for the ARP mechanism are calculated according to equation 4-9 which uses values of k_{ARP} presented in Table 4-7. As observed in Fig. 4-6, ARP quantum yields do not show any trend with pH. Electrical efficiency values are also presented in Table 4-7. The UV/sulfite ARP is most energy efficient at a high pH around 11. The data also indicate that the direct photolysis mechanism that dominates at pH 5, is more energy efficient than the combination of photolysis and ARP mechanisms at pH 7 and 9. However, direct photolysis may be limited in its application due to attenuation of UV by interferences such as NOM, iron and nitrate in water/wastewater. Under a direct photolytic removal process, UV absorbance due to NOM would be greater than UV absorbed by bromate, as the extinction coefficient of NOM is 25 times greater than that of bromate. In an ARP system this effect could be reduced by increasing the dose of sulfite which increases the rate of UV absorbance by sulfite to produce hydrated electrons. As sulfite concentration is a variable that can be controlled optimum dosage could reduce the UV filtering by NOM.

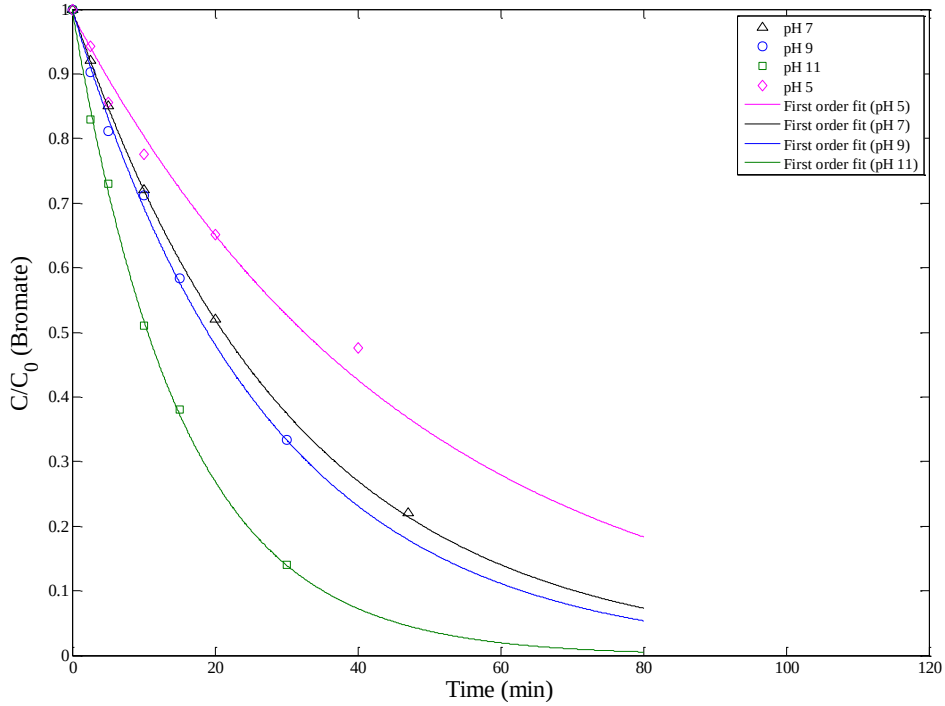

Figure 4-4. Bromate removal with UV-L/Sulfite ARP at different pH conditions, $[BrO_3^-]_0$ = 250 µg/L, S(IV) dose=70 µM, $I'_{0,uv-l}$=9 mW/cm^2

Table 4-5. Rate constants and quantum yields for bromate removal with UV-L/Sulfite ARP at different pH conditions, $[BrO_3^-]_0$=250 µg/L, S(IV) dose=70 µM, UV-I=9 mW/cm^2

pH	k_{obs} (min^{-1})	95% CI	R^2	SSE	RMSE	k_{ARP} (min^{-1})
5.0	0.019	0.004	0.985	139.90	5.91	0.001
7.1	0.033	0.000	1.000	0.41	0.32	0.015
9.0	0.036	0.003	0.997	55.96	3.74	0.017
10.9	0.065	0.003	0.999	17.45	2.09	0.047

Table 4-6. Molar absorptivity of sulfite solutions at different pH conditions

pH	Ionization fraction of $[SO_3^{2-}]$	Molar absorptivity at 222 nm, (log_{10} base) (M^{-1} cm^{-1})	Molar absorptivity at 254 nm, (log_{10} base) (M^{-1} cm^{-1})
7.2	0.454	955	16.7
9.0	0.981	1316	21.2
10.3	1.000	1324	22.3

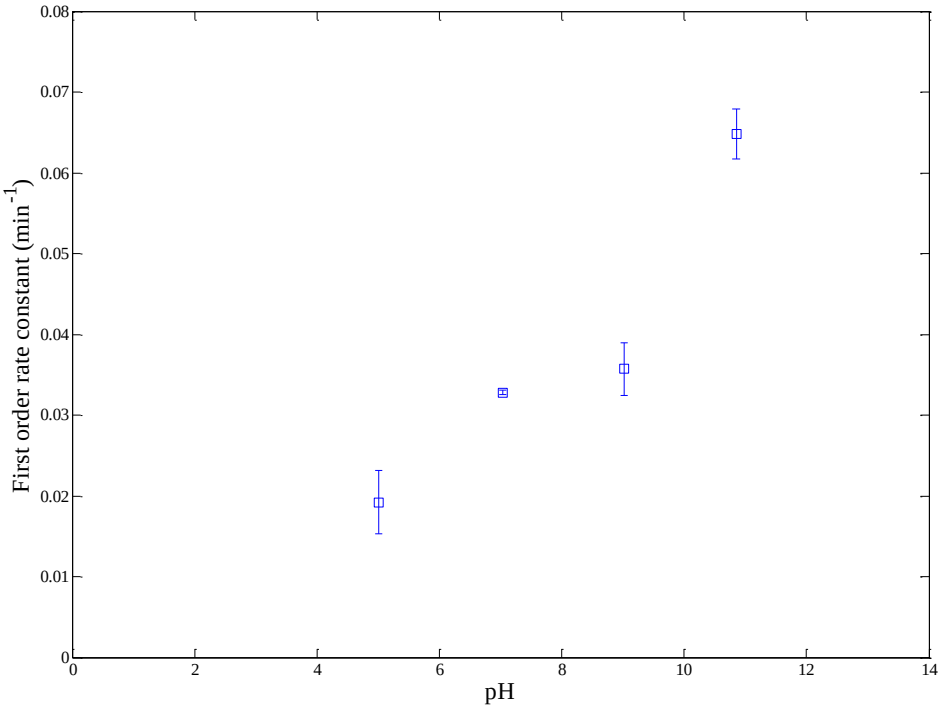

Figure 4-5. Effect of pH on first-order rate constant for bromate removal with UV-L/Sulfite ARP, $[BrO_3^-]_0$=250 µg/L, S(IV) dose=70 µM, $I'_{0,uv-l}$=9 mW/cm^2

Table 4-7. Quantum yields and energy requirements for bromate removal with UV-L/Sulfite ARP, $[BrO_3^-]_0$=250 µg/L, S(IV) dose=70 µM, UV-I=9 mW/cm^2

pH	fraction of UV absorbed	ARP Quantum Yield (mol/Ein)	E_{EO} (kWh/m^3)
5.0	1.67E-03	-	0.069
7.1	3.57E-03	0.015	0.087
9.0	4.53E-03	0.010	0.101
10.9	4.75E-03	0.022	0.058

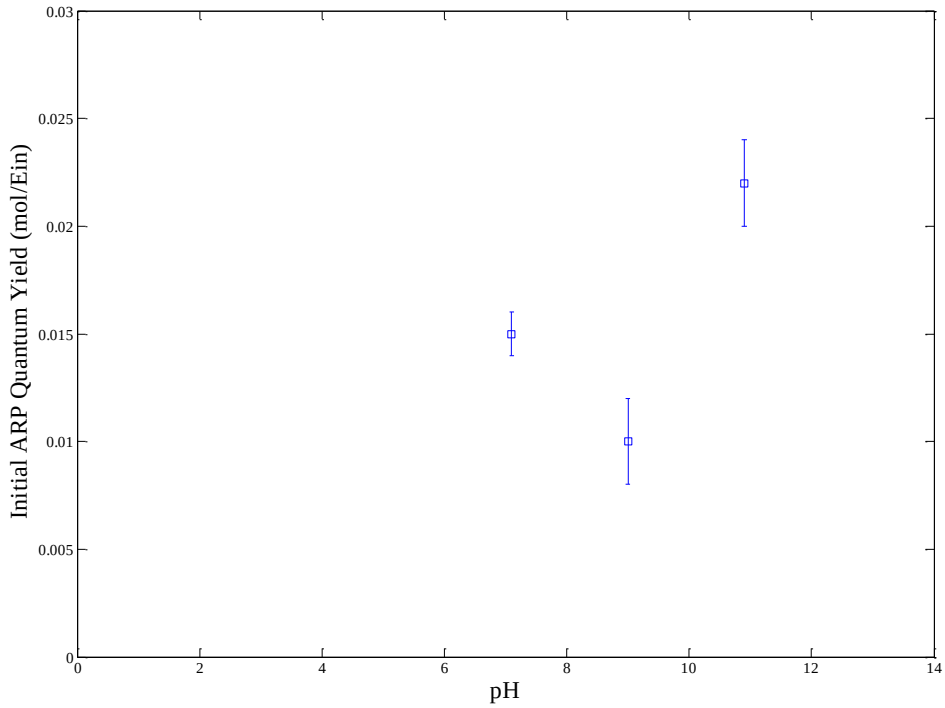

Figure 4-6. Effect of pH on quantum yield for bromate removal with the UV-L/Sulfite ARP, $[BrO_3^-]_0$=250 µg/L, S(IV) dose=70 µM, $I'_{0,uv-l}$=9 mW/cm^2

Effect of sulfite dose

Bromate removal with varying doses of sulfite at pH 7, and a UV-L irradiance of 9 mW/cm^2 can be observed in Fig. 4-7. Observed rate constants estimated from fitting first-order decay model to experimental data, and ARP rate constants calculated from the difference in observed and direct photolysis rate constants are presented in Table 4-8. Initial ARP quantum yields calculated according to equation 4-9 are presented in Table 4-9. According to the Beer-Lambert law, increasing sulfite concentration leads to a higher absorbance of the incident UV radiation, which results in increased rate of production of hydrated electrons in reaction (1). Equation 4-5v indicates the dependence of k_{obs} on the concentration of sulfite. Under conditions where, scavenger concentration is very low, equation 4-5 can be simplified as equation 4-14. This indicates a linear relationship between first-order rate constant and sulfite concentration. The rate constants presented in Fig. 4-8 support this model by showing a linear relationship between k_{obs} and S(IV) dose.

$$k = \left\{ \phi_T I_{avg} \varepsilon_T + \left(\frac{\phi_S I_{avg} \varepsilon_S}{C_T} \right) C_S \right\} \qquad 4\text{-}14$$

The intercept in Fig. 4-8 corresponds to '$\phi_T I_{avg} \varepsilon_T$' in equation 4-14, which is the term related to bromate photolysis. The other term in equation 4-14 is associated with bromate reduction by hydrated electrons. These are two reaction pathways contributing to bromate reduction. If direct photolysis is the dominant mechanism, higher sulfite doses could decrease the average UV irradiance in the reactor and thereby slow down the bromate reduction kinetics. The results shown in Fig. 4-8 indicate the contrary and a

significant linear trend can be observed. Higher sulfite concentrations increase the overall absorbance of UV in the solution and thereby increase k_{obs} as suggested by equation 4-14. The fraction of UV absorbed in the reactor and the energy requirements are also presented in Table 4-9. At the level of sulfite concentrations used in this study, the transmittance of the solution is greater than 99%. This means that only a minor fraction of UV irradiance applied is being utilized for bromate removal. In a real treatment process, the reactor would be designed to maximize the utilization of UV dose, resulting in substantially all of the light energy being absorbed. The results in Table 4-9 show that the energy required per order (E_{EO}) increases with sulfite dose, which indicates that direct photolysis is more energy efficient than reduction through ARP. Initial quantum yields ($\phi_{ARP,0}$) presented in Fig. 4-7, do not show any trend with sulfite dose, as increases in the rate of bromate removal are offset by increases in the rate of absorption of UV photons.

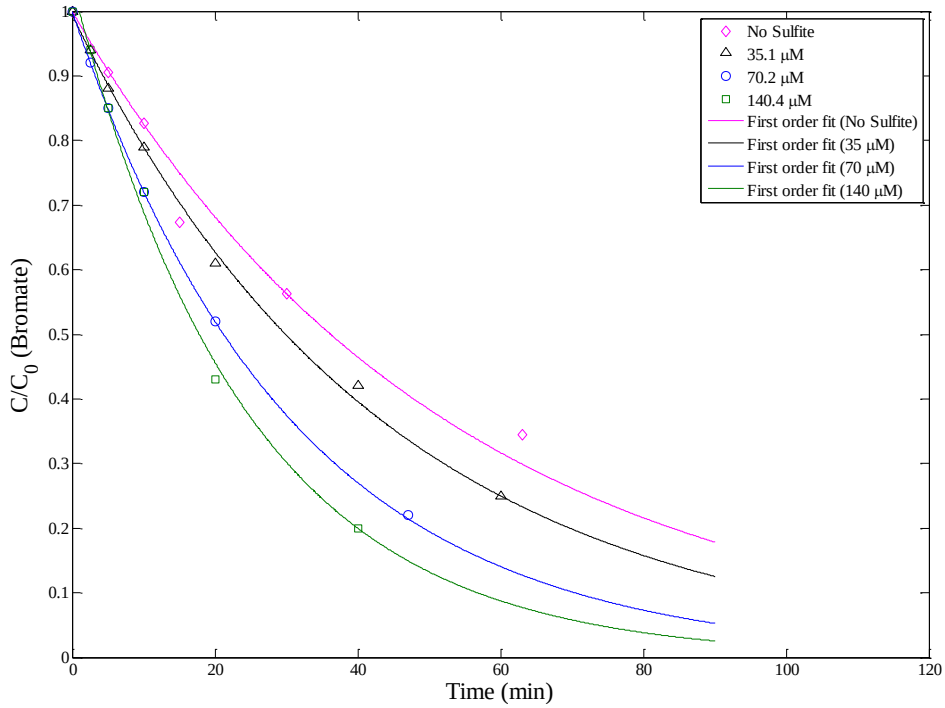

Figure 4-7. Bromate removal with UV-L/Sulfite ARP at different sulfite doses, $[BrO_3^-]_0$=250 µg/L, pH=7, $I'_{0,uv-l}$=9 mW/cm^2

Table 4-8. Rate constants and quantum yields for bromate removal with UV-L/Sulfite ARP at different sulfite doses, $[BrO_3^-]_0$=250 µg/L, pH=7, $I'_{0,uv-l}$=9 mW/cm^2

S(IV) Dose (µM)	K_{obs} (min^{-1})	95% CI	R^2	SSE	RMSE	k_{ARP} (min^{-1})
0	0.018	0.005	0.977	457.2	10.7	0.000
35	0.023	0.002	0.996	41.7	3.2	0.005
70	0.033	0.001	1.000	0.4	0.3	0.015
140	0.042	0.006	0.994	171.2	6.5	0.023

Table 4-9. Energy requirements for bromate removal with UV-L/Sulfite ARP, $[BrO_3^-]_0$=250 µg/L, pH=7

S(IV) Dose (µM)	fraction of UV absorbed	ARP Quantum Yield (mol/Ein)	E_{EO} (kWh/m^3)
0	8.32E-05	-	0.004
35	1.82E-03	0.011	0.064
70	3.57E-03	0.015	0.087
140	7.07E-03	0.014	0.136

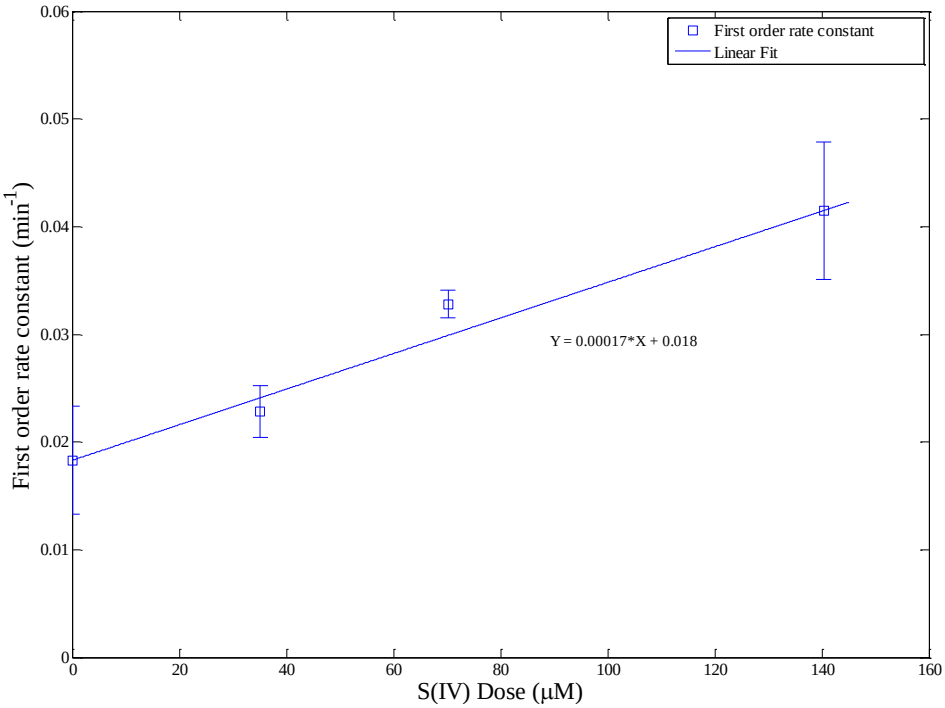

Figure 4-8. Effect of sulfite dose on first-order rate constant for bromate removal with UV-L/Sulfite ARP, $[BrO_3^-]_0$=250 µg/L, pH=7, $I'_{0,uv-l}$=9 mW/cm^2

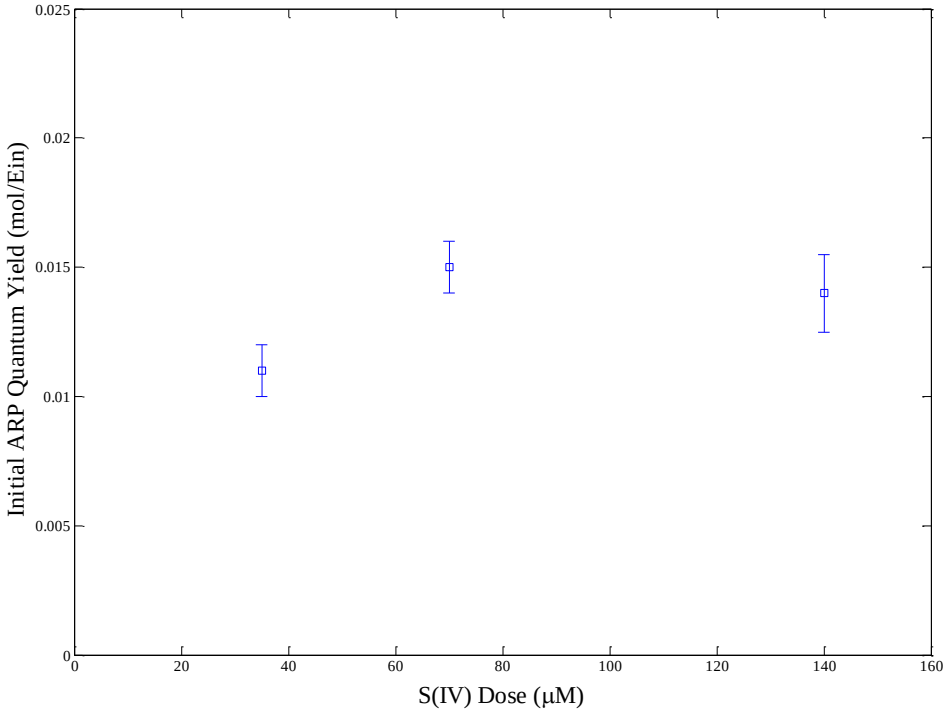

Figure 4-9. Effect of sulfite dose on quantum yield for bromate removal with UV-L/Sulfite ARP, $[BrO_3^-]_0$=250 μg/L, pH=7, $I'_{0,uv-l}$=9 mW/cm^2

Effect of UV irradiance

Bromate removal by the UV-L/sulfite ARP at varying UV irradiance values is presented in Fig. 4-10. Table 4-10 presents the observed first-order rate constants for the data in Fig. 4-10. The data indicate faster observed rates of bromate removal with increasing UV irradiance. This behavior is in accordance with equation 4-5. Higher I_0 leads to an increased rate of direct photolysis and an increased rate of production of e_{aq}^-. This combination results in faster kinetics of bromate removal. From Fig. 4-11, it can be inferred that a proportional relationship exists between I_0 and k_{obs} as predicted by equation 4-14. In the absence of UV irradiation, bromate reduction by sulfite is negligible, which is in agreement with previous studies conducted on bromate removal.[126] ARP rate constants were calculated as the difference between the observed rate constant and the direct photolysis rate constant. The ARP rate constants and the quantum yields for ARP mechanism are presented in Table 4-11. As shown in Fig. 4-12, ARP quantum yields do not have any significant trend with varying UV intensities. As the quantum yield is a ratio of rate of the reaction to rate of photon absorption, increasing UV irradiance should not have any effect. Energy requirements (E_{EO}) for bromate removal are presented in Table 4-10 and do not change significantly with UV irradiance. In calculating E_{EO}, an increased rate is offset by a proportional increase in power absorbed per volume ($Pv = I_0/L.(1-e^{-\varepsilon CL})$).

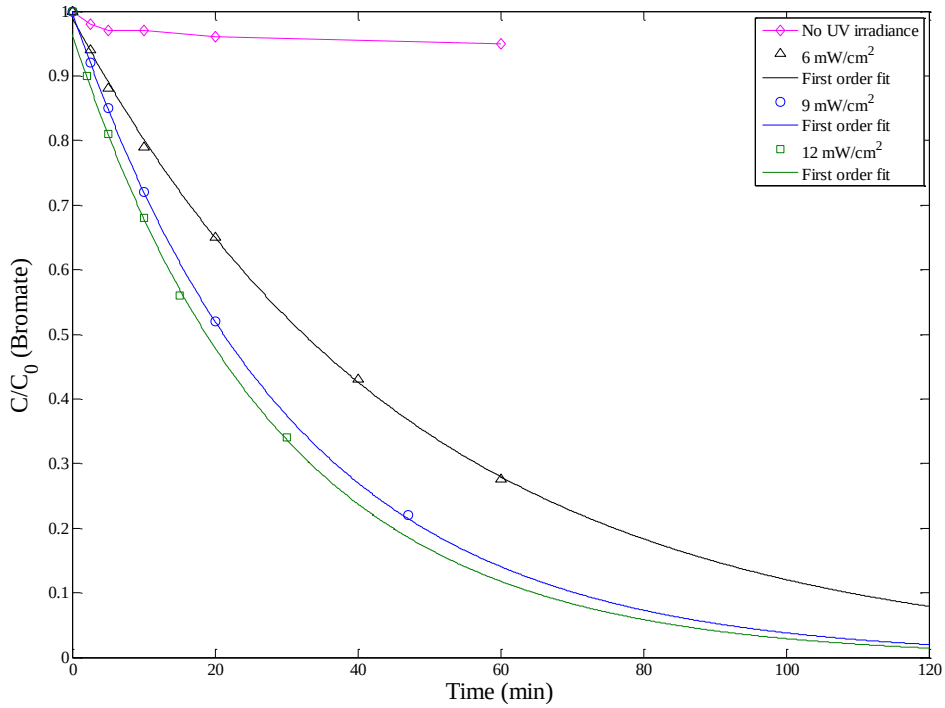

Figure 4-10. Bromate removal with the UV-L/Sulfite ARP at different UV irradiance values, [BrO_3^-], $I'_{0,uv-l}$=250 µg/L, pH=7, S(IV) dose=70 µM

Table 4-10. Rate constants and quantum yields for bromate removal with UV-L/Sulfite ARP at different UV irradiance values, $[BrO_3^-]_0$=250 µg/L, S(IV) dose=70 µM, pH=7

UV_I (mW/cm^2)	k_{obs} (min^{-1})	95% CI	R^2	SSE	RMSE	k_{ARP} (min^{-1})
0	-	-	-	-	-	-
6	0.021	0.002	0.998	36.03	3.00	0.009
9	0.033	0.001	1.000	0.41	0.32	0.015
12	0.036	0.003	0.997	52.88	3.64	0.012

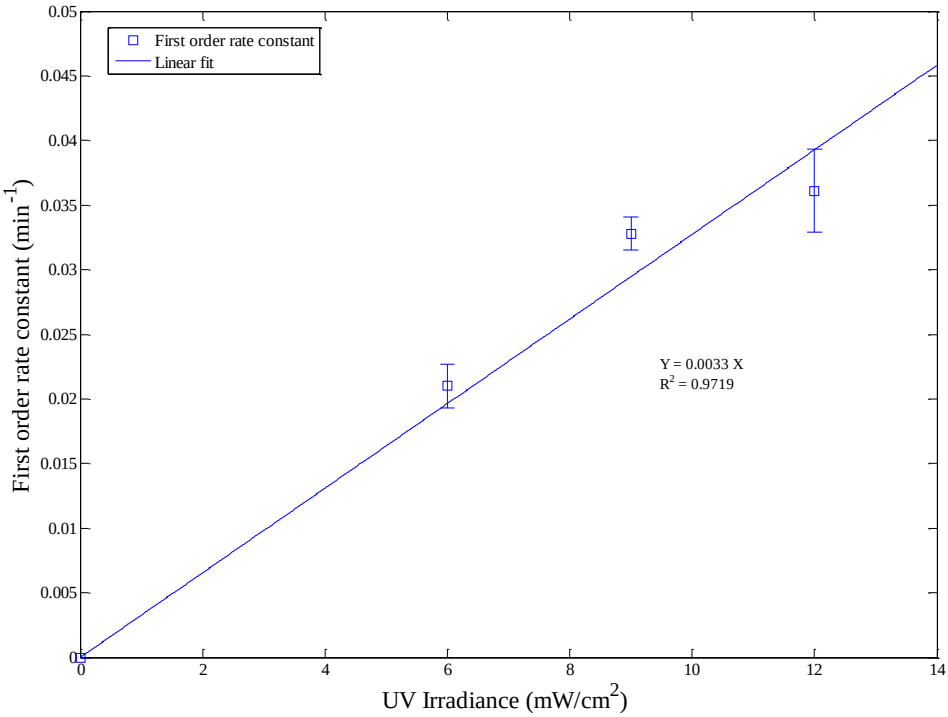

Figure 4-11. Effect of UV irradiance on first-order rate constant for bromate removal with UV-L/Sulfite ARP, $[BrO_3^-]_0$=250 µg/L, S(IV) dose=70 µM, pH=7

Table 4-11. Energy requirements for bromate removal with UV-L/Sulfite ARP, $[BrO_3^-]_0$=250 µg/L, S(IV) dose=70 µM, pH=7 mW/cm^2

UV_I (mW/cm^2)	fraction of UV absorbed	ARP Quantum Yield (mol/Ein)	E_{EO} (kWh/m^3)
0	3.60E-03	-	-
6	3.59E-03	0.011	0.091
9	3.57E-03	0.015	0.087
12	3.59E-03	0.012	0.106

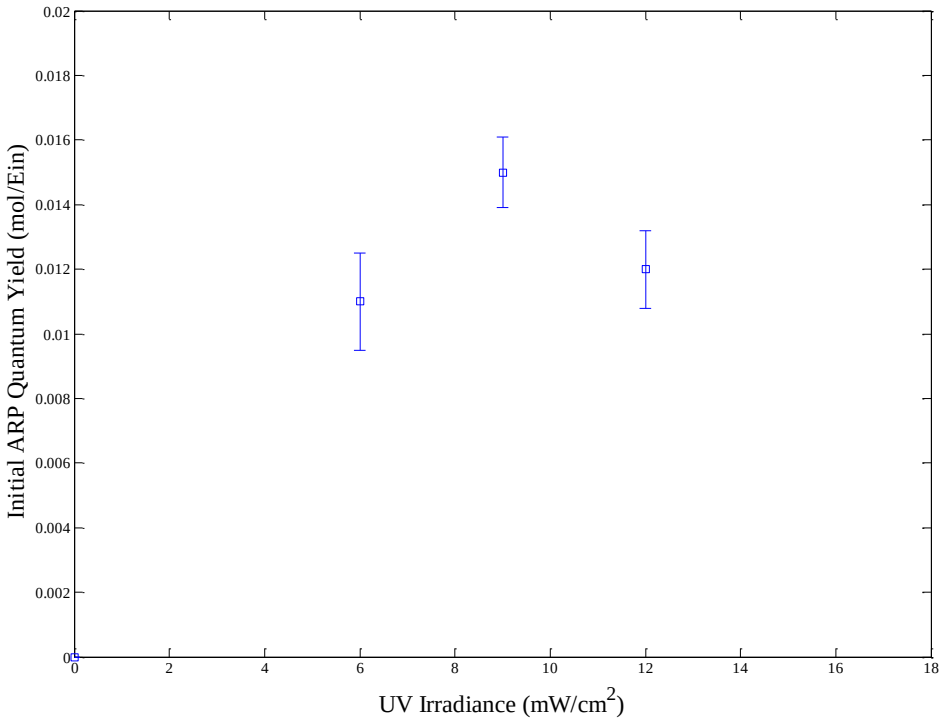

Figure 4-12. Effect of UV irradiance on quantum yield for bromate removal with UV-L/Sulfite ARP, $[BrO_3^-]_0$=250 µg/L, S(IV) dose=70 µM, pH=7

Effect of UV lamp

Results for bromate removal at S(IV) dose of 70 μM, with two different sources of UV radiation at 6 mW/cm^2 are shown in Fig. 4-13. The observed and ARP rate constants are presented in Table 4-12. According to the Beer-Lambert law, absorbance of UV is proportional to the molar extinction coefficient of the compound absorbing the light, bromate and sulfite in this case. Both bromate and sulfite have significantly higher molar absorptivity at 222 nm that at 254 nm. Thus, operating the ARP with a lower wavelength of UV light increases both components of the relationship for the observed rate constant (equation 4-5), resulting in a higher photolysis rate and a greater rate of hydrated electron generation. The overall improvement in kinetics by a factor of 60 could be attributed to the cumulative effect of these two individual reaction pathways. E_{EO} values presented in Table 4-13 indicate that the UV-L lamp is an order of magnitude more efficient than the excimer lamp with respect to energy use. When scaling up ARPs to a real water treatment process, operating costs will depend on the efficient usage of energy. In such a case, although the excimer lamp provides better kinetics, it lacks energy efficiency. Significant technological improvements need to be made in production of low wavelength UV lamps to make them suitable for water treatment. The tradeoff between kinetics and efficiency would also be influenced by design of the UV reactor and by constituents in the treated water. Water/wastewater constituents such as NOM, nitrate, nitrite and iron absorb UV and attenuate the UV irradiance available for photolytic treatment. UV absorbance of these compounds is different at 254 and 222 nm. As NOM, nitrate, nitrite and iron have greater absorbance at low wavelength UV,

attenuation of UV at high concentration of interfering compounds would be a greater problem with excimer lamp.[130-132] The nature of the effect of NOM on both lamps is discussed in the next section.

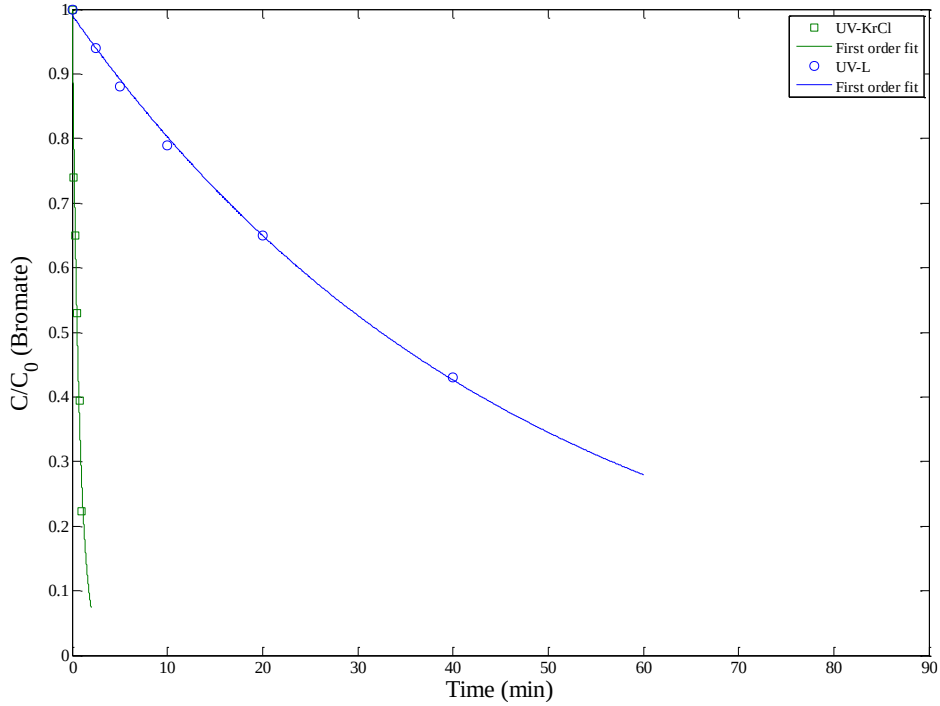

Figure 4-13. Bromate removal with UV/Sulfite ARP [BrO_3^-]$_0$=250 µg/L, S(IV) dose=70 µM, pH=7, I'$_{0,uv-l}$=6 mW/cm^2 I'$_{0,uv-krcl}$ = 6 mW/cm^2

Table 4-12. Rate constants and quantum yields for bromate removal with the UV/Sulfite ARP [BrO_3^-]$_0$=250 µg/L, S(IV) dose=70 µM, pH=7, I'$_{0,uv-l}$=6 mW/cm^2, I'$_{0,uv-krcl}$ = 6 mW/cm^2

UV Lamp	ƛ (nm)	Kobs (min^{-1})	95% CI	R^2	SSE	RMSE	k_{ARP} (min^{-1})
UV-KrCl	222	1.294	0.292	0.981	349.00	9.34	0.886
UV-L	254	0.021	0.002	0.998	36.03	3.00	0.009

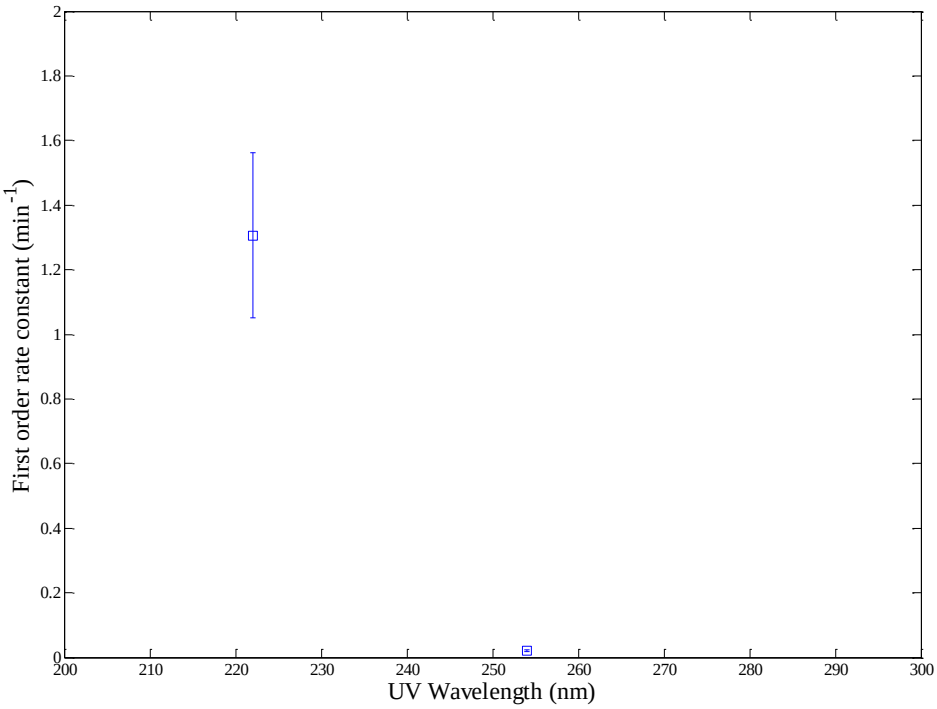

Figure 4-14. Effect of UV wavelength on rate constants for bromate removal with UV-L/Sulfite ARP, $[BrO_3^-]_0$=250 µg/L, S(IV) dose=70 µM, pH=7, $I'_{0,uv-l}$=6 mW/cm^2, $I'_{0,uv-krcl}$, = 6 mW/cm^2

Table 4-13. Energy requirements for bromate removal with UV /Sulfite ARP, $[BrO_3^-]_0$=250 µg/L, S(IV) dose=70 µM, pH=7 mW/cm^2, $I'_{0,uv\text{-}l}$=6 mW/cm^2, $I'_{0,uv\text{-}krcl}$ = 6 mW/cm^2

UV Lamp	fraction of UV absorbed	E_{EO} (kWh/m^3)
UV-KrCl	1.844E-01	1.114
UV-L	3.578E-03	0.091

Effect of NOM

Any treatment process that utilizes UV irradiation for target removal is sensitive to natural water constituents that absorb UV. One such group of UV absorbing compounds that is ubiquitous in surface waters is referred to as Natural Organic Matter (NOM).[99, 134, 135] NOM is a generic term that covers a heterogeneous mixture of multi-functional organic compounds. Composition of aquatic NOM is dependent on spatial, seasonal and climatic variations in source water. The major structural groups comprising NOM are aromatic, aliphatic, phenolic and quinonic compounds. NOM contains both hydrophobic and hydrophilic fractions. Humic substances that include humic acids, fulvic acids and humin are the principal group that impart color and UV absorbance to water.[134] NOM absorbs UV light in the wavelength range of 200-300 nm, commonly used in water treatment. Specific UV absorbance (SUV) is a parameter calculated as the UV absorbance of water at a single wavelength normalized for dissolved organic carbon

concentration. Specific UV absorbance at 254 nm (SUV_{254}) is used as an indicator for estimating the aromatic fraction of NOM. In drinking water treatment, the necessity for enhanced coagulation and softening is determined by SUV_{254}. For water systems with SUV_{254} values greater than 2 $Lmg^{-1}m^{-1}$, enhanced coagulation is required to meet USEPA DBP rule.[99]

The photochemical transformations of NOM under UV irradiation have been the subject of several studies.[135-137] The fundamental photolytic process that occurs is the breakdown of high molecular weight hydrophobic fractions of NOM to low molecular weight compounds. This process is visualized as photo bleaching.[136-138] This, process attenuates UV in the reactor and it is imperative to test effectiveness of the UV/sulfite ARP in presence of NOM. Fig. 4-16 presents the UV absorbance of NOM used in the current study. Fig. 4-17 and Fig. 4-18 present effect of NOM on bromate removal with UV-L and UV-KrCL lamps respectively. Table 4-14 lists the molar extinction coefficients values for all three UV absorbing compounds present in water samples for current experiments.

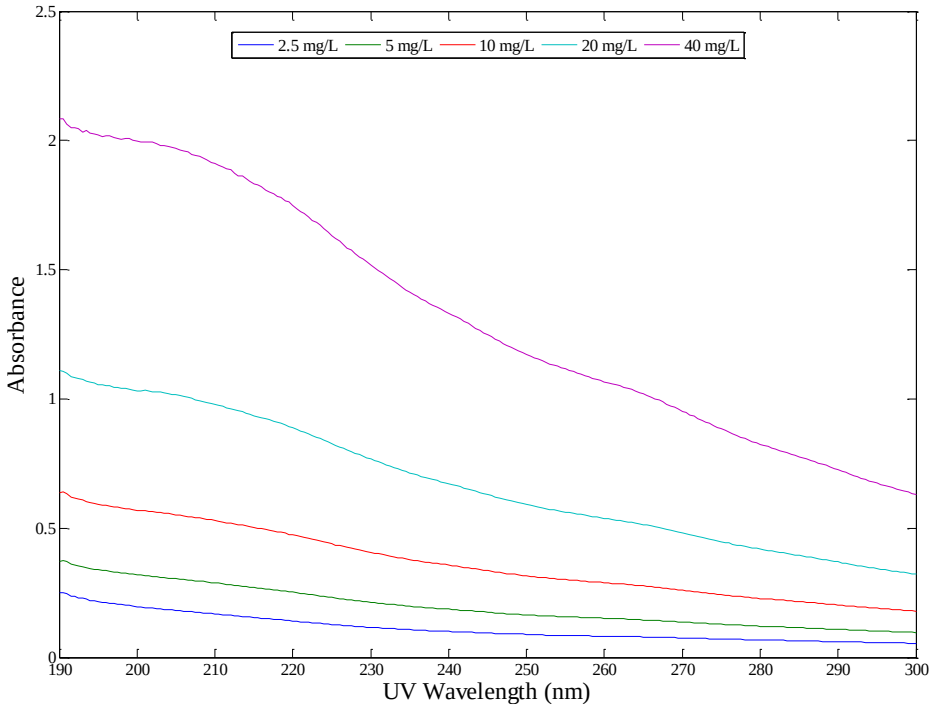

Figure 4-15. UV Absorbance spectrum of NOM

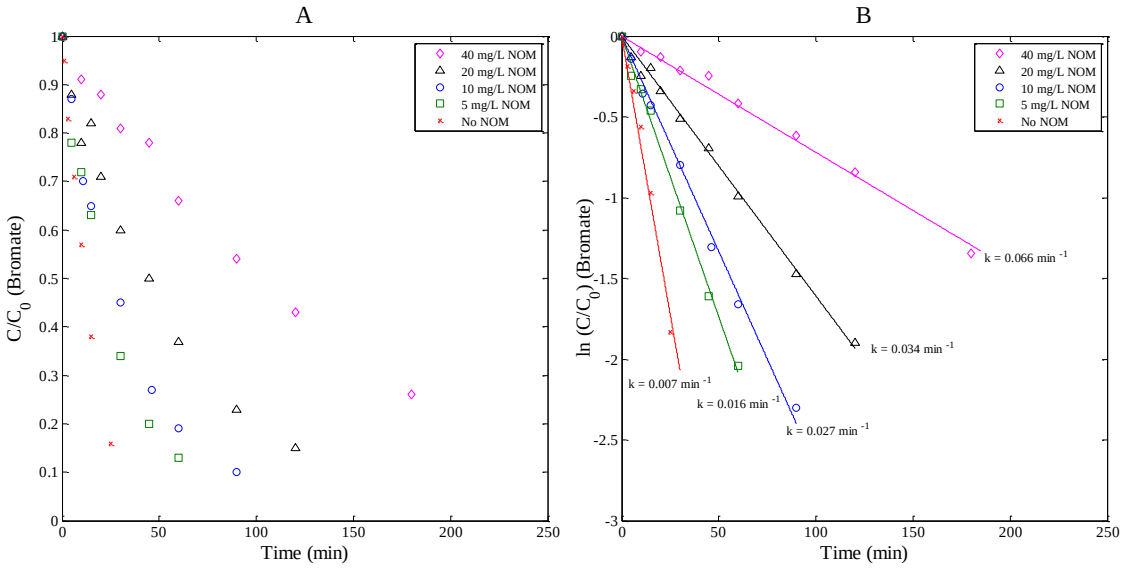

Figure 4-16. Bromate removal with UV-L/Sulfite ARP in presence of NOM, [BrO_3^-]$_0$=1 mg/L, pH=7, S(IV) dose=234 µM, I'$_{0,uv-l}$=4.82 mW/cm^2

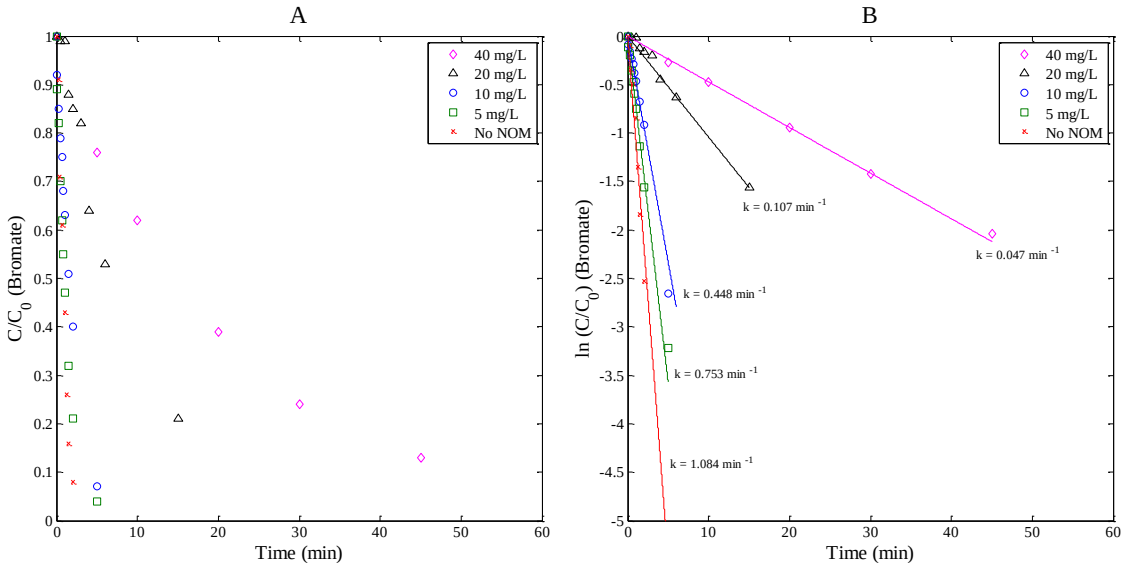

Figure 4-17. Bromate removal with UV-KrCl/Sulfite ARP in presence of NOM, $[BrO_3^-]_0$=1 mg/L, pH=7, S(IV) dose=234 µM, $I'_{0,uv\text{-}krcl}$=2.00 mW/cm^2

Table 4-14. Molar extinction coefficients (M^{-1} cm^{-1}) (log_e base) at pH 7

Compound	222 nm	254 nm
Bromate	1207	31.8
Sulfite	2199	38.5
NOM (as C)	1213	800

Attenuation coefficient (α) and I_{avg} in the reactor are calculated as in equations 4-1 and 4-2 respectively. Table 4-15 and 4-16 present the effect of NOM on α, I_{avg}, bromide recovery and first order rate constant (k_{obs}) for bromate removal with UV-L and UV-KrCl lamps, respectively. Fig. 4-19 shows a linear increase in α with increasing NOM concentration. Fig. 4-20 presents the decrease in I_{avg} as a function of attenuation coefficient. As NOM absorbs a greater fraction of UV at 222 nm, at high NOM level, I_{avg} in the reactor under UV-KrCl lamp is 80% lower than the UV-L lamp.

From the generic ARP model, the first-order rate constant for bromate removal can be expressed as shown in Equation 4-5, which can be rearranged as Equation 4-15. Equation xiv shows that reduction in rate constant can occur due to two distinct phenomenon: lowering of I_{avg} causing reduction in photolysis rate and increase in the C_{SC}, causing NOM to act as a scavenger of radicals. In order to isolate the two distinct effects and to determine the significant phenomenon, the rate constants for bromate reduction are plotted against I_{avg} in Fig. 4-21. The near linear dependence of rate

constant on I_{avg} is evident from the strong linear fit in Fig. 4-21 and goodness of fit Table 4-17.

$$k = I_{avg}\left\{\phi_T \varepsilon_T + \left[\frac{K_{TR}\phi_S \varepsilon_S C_S}{K_{TR}C_T + K_{SCR}C_{SC}}\right]\right\} \quad 4\text{-}15$$

Equation 4-14 can be rearranged as Equation 4-15, in order to isolate the scavenging effect of increasing NOM concentration (C_{SC}).

$$\left(\frac{k}{I_{avg}} - \phi_T \varepsilon_T\right) = \left[\frac{K_{TR}\phi_S \varepsilon_S C_S}{K_{TR}C_T + K_{SCR}C_{SC}}\right] \quad 4\text{-}16$$

Fig. 4-22 presents the values for $\left(\frac{k}{I_{avg}} - \phi_T \varepsilon_T\right)$ as a function of scavenger/NOM concentration. If scavenging effect of NOM is significant, the data should be inversely dependent on C_{SC}. The data in Table 4-17 show that scavenging effect is more pronounced for the UV-L lamp and UV attenuation effect is stronger for the excimer lamp. However, the overall effect of decreasing rates observed with increasing NOM concentration is a combination of these two effects. Additionally bromide recovery under the excimer lamp is consistently higher than the UV-L lamp. This loss could be due to three possible reasons: a) formation of brominated organics under the UV-L

irradiation b) volatilization of hypobromous acid formed during bromate reduction to bromide c) formation of stable bromine compounds.

Table 4-15. Average UV irradiance in the reactor for UV-L lamp, $[BrO_3^-]_0$=1 mg/L, pH=7, S(IV) dose=234 µM, UV-L irradiance=4.82 mW/cm^2, I_0 = 6.135E-03 Ein/m^2-min

C_{NOM} (mg/L, C)	k_{obs} (min^{-1})	95% CI	α (cm^{-1})	I_{avg} (Ein/m^2-min)	Bromide Recovery
0	0.066	0.009	0.009	6.099E-03	100%
5	0.034	0.005	0.343	4.952E-03	92.3%
10	0.027	0.002	0.676	4.083E-03	91.8%
20	0.016	0.002	1.342	2.902E-03	90.6%
40	0.007	0.001	2.675	1.710E-03	94.5%

Table 4-16. Average UV irradiance in the reactor for UV-KrCl lamp, $[BrO_3^-]_0$=1 mg/L, pH=7, S(IV) dose=234 µM, UV-L irradiance=2.00 mW/cm^2, I_0 = 2.225E-03 Ein/m^2-min

C_{NOM} (mg/L, C)	k_{obs} (min^{-1})	95% CI	α (cm^{-1})	I_{avg} (Ein/m^2-min)	Bromide Recovery
0	1.084	0.170	0.525	1.613E-03	98.6%
5	0.753	0.078	1.030	1.226E-03	102%
10	0.448	0.018	1.535	9.633E-04	98.2%
20	0.107	0.021	2.546	6.478E-04	101%
40	0.047	0.004	4.567	3.738E-04	102%

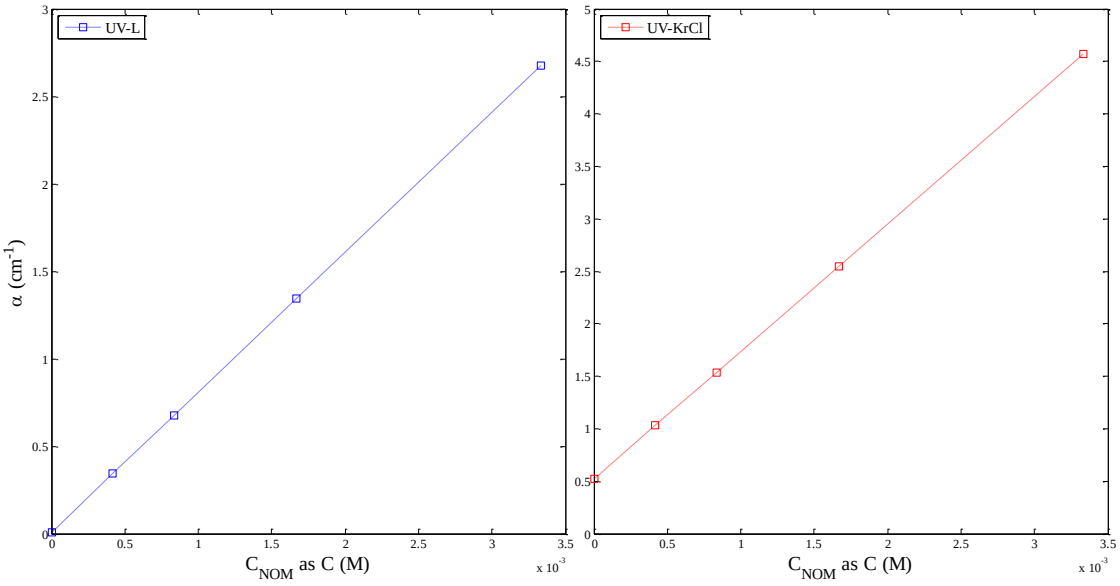

Figure 4-18. Increase in attenuation coefficient α (cm^{-1}) with C_{NOM}

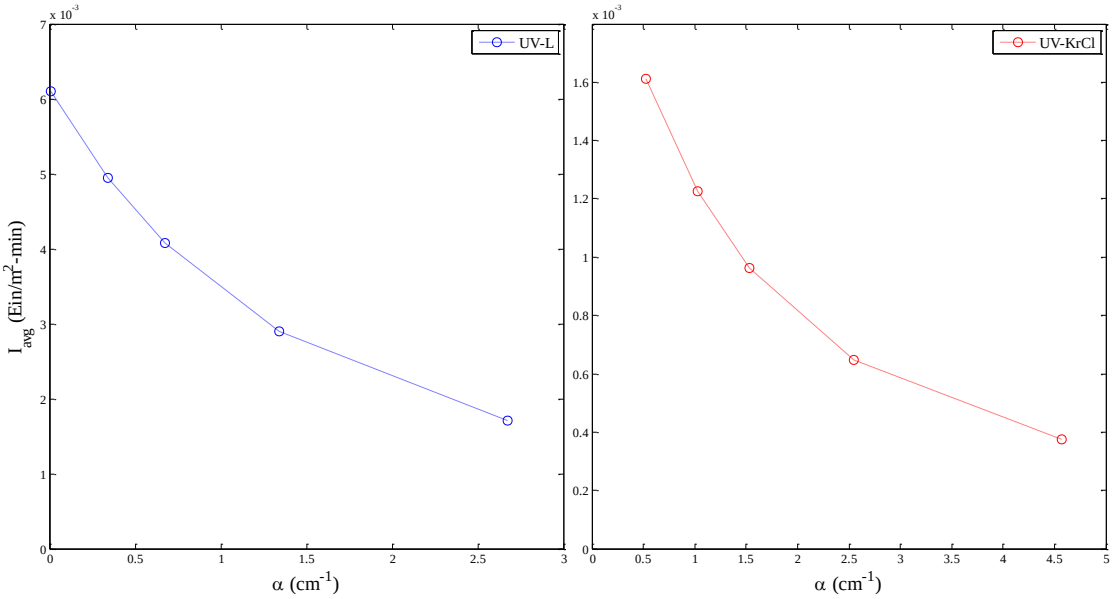

Figure 4-19. Decrease in average UV irradiance in the reactor with attenuation coefficient, $[BrO_3^-]_0$=1 mg/L, pH=7, S(IV) dose=234 µM, $I'_{0,uv\text{-}krcl}$=2.00 mW/cm^2, $I'_{0,uv\text{-}L}$=4.82 mW/cm^2

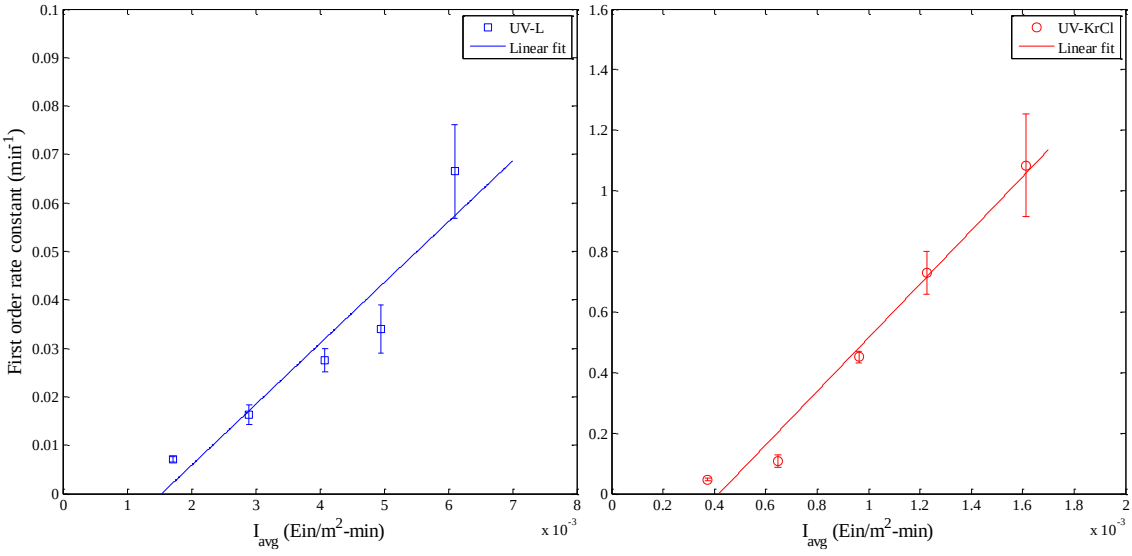

Figure 4-20. Effect of I_{avg} on the observed rate constant, $[BrO_3^-]_0$=1 mg/L, pH=7, S(IV) dose=234 µM, $I'_{0,uv\text{-}krcl}$=2.00 mW/cm^2, $I'_{0,uv\text{-}L}$=4.82 mW/cm^2

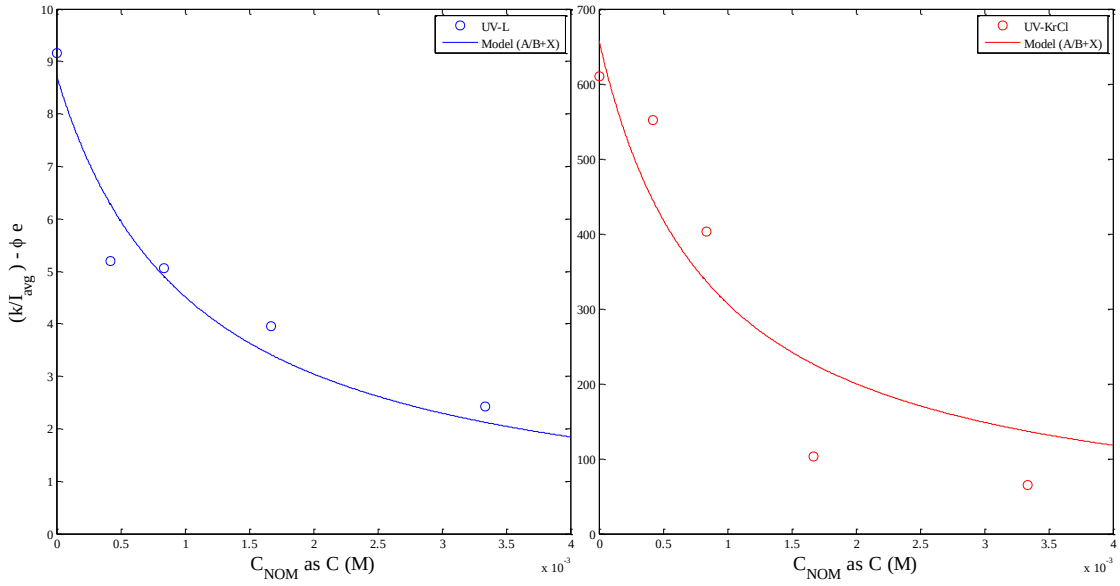

Figure 4-21. Verification of scavenging effect of NOM on bromate reduction kinetics, $[BrO_3^-]_0$=1 mg/L, pH=7, S(IV) dose=234 µM, $I'_{0,uv\text{-}krcl}$=2.00 mW/cm^2, $I'_{0,uv\text{-}L}$=4.82 mW/cm^2

Table 4-17. Model goodness of fit parameters for NOM effect on bromate kinetics

Lamp	Type of fit	R^2	C_V of RMSE
UV-L	Linear $(k = a.\ I_{avg} + b)$	0.899	0.276
	Inverse $(k/I_{avg} - \phi\varepsilon) = a / (b + C_{SC})$	0.918	0.160
UV-KrCl	Linear $(k = a.\ I_{avg} + b)$	0.828	0.161
	Inverse $(k/I_{avg} - \phi\varepsilon) = a / (b + C_{SC})$	0.976	0.348

Conclusions

The UV/Sulfite ARP was effective in completely removing bromate. The removal kinetics at alkaline pH were faster than at acidic and neutral pH. Operating the ARP with a low wavelength excimer UV lamp significantly increased the rate of bromate degradation, but did not result in improved quantum yield for the process. Higher sulfite doses and UV intensities also contributed to overall improvement in kinetics. Operating the ARP with the UV-L lamp offers better energy efficiency comparable to other advanced treatment processes, and thereby it is more suitable for practical applications. Direct photolysis and reaction with reducing radicals from sulfite irradiation were the two principal reduction mechanisms of bromate. NOM had a significant effect on lowering the rates by impacting both reduction pathways for bromate. The primary end products of this process were the relatively innocuous bromide and sulfate. Thus, UV/Sulfite ARP demonstrates the potential to become as a water treatment process for the removal of oxidized contaminants and disinfection byproducts.

CHAPTER V

SUMMARY AND CONCLUSIONS

This research demonstrates the effectiveness of UV/SO_3^{2-} ARP for application to the treatment of organic and inorganic contaminants. Results from the study reveal kinetic data on defluorination of PFOA and reduction of bromate and chlorite. Direct UV photolysis and reduction through hydrated electrons, were the principal mechanisms responsible for degradation of the target contaminants. The major end products of the reduction process for PFOA, bromate and chlorite were inorganic ions fluoride, bromide and chloride. Batch reactor testing of the UV/SO_3^{2-} ARP under different process conditions identified the optimum conditions of process variables such as pH, reagent dose, nature of UV lamp, and scavenger effects. The rate constants, quantum yields and energy requirement data developed in this research could form the basis for further testing of the ARP at pilot scale.

The major conclusions from this research can be summarized as:

1. Emission spectrum of the UV lamp plays a significant role in determining the degradation rate of contaminants in the UV/SO_3^{2-} ARP
2. Excimer UV lamp with low wavelength emission matching the absorbance spectrum of sulfite offers significant improvement in kinetics of bromate and PFOA removal in comparison to UV-L lamp.
3. UV-L lamp due to high electrical to UV conversion ratio offers greater energy efficiency for the large scale application of treatment process.

4. Research and development of energy efficient UV lamps would be the determining factor for the viability of the results of the UV/SO_3^{2-} ARP.
5. Neutral to alkaline pH would be suitable for achieving greater removal kinetics.
6. Under conditions of low UV attenuation kinetics of target removal would be proportional to sulfite dose, when UV attenuation is very high scavenging and mixing effects would counteract increasing sulfite doses.
7. UV attenuation and scavenging of hydrated electrons by NOM would be a major hindrance in application of UV/SO_3^{2-} ARP for treating natural waters.
8. Radical scavengers such as NOM, alkalinity and nitrate present in natural waters could aid in inhibiting chlorate formation during photolytic removal of chlorite.
9. Waters with high DO would require greater doses of sulfite in order to maintain adequate reducing conditions for target contaminants and prevent formation of oxidizing radicals through sulfite photochemistry.
10. The generic ARP model developed according to the fundamental processes occurring adequately describes the effect of variables such as reagent dose, UV intensity and scavenger concentration on the degradation rate of target contaminants.

REFERENCES

1. Snoeyink, V. L., *Water Chemistry / Vernon L. Snoeyink, David Jenkins*. Wiley: New York, 1980.

2. Tchobanoglous, G.; Burton, F. L.; Stensel, H. D.; Metcalf; Eddy, *Wastewater Engineering: Treatment and Reuse*. McGraw-Hill Education: 2003.

3. Ayscough, P. B.; Burchill, C. E.; Ivin, K. J.; Logan, S. R., The Photochemical Oxidation of Aqueous Iodide Solutions. An Experiment Demonstrating the Competitive Reactions of the Hydrated Electron. *J. Chem. Educ.* **1967,** *44*, (6), 349-53.

4. Walker, D. C., The Hydrated Electron. *Q. Rev., Chem. Soc.* **1967,** *21*, (1), 79-108.

5. Buxton, G. V.; Greenstock, C. L.; Helman, W. P.; Ross, A. B., Critical Review of Rate Constants for Reactions of Hydrated Electrons, Hydrogen Atoms and Hydroxyl Radicals (·Oh/·O-) in Aqueous Solution. *J. Phys. Chem. Ref. Data* **1988,** *17*, (2), 513-886.

6. Airey, P. L.; Dainton, F. S., The Photochemistry of Aqueous Solutions of Fe (Ii). I. Photoelectron Detachment from Ferrous and Ferrocyanide Ions. *Proceedings of the Royal Society of London. Series A, Mathematical and Physical Sciences* **1966,** *291*, (1426), 340-352.

7. Getoff, N.; Schenck, G. O., Primary Products of Liquid Water Photolysis at 1236 Å, 1470 Å and 1849 Å. *Berichte der Bunsengesellschaft für physikalische Chemie* **1968,** *72*, (2), 288-288.

8. Iwata, A.; Nakashima, N.; Kusaba, M.; Izawa, Y.; Yamanaka, C., Quantum Yields of Hydrated Electrons by Uv Laser Irradiation. *Chem. Phys. Lett.* **1993,** *207*, (2-3), 137-42.

9. Fischer, M.; Warneck, P., Photodecomposition and Photooxidation of Hydrogen Sulfite in Aqueous Solution. *J. Phys. Chem.* **1996,** *100*, (37), 15111-15117.

10. Heit, G.; Neuner, A.; Saugy, P.-Y.; Braun, A. M., Vacuum-Uv (172 Nm) Actinometry. The Quantum Yield of the Photolysis of Water. *The Journal of Physical Chemistry A* **1998,** *102*, (28), 5551-5561.

11. Sauer, M. C., Jr.; Crowell, R. A.; Shkrob, I. A., Electron Photodetachment from Aqueous Anions. 1. Quantum Yields for Generation of Hydrated Electron by 193 and 248 Nm Laser Photoexcitation of Miscellaneous Inorganic Anions. *J. Phys. Chem. A* **2004,** *108*, (25), 5490-5502.

12. Yang, Y.; Jiang, J.; Lu, X.; Ma, J.; Liu, Y., Production of Sulfate Radical and Hydroxyl Radical by Reaction of Ozone with Peroxymonosulfate: A Novel Advanced Oxidation Process. *Environ. Sci. Technol.* **2015,** *49*, (12), 7330-7339.

13. Li, X.; Ma, J.; Liu, G.; Fang, J.; Yue, S.; Guan, Y.; Chen, L.; Liu, X., Efficient Reductive Dechlorination of Monochloroacetic Acid by Sulfite/Uv Process. *Environ. Sci. Technol.* **2012,** *46*, (13), 7342-7349.

14. Liu, X.; Yoon, S.; Batchelor, B.; Abdel-Wahab, A., Degradation of Vinyl Chloride by Sulfite/Uv Advanced Reduction Process: Effects of Process Variables and a Kinetic Model. *Sci. Total Environ.* **2013,** *454-455*, 578-583.

15. Vellanki, B. P.; Batchelor, B., Perchlorate Reduction by the Sulfite/Ultraviolet Light Advanced Reduction Process. *J Hazard Mater* **2013,** *262*, 348-56.

16. Yoon, S.; Han, D. S.; Liu, X.; Batchelor, B.; Abdel-Wahab, A., Degradation of 1,2-Dichloroethane Using Advanced Reduction Processes. *J. Environ. Chem. Eng.* **2014,** *2*, (1), 731-737.

17. Dogliotti, L.; Hayon, E., Flash Photolysis Study of Sulfite, Thiocyanate, and Thiosulfate Ions in Solution. *J. Phys. Chem.* **1968,** *72*, (5), 1800-7.

18. Neta, P.; Huie, R. E., Free-Radical Chemistry of Sulfite. *EHP, Environ. Health Perspect.* **1985,** *64*, 209-17.

19. Vellanki, B. P. Advanced Reduction Processes - a New Class of Treatment Processes. Texas A&M University, College Station, TX, 2012.

20. Hart, E. J.; Gordon, S.; Thomas, J. K., Rate Constants of Hydrated Electron Reactions with Organic Compounds. *J. Phys. Chem.* **1964,** *68*, (6), 1271-4.

21. Goss K U, B. G., What Is So Special About the Sorption Behavior of Highly Fluorinated Compounds. *Journal of Physical Chemistry* **2006,** *110*, (30), 9518-9522.

22. Goss, K.-U., The Pka Values of Pfoa and Other Highly Fluorinated Carboxylic Acids. *Environ. Sci. Technology* **2008,** *42*, (13), 5032-5032.

23. Chad D. Vecitis, H. P., Jie Cheng, Brian T. Mader, Michael R. Hoffmann, Treatment Technologies for Aqueous Perfluorooctanesulfonate (Pfos) and Perfluorooctanoate (Pfoa). *Front. Environ. Sci. Engin. China* **2009,** *3*, (2), 129-151.

24. Bryan Boulanger, J. V., Jerald Schnoor , Keri Hornbuckle, Detection of Perfluorooctane Surfactants in Great Lakes Water. *Environ. Sci. Technology* **2004,** *38*, (15), 4064-4070.

25. K. J. Hansen, H. O. J., J. S. Eldridge, J. L. Butenhoff, and L. A. Dick, Quantitative Characterization of Trace Levels of Pfos and Pfoa in the Tennessee River. *Environ. Sci. Technology* **2002,** *36*, (8), 1681-1685.

26. Sinclair E, M. D. T., Roblee K, Yamashita N, Kannan K., Occurrence of Perfluoroalkyl Surfactants in Water, Fish, and Birds from New York State. *Archives of Environmental Contamination and Toxicology* **2006,** *50*, (3), 398-410.

27. Smithwick M, M. S. A., Solomon K R, Sonne C, Martin J W, Born E W, Dietz R, Derocher A E, Letcher R J, Evans T J, Gabrielsen G W, Nagy J, Stirling I, Taylor M K, Muir D C G., Circumpolar Study of Perfluoroalkyl Contaminants in Polar Bears. *Environ. Sci. Technology* **2005,** *39*, (15), 5517-5523.

28. Antonia M. Calafat , Z. K., Samuel P. Caudill , John A. Reidy , Larry L. Needham, Perfluorochemicals in Pooled Serum Samples from United States Residents in 2001 and 2002. *Environ. Sci. Technology* **2006,** *40*, (7), 2128–2134.

29. *Phase-out Plan for Posf-Based Products*; US Environmental Protection Agency: Washington DC, 2000.

30. Ellis D A, M. J. W., De Silva A O, Mabury S A, Hurley M D, Andersen M P S, Wallington T J., Degradation of Fluorotelomer Alcohols: A Likely Atmospheric Source of Perfluorinated CarboxylicAcids. *Environ. Sci. Technology* **2004,** *38*, (12), 3316-3321.

31. Nobuyoshi Yamashitaa, K. K., Sachi Taniyasua, Yuichi Horiia, Gert Petrickc, Toshitaka Gamod, A Global Survey of Perfluorinated Acids in Oceans. *Marine Pollution Bulletin* **2005,** *51*, (8-12), 658-668.

32. T. Wang, Y. W. W., C.Y. Liao, Y.Q. Cai, G.B. Jiang, Perspectives on the Inclusion of Perfluorooctane Sulfonate into the Stockholm Convention on Persistent Organic Pollutants. *Environ. Sci. Technology* **2009,** *43*, 5171-5175.

33. Comparative Assessment of the Global Fate and Transport Pathways of Long-Chain Perfluorocarboxylic Acids (Pfcas) and Perfluorocarboxylates (Pfcs) Emitted from Direct Sources. *Environmental Science and Technology* **2009,** *43*, (15), 5830-5836.

34. Xiaodong Ju, Y. J., Kazuaki Sasaki,Norimitsu Saito, Perfluorinated Surfactants in Surface, Subsurface Water and Microlayer from Dalian Coastal Waters in China. *Environmental Science and Technology* **2008,** *42*, (10), 3538-3542.

35. Lena Vierke*, C. S., Annegret Biegel-Engler, Wiebke Drost, Christoph Schulte, Perfluorooctanoic Acid (Pfoa) — Main Concerns and Regulatory Developments in Europe from an Environmental Point of View. *Environmental Sciences Europe* **2012,** *24*, (16).

36. Hites, R. A., *Persistant Organic Pollutants in the Great Lakes*. Springer: Germany, 2006; Vol. 5.

37. *Removal of Pfoa with Granular Activated Carbon: 3m Wastewater Treatment System Monitoring*; US Environmental Protection Agency: Washington DC, 2004.

38. Sinclair E, K. K., Mass Loading and Fate of Perfluoroalkyl Surfactants in Wastewater Treatment Plants. *Environ. Sci. Technology* **2006,** *40*, (5), 1408-1414.

39. Heqing Tanga, Q. X., Min Lei, Jingchun Yan, Lihua Zhub, Jing Zouc, Efficient Degradation of Perfluorooctanoic Acid by Uv–Fenton Process. *Chemical Engineering Journal* **2012,** *184*, 156-162.

40. H. Hori, A. Y., K. Koike, S. Kutsuna, I. Osaka, R. Arakawa, Persulfate-Induced Photochemical Decomposition of Fluorotelomer Unsaturated Carboxylic Acid in Water. *water research* **2007,** *41*, 2962-2968.

41. Y. Wang, P. Z., G. Pan, H. Chen, Ferric Ion Mediated Photochemical Decomposition of Perfluorooctanoic Acid by 254 Nm Uv Light. *journal of hazardous materials* **2008,** *160*, 181-186.

42. C.R. Estrellan, C. S., H. Hinode,, Photocatalytic Decomposition of Perfluorooctanoic Acid by Iron and Niobium Co-Doped Titanium Dioxide. *Journal of hazardous materials* **2010,** *179*, 79-83.

43. H. Hori, A. Y., K. Koike, S. Kutsuna, I. Osaka, R. Arakawa, Photochemical Decomposition of Environmentally Persistent Short-Chain Perfluorocarboxylic Acids in Water Mediated by Iron(Ii)/(Iii) Redox Reactions. *Chemosphere* **2007,** *68*, 572-578.

44. J. Chen, P. Z., J. Liu, Photodegradation of Perfluorooctanoic Acid by 185 Nm Vacuum Ultraviolet Light. *journal of environmental Sci.* **2007,** *19*, 387-390.

45. R.R. Giri, H. O., T. Morigaki, S. Taniguchi, R. Takanami, Uv Photolysis of Perfluorooctanoic Acid (Pfoa) in Dilute Aqueous Solution. *Water Sci. Technol.* **2011,** *2*, 276-282.

46. Weeks, J. L.; Meaburn, G. M. A. C.; Gordon, S., Absorption Coefficients of Liquid Water and Aqueous Solutions in the Far Ultraviolet. *Radiat. Res.* **1963,** *19*, (3), 559-67.

47. Vellanki, B. P.; Batchelor, B.; Abdel-Wahab, A., Advanced Reduction Processes: A New Class of Treatment Processes. *Environ. Eng. Sci.* **2013,** *30*, (5), 264-271.

48. Bhanu Prakash Vellanki, B. B., Perchlorate Reduction by the Sulfite/Ultraviolet Light Advanced Reduction Process. *Journal of Hazardous Materials* **2013,** *262*, 348-356.

49. Vellanki, B. P. Advanced Reduction Processes - a New Class of Treatment Processes. Texas A&M University, College Station, 2012.

50. Xu Liu, S. Y., Bill Batchelor, Ahmed Abdel-Wahab, Photochemical Degradation of Vinyl Chloride with an Advanced Reduction Process (Arp) – Effects of Reagents and Ph. *chemical engineering journal* **2013,** *215-216*, 868-875.

51. Xu Liu, S. Y., Bill Batchelor, Ahmed Abdel-Wahab, Degradation of Vinyl Chloride (Vc) by the Sulfite/Uv Advanced Reduction Process (Arp): Effects of Process Variables and a Kinetic Model. *Science of the total environment* **2013,** *454-455*, 578-583.

52. Huie, P. N. a. R. E., Free-Radical Chemistry of Sulfite. *Environmental Health Perspectives* **1985,** *64*, 209-217.

53. Shi, X. L. S., Generation of So3.Bul- and Oh Radicals in So32- Reactions with Inorganic Environmental Pollutants and Its Implications to So32- Toxicity. *Journal of inorganic biochemistry* **1994,** *56*, (3), 155-165.

54. Michael Fischer, P. W., Photodecomposition and Photooxidation of Hydrogen Sulfite in Aqueous Solution. *Journal of Physical Chemistry* **1996,** *100*, 15111-15117.

55. Huang, L.; Dong, W.; Hou, H., Investigation of the Reactivity of Hydrated Electron toward Perfluorinated Carboxylates by Laser Flash Photolysis. *Chem. Phys. Lett.* **2007,** *436*, (1-3), 124-128.

56. Qu, Y.; Zhang, C.; Li, F.; Chen, J.; Zhou, Q., Photo-Reductive Defluorination of Perfluorooctanoic Acid in Water. *Water Res.* **2010,** *44*, (9), 2939-2947.

57. Zhou Song, H. T., Nan Wangb, Lihua ZhubaKey, Reductive Defluorination of Perfluorooctanoic Acid by Hydratedelectrons in a Sulfite-Mediated Uv Photochemical System. *Journal of Hazardous Materials* **2013,** *262*, 332-338.

58. Wang, Y.; Zhang, P.; Pan, G.; Chen, H., Ferric Ion Mediated Photochemical Decomposition of Perfluorooctanoic Acid (Pfoa) by 254nm Uv Light. *J. Hazard. Mater.* **2008,** *160*, (1), 181-186.

59. Ohno, M.; Ito, M.; Ohkura, R.; Mino A, E. R.; Kose, T.; Okuda, T.; Nakai, S.; Kawata, K.; Nishijima, W., Photochemical Decomposition of Perfluorooctanoic Acid Mediated by Iron in Strongly Acidic Conditions. *J. Hazard. Mater.* **2014,** *268*, 150-155.

60. Cao, M. H.; Wang, B. B.; Yu, H. S.; Wang, L. L.; Yuan, S. H.; Chen, J., Photochemical Decomposition of Perfluorooctanoic Acid in Aqueous Periodate with Vuv and Uv Light Irradiation. *J. Hazard. Mater.* **2010,** *179*, (1-3), 1143-1146.

61. Tang, H.; Xiang, Q.; Lei, M.; Yan, J.; Zhu, L.; Zou, J., Efficient Degradation of Perfluorooctanoic Acid by Uv-Fenton Process. *Chem. Eng. J. (Amsterdam, Neth.)* **2012,** *184*, 156-162.

62. Cheng, J.-h.; Liang, X.-y.; Yang, S.-w.; Hu, Y.-y., Photochemical Defluorination of Aqueous Perfluorooctanoic Acid (Pfoa) by Vuv/Fe3+ System. *Chem. Eng. J. (Amsterdam, Neth.)* **2014,** *239*, 242-249.

63. Ho, C. K., Evaluation of Reflection and Refraction in Simulations of Ultraviolet Disinfection Using the Discrete Ordinates Radiation Model. *Water Sci Technol* **2009,** *59*, (12), 2421-8.

64. Bolton, J. R.; Linden, K. G., Standardization of Methods for Fluence (Uv Dose) Determination in Bench-Scale Uv Experiments. *J. Environ. Eng. (Reston, VA, U. S.)* **2003,** *129*, (3), 209-215.

65. Rabindra Raj Giri, H. O., Tatsuya Okada, Shogo Taniguchia, Ryohei Takanamia, Factors Influencing Uv Photodecomposition of Perfluorooctanoic Acid in Water. *Chemical Engineering Journal* **2012,** *180*, 197-203.

66. Bolton, J. R.; Bircher, K. G.; Tumas, W.; Tolman, C. A., Figures-of-Merit for the Technical Development and Application of Advanced Oxidation Technologies for Both Electric- and Solar-Driven Systems. *Pure Appl. Chem.* **2001,** *73*, (4), 627-637.

67. Zoschke, K.; Börnick, H.; Worch, E., Vacuum-Uv Radiation at 185 nm in Water Treatment – a Review. *Water Research* **2014,** *52*, 131-145.

68. Huang, J. Carbonate Radical in Natural Waters. Dissertation, University of Toronto, Toronto, Canada, 2000.

69. Huie, R. E.; Clifton, C. L.; Neta, P., Electron Transfer Reaction Rates and Equilibria of the Carbonate and Sulfate Radical Anions. *Radiat. Phys. Chem.* **1991,** *38*, (5), 477-81.

70. Ichino, T.; Fessenden, R. W., Reactions of Hydrated Electron with Various Radicals: Spin Factor in Diffusion-Controlled Reactions. *J. Phys. Chem. A* **2007,** *111*, (13), 2527-2541.

71. Das, T. N.; Huie, R. E.; Neta, P., Reduction Potentials of So3•-, So5•-, and S4o6•3- Radicals in Aqueous Solution. *J. Phys. Chem. A* **1999,** *103*, (18), 3581-3588.

72. Lu, N.; Gao, N.-Y.; Deng, Y., Nitrite Formation During Low Pressure Ultraviolet Lamp Irradiation of Nitrate. *Water Sci. Technol.* **2009,** *60*, (6), 1393-1400.

73. Crook, M. J.; Jefferson, B.; Autin, O.; MacAdam, J.; Nocker, A., Comparison of Ultraviolet Light Emitting Diodes with Traditional Uv for Greywater Disinfection. *J. Water Reuse Desalin.* **2015,** *5*, (1), 17-27.

74. Ibrahim, M. A. S.; MacAdam, J.; Autin, O.; Jefferson, B., Evaluating the Impact of Led Bulb Development on the Economic Viability of Ultraviolet Technology for Disinfection. *Environ. Technol.* **2014,** *35*, (4), 400-406.

75. Tchobanoglous, G.; Stensel, H. D.; Tsuchihashi, R.; Burton, F. L.; Abu-Orf, M.; Bowden, G.; Pfrang, W., *Wastewater Engineering : Treatment and Resource Recovery*. New York, NY : McGraw-Hill Education, 2014.
Fifth edition / revised by George Tchobanoglous (Professor Emeritus of Civil and Environmental Engineering, University of California at Davis), H. David Stensel (Professor of Civil and Environmental Engineering, University of Washington, Seattle), Ryujiro Tsuchihashi (Wastewater Technical Leader, AECOM), Franklin Burton (Consulting Engineer, Los Altos, CA) ; contributing authors, Mohammad Abu-Orf (North America Biosolids Practice Leader, AECOM), Gregory Bowden (Wastewater Technical Leader, AECOM), William Pfrang (Wastewater Treatement Technology Leader, AECOM). 2014.

76. *Electric Power Monthly*; U.S. Energy Information Administration: Washington, DC, 2015.

77. Kirschner, M., Sodium Sulfite. *ICIS Chemical Business* **2008,** *273*, (10), 42.

78. Crittenden, J. C.; Trussell, R. R.; Hand, D. W.; Howe, K. J.; Tchobanoglous, G., Advanced Oxidation. In *Mwh's Water Treatment: Principles and Design, Third Edition*, John Wiley & Sons, Inc.: 2012; pp 1415-1484.

79. Yasar, A.; Ahmad, N.; Khan, A. A. A., Energy Requirement of Ultraviolet and Aops for the Post-Treatment of Treated Combined Industrial Effluent. *Coloration Technology* **2006,** *122*, (4), 201-206.

80. David Sedlak, M. K. *Removal and Destruction of Ndma and Ndma Precursors During Wastewater Treatment*; Water Reuse Foundation: Alexandria, VA, 2006.

81. Alexander A. Mofidi, J. H. M. L. S. P., Bradley M. Coffey Sun Liang, James F. Green *Advanced Oxidation Processes and Uv Photolysis for Treatment of Drinking Water*; California Energy Commission: Sacramento, California, 2002.

82. USEPA *Alternative Disinfectants and Oxidants Guidance Manual*; United States Environmental Protection Agency: April, 1999; pp 4-1 to 4-35.

83. Voukkali, I.; Zorpas, A. A., Disinfection Methods and by-Products Formation. *Desalin. Water Treat.* **2014**, Ahead of Print.

84. Werdehoff, K. S.; Singer, P. C., Chlorine Dioxide Effects on Thmfp, Toxfp, and the Formation of Inorganic by-Products. *J. - Am. Water Works Assoc.* **1987,** *79*, (9), 107-13.

85. Lurie Mclntyre, L. N., Chlorates: A Literature Review of Aspects Relevant to the Aquatic Environment In Services, E. P., Ed. Alberta Environment Alberta, 1990.

86. EPA, U., Inorganic Chlorates Facts. In Agency, E. P., Ed. Washington, DC, 2008.

87. Grant-Trusdale, S. *Chlorite and Chlorate in Drinking Water*; World Health Organization: Geneva, Switzerland, 2005.

88. National Primary Drinking Water Regulations: Disinfectants and Disinfection Byproducts. In Agency, E. P., Ed. 1998; Vol. 63, pp 69390-69476.

89. Dixon, K. L.; Lee, R. G., The Effect of Sulfur-Based Reducing Agents and Gac Filtration on Chlorine Dioxide by-Products. *J. - Am. Water Works Assoc.* **1991,** *83*, (5), 48-55.

90. Griese, M. H.; Hauser, K.; Berkemeier, M.; Gordon, G., Using Reducing Agents to Eliminate Chlorine Dioxide and Chlorite Ion Residuals in Drinking Water. *J. - Am. Water Works Assoc.* **1991,** *83*, (5), 56-61.

91. Gordon, G.; Slootmaekers, B.; Tachiyashiki, S.; Wood, D. W., III, Minimizing Chlorite Ion and Chlorate Ion in Water Treated with Chlorine Dioxide. *J. - Am. Water Works Assoc.* **1990,** *82*, (4), 160-5.

92. Griese, M. H.; Kaczur, J. J.; Gordon, G., Combining Methods for the Reduction of Oxychlorine Residuals in Drinking Water. *J. - Am. Water Works Assoc.* **1992,** *84*, (11), 69-77.

93. Iatrou, A.; Knocke, W. R., Removing Chlorite by the Addition of Ferrous Iron. *J. - Am. Water Works Assoc.* **1992,** *84*, (11), 63-8.

94. Hurst, G. H.; Knocke, W. R., Evaluating Ferrous Iron for Chlorite Ion Removal. *J. - Am. Water Works Assoc.* **1997,** *89*, (8), 98-105.

95. Leitner, N. K. V.; De Laat, J.; Dore, M., Photodecomposition of Chlorine Dioxide and Chlorite by U.V.-Irradiation - Part Ii. Kinetic Study. *Water Res.* **1992,** *26*, (12), 1665-72.

96. Leitner, N. K. V.; De Laat, J.; Dore, M., Photodecomposition of Chlorine Dioxide and Chlorite by U.V.-Irradiation - Part I. Photo-Products. *Water Res.* **1992,** *26*, (12), 1655-64.

97. Cosson, H.; Ernst, W. R., Photodecomposition of Chlorine Dioxide and Sodium Chlorite in Aqueous Solution by Irradiation with Ultraviolet Light. *Ind. Eng. Chem. Res.* **1994,** *33*, (6), 1468-75.

98. Wu, C.; Linden, K. G., Phototransformation of Selected Organophosphorus Pesticides: Roles of Hydroxyl and Carbonate Radicals. *Water Res.* **2010,** *44*, (12), 3585-3594.

99. Weishaar, J. L.; Aiken, G. R.; Bergamaschi, B. A.; Fram, M. S.; Fujii, R.; Mopper, K., Evaluation of Specific Ultraviolet Absorbance as an Indicator of the Chemical Composition and Reactivity of Dissolved Organic Carbon. *Environ. Sci. Technol.* **2003,** *37*, (20), 4702-4708.

100. Legrini, O.; Oliveros, E.; Braun, A. M., Photochemical Processes for Water Treatment. *Chem. Rev.* **1993,** *93*, (2), 671-98.

101. Haag, W. R.; Hoigne, J., Photo-Sensitized Oxidation in Natural Water Via Hydroxyl Radicals. *Chemosphere* **1985,** *14*, (11-12), 1659-71.

102. Buxton, G. V.; Elliot, A. J., Rate Constant for Reaction of Hydroxyl Radicals with Bicarbonate Ions. *Radiat. Phys. Chem.* **1986,** *27*, (3), 241-3.

103. Liu, X.; Yoon, S.; Batchelor, B.; Abdel-Wahab, A., Photochemical Degradation of Vinyl Chloride with an Advanced Reduction Process (Arp) - Effects of Reagents and Ph. *Chem. Eng. J. (Amsterdam, Neth.)* **2013,** *215-216*, 868-875.

104. Morowitz, H. J., Absorption Effects in Volume Irradiation of Microorganisms. *Science* **1950,** *111*, (2879), 229.

105. Haag, W. R.; Hoigne´, J. r.; Gassman, E.; Braun, A. M., Singlet Oxygen in Surface Waters — Part Ii: Quantum Yields of Its Production by Some Natural Humic Materials as a Function of Wavelength. *Chemosphere* **1984,** *13*, (5), 641-650.

106. Corin, N.; Backlund, P.; Kulovaara, M., Degradation Products Formed During Uv-Irradiation of Humic Waters. *Chemosphere* **1996,** *33*, (2), 245-255.

107. Parkinson, A.; Roddick, F. A.; Hobday, M. D., Uv Photooxidation of Nom: Issues Related to Drinking Water Treatment. *Journal of Water Supply: Research and Technology - Aqua* **2003,** *52*, (8), 577-586.

108. Buxton, G. V.; Subhani, M. S., Radiation Chemistry and Photochemistry of Oxychlorine Ions. 3. Photodecomposition of Aqueous Solutions of Chlorite Ions. *J. Chem. Soc., Faraday Trans. 1* **1972,** *68*, (Pt. 5), 970-9.

109. Buxton, G. V.; Subhani, M. S., Radiation Chemistry and Photochemistry of Oxychlorine Ions. 2. Photodecomposition of Aqueous Solutions of Hypochlorite Ions. *J. Chem. Soc., Faraday Trans. 1* **1972,** *68*, (Pt. 5), 958-69.

110. Buxton, G. V.; Subhani, M. S., Radiation Chemistry and Photochemistry of Oxychlorine Ions. 1. Radiolysis of Aqueous Solutions of Hypochlorite and Chlorite Ions. *J. Chem. Soc., Faraday Trans. 1* **1972,** *68*, (Pt. 5), 947-57.

111. Autin, O.; Hart, J.; Jarvis, P.; MacAdam, J.; Parsons, S. A.; Jefferson, B., Impact of Background Organic Matter and Alkalinity on Degradation of Pesticide Metaldehyde by Oxidation Processes: Uv/H2o2 and Uv/Tio2. *Water Res.* **2013,** *47*, (6), 2041-2049.

112. Huang, J.; Mabury, S. A., Steady-State Concentrations of Carbonate Radicals in Field Waters. *Environ. Toxicol. Chem.* **2000,** *19*, (9), 2181-2188.

113. Jankowski, J. J.; Kieber, D. J.; Mopper, K., Nitrate and Nitrite Ultraviolet Actinometers. *Photochem. Photobiol.* **1999,** *70*, (3), 319-328.

114. Sharpless, C. M.; Page, M. A.; Linden, K. G., Impact of Hydrogen Peroxide on Nitrite Formation During Uv Disinfection. *Water Res.* **2003,** *37*, (19), 4730-4736.

115. Goldstein, S.; Rabani, J., Mechanism of Nitrite Formation by Nitrate Photolysis in Aqueous Solutions: The Role of Peroxynitrite, Nitrogen Dioxide, and Hydroxyl Radical. *J. Am. Chem. Soc.* **2007,** *129*, (34), 10597-10601.

116. IARC *Potassium Bromate (Summary of Data Reported and Evaluation)*; IARC: Lyon, 1999; pp 481-496.

117. EPA, U. *National Primary Drinking Water Regulations: Stage 2 Disinfectants and Disinfection Byproducts Rule*; United States Environmental Protection Agency: Washington, DC, 2006.

118. Butler, R.; Godley, A.; Lytton, L.; Cartmell, E., Bromate Environmental Contamination: Review of Impact and Possible Treatment. *Crit. Rev. Environ. Sci. Technol.* **2005,** *35*, (3), 193-217.

119. Ratpukdi, T.; Casey, F.; DeSutter, T.; Khan, E., Bromate Formation by Ozone-Vuv in Comparison with Ozone and Ozone-Uv: Effects of Ph, Ozone Dose, and Vuv Power. *J. Environ. Eng. (Reston, VA, U. S.)* **2011,** *137*, (3), 187-195.

120. Amy, G.; Siddiqui, M.; Zhai, W.; DeBroux, J.; Odem, W., Nation-Wide Survey of Bromide Ion Concentrations in Drinking Water Sources. *Proc. - Annu. Conf., Am. Water Works Assoc.* **1993**, (WATER RESEARCH), 1-19.

121. Flury, M.; Papritz, A., Bromide in the Natural Environment: Occurrence and Toxicity. *J. Environ. Qual.* **1993,** *22*, (4), 747-58.

122. Association, I. D. Desalination 101: Dealination by the Numbers. http://idadesal.org/desalination-101/desalination-by-the-numbers/ (6/4/2014),

123. Siddiqui, M.; Amy, G.; Ozekin, K.; Zhai, W.; Westerhoff, P., Alternative Strategies for Removing Bromate. *J. - Am. Water Works Assoc.* **1994,** *86*, (10), 81-96.

124. Siddiqui, M.; Zhai, W.; Amy, G.; Mysore, C., Bromate Ion Removal by Activated Carbon. *Water Res.* **1996,** *30*, (7), 1651-1660.

125. Prados-Ramirez, M. J.; Ciba, N.; Bourbigot, M. M., Available Techniques for Reducing Bromate in Drinking Water. *Water Supply* **1995,** *13*, (1), 61-70.

126. Gordon, G.; Gauw, R. D.; Emmert, G. L.; Walters, B. D.; Bubnis, B., Treatment Technologies: Chemical Reduction Methods for Bromate Ion Removal. *J. - Am. Water Works Assoc.* **2002,** *94*, (2), 91-98.

127. Phillip, N. H.; Gurten, E.; Diyamandoglu, V., Transformation of Bromine Species During Decomposition of Bromate under Uv Light from Low Pressure Mercury Vapor Lamps. *Ozone: Sci. Eng.* **2006,** *28*, (4), 217-228.

128. Peldszus, S.; Andrews, S. A.; Souza, R.; Smith, F.; Douglas, I.; Bolton, J.; Huck, P. M., Effect of Medium-Pressure Uv Irradiation on Bromate Concentrations in Drinking Water, a Pilot-Scale Study. *Water Res.* **2003,** *38*, (1), 211-217.

129. Farkas, L.; Klein, F. S., The Photochemistry of Some Ions in Solution. *J. Chem. Phys.* **1948,** *16*, 886-93.

130. Duan, Y.; Batchelor, B., Impacts of Natural Organic Matter on Perchlorate Removal by an Advanced Reduction Process. *J Environ Sci Health A Tox Hazard Subst Environ Eng* **2014,** *49*, (6), 731-40.

131. Hioki, A.; McLaren, J. W., Direct Determination Method of Nitrate Ions in Seawater by Uv-Detection Ion-Chromatography with Hydrochloric Acid/Sodium Chloride Eluent. *Sansoken Keiryo Hyojun Hokoku* **2008,** *7*, (2), 51-59.

132. Turner, R. C.; Miles, K. E., The Ultraviolet Absorption Spectra of the Ferric Ion and Its First Hydrolysis Product in Aqueous Solutions. *Can. J. Chem.* **1957,** *35*, 1002-9.

133. Hayon, E.; Treinin, A.; Wilf, J., Electronic Spectra, Photochemistry, and Autoxidation Mechanism of the Sulfite-Bisulfite-Pyrosulfite Systems. So2-, So3-, So4-, and So5- Radicals. *J. Amer. Chem. Soc.* **1972,** *94*, (1), 47-57.

134. Minear, R. A.; Amy, G. L., Water Disinfection and Natural Organic Matter: History and Overview. *ACS Symp. Ser.* **1996,** *649*, (Water Disinfection and Natural Organic Matter), 1-9.

135. Guo, Q.; Zhang, Z.; Ma, Z.; Liang, Y.; Liu, W., Fluorescence Characteristics of Natural Organic Matter in Waterunder Sequential Exposure to Uv Irradiation/Chlor(Am)Ination. *Water Sci. Technol.: Water Supply* **2014,** *14*, (1), 22-30.

136. Thomson, J.; Roddick, F.; Drikas, M., Natural Organic Matter Removal by Enhanced Photo-Oxidation Using Low Pressure Mercury Vapor Lamps. *Water Sci. Technol.: Water Supply* **2002,** *2*, (5-6), 435-443.

137. Xie, H.; Zafiriou, O. C.; Cai, W.-J.; Zepp, R. G.; Wang, Y., Photooxidation and Its Effects on the Carboxyl Content of Dissolved Organic Matter in Two Coastal Rivers in the Southeastern United States. *Environ. Sci. Technol.* **2004,** *38*, (15), 4113-4119.

138. Thomson, J.; Roddick, F. A.; Drikas, M., Vacuum Ultraviolet Irradiation for Natural Organic Matter Removal. *J. Water Supply: Res. Technol.--AQUA* **2004,** *53*, (4), 193-206.

139. Ritchie, J. D.; Perdue, E. M., Proton-Binding Study of Standard and Reference Fulvic Acids, Humic Acids, and Natural Organic Matter. *Geochimica et Cosmochimica Acta* **2003,** *67*, (1), 85-96.

140. Shamus, J. D.; Perdue, E. M., Acidic Functional Groups of Suwannee River Natural Organic Matter, Humic Acids, and Fulvic Acids. In *Advances in the Physicochemical Characterization of Dissolved Organic Matter: Impact on Natural and Engineered Systems*, American Chemical Society: 2014; Vol. 1160, pp 75-86.

APPENDIX A

DERIVATION OF ONE PSEUDO COMPONENT MODEL

Defluorination of PFOA is considered to be represented by reactions 1 and 2:

Reaction 1: $A \rightarrow B + n_1 F$,

Rate of the reaction, $r_1 = k_1 A$

A is molar concentration of PFOA,

It is assumed that r_1 is first order reaction. So, the concentration of A at any time t, in a batch reactor can be calculated as,

$A = A^0 \exp(-k_1 t)$

Reaction 2: $B \rightarrow C + n_2 F$,

Rate of the reaction $r_2 = k_2 B$

B is molar concentration of the pseudo-component

C is molar concentration of the completely defluorinated product

Initial conditions at time t = 0,

$A = A^0$, B = 0, C = 0

The total fluoride (F_t) in the system is present as

a. Fluoride attached to PFOA, A
b. Fluoride attached to pseudo component, B
c. Inorganic fluoride, F

$F_t = 15 A^0 = 15 A + n B + F$

The number of fluorine attached to compound B can be in the range 6-9, but the optimum value for n was selected as 9 to obtain best goodness of fit parameters for the model.

Conducting a material balance for compound B in a batch system,

$dB/dt = r_1 – r_2 = k_1A – k_2B = k_1 A^0\exp(-k_1t) – k_2B$

$dB/dt + k_2B = k_1 A^0\exp(-k_1t)$

Multiplying by integrating factor $\exp(k_2t)$

$dB/dt (\exp(k_2t))+ k_2B(\exp(k_2t)) = k_1 A^0\exp(-k_1t) (\exp(k_2t))$

$d\{B(\exp(k_2t))\}/dt = k_1 A^0\exp(k_2-k_1)t))$

$[B(\exp(k_2t))]_0^t = \{k_1 A^0/(k_2-k_1)\}[(\exp(k_2-k_1t)]_0^t$

$B(\exp(k_2t)) – B_0 = \{k_1 A^0/(k_2-k_1)\}\{(\exp(k_2-k_1t)-1\}$

$B_0 = 0,$

$B = \{k_1 A^0/(k_2-k_1)\}\{(\exp(k_2-k_1t)-1\}(\exp(-k_2t))$

$B = \{k_1 A^0/(k_2-k_1)\}(\exp(-k_1t)-\exp(-k_2t)\}$

Conducting a material balance for fluoride in the system gives,

$F = 15 A^0 -15 A - n B$

$F = 15 A^0 -15 A^0 \exp(-k_1t) - n \{k_1 A^0/(k_2-k_1)\}(\exp(-k_1t)-\exp(-k_2t)\}$

The residual plot for errors, i.e. difference between model value and measured fluoride concentration is shown as a function of ‘n’ value in figures 73 and 74

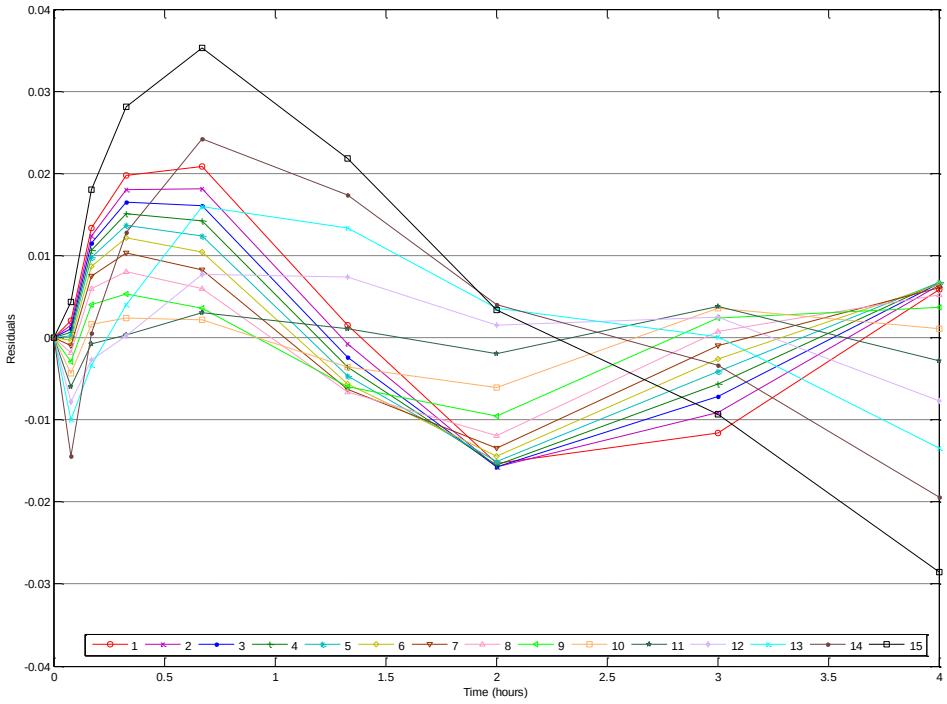

Figure A-1. Residual plot for model predictions, 'n' values 1 to 15

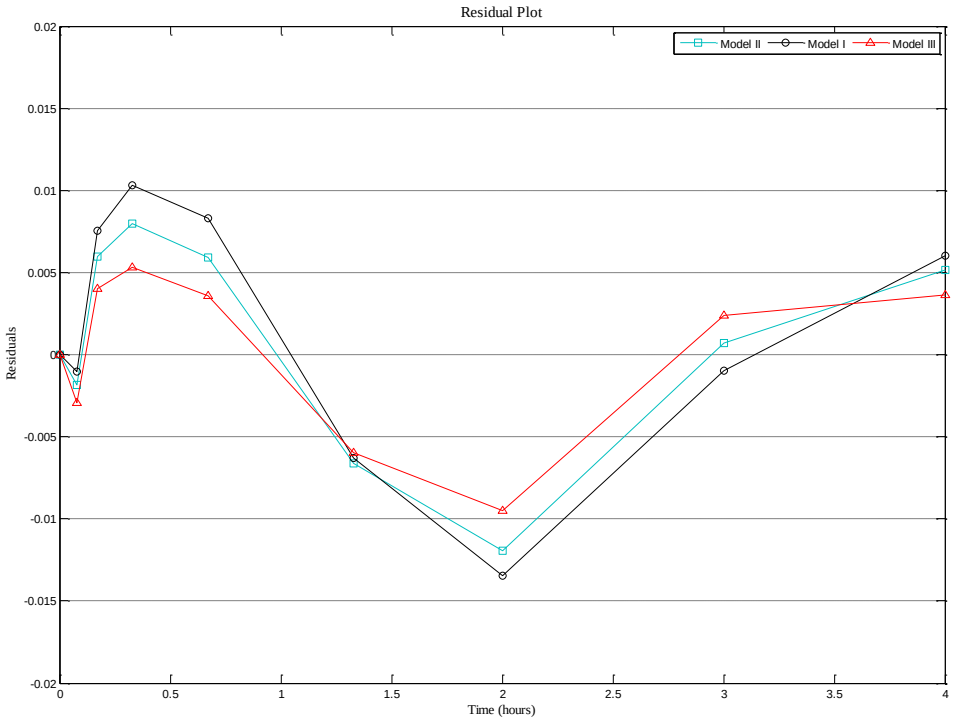

Figure A-2. Residual plot for model predictions 'n' =7, 8, 9

APPENDIX B

COMPOSITION OF FULVIC ACID (NOM)

Table B-1. Elemental compositions of Suwannee River NOM[30]

Cat. No.	H_2O	Ash	C	H	O	N	S	P	$\delta^{13}C$	$\delta^{15}N$
1R101F	8.9	0.98	53.04	4.36	43.91	0.75	0.46	<0.01	-27.9	-2.76

H_2O content is the % (w/w) of H_2O in the air-equilibrated sample; Ash is the % (w/w) of inorganic residue in a dry sample; C, H, O, N, S, and P are the elemental composition in %(w/w) of a dry, ash-free sample.

Table B-2. Acidic functional groups of Suwannee River NOM[30, 139, 140]

Cat. No.	Carboxyl	Phenolic	Q_1	log K_1	n_1	Q_2	log K_2	n_2	N	RMSE
1R101F	12.23	3.11	12.94	3.81	3.36	1.60	9.62	1.00	115	0.1312

Q_1 and Q_2 are the maximum charge densities of the two classes of binding sites, log K_1 and log K_2 are the mean log K values for proton binding by the two classes of sites, and n_1 and n_2 are empirical parameters that control the width (in log K) of a class of proton binding sites. The fitting parameters were obtained with a modified Henderson–Hasselbalch equation:

$$Q_{TOT} = \left(\frac{Q1}{1+\left(K_1[H^+]^{1/n1}\right)} \right) + \left(\frac{Q2}{1+\left(K_2[H^+]^{1/n_2}\right)} \right)$$

APPENDIX C

NONLINEAR REGRESSION FOR CALCULATING PHOTOLYSIS QUANTUM YIELD FOR TARGET CONTAMINANT

Three m-files (MATLAB) were used to obtain the quantum yield

m-file 1: deriv_ode.m

```
%This coding is kinetic equation
function dcdt=deriv_ode(t,cmeas,k) % k represents quantum,
L=0.013 % path length in meter
e=1.380 % molar absorbtivity in m^2/mol
e_1=2.303*e % base e molar absorbtivity
I_0=90.0 % light intensity in unit J/m^2/s, 1 uW/cm^2=0.01 J/m^2/s
w=254*10^-9 % wavelength of UV light in meter
Na=6.02*10^23 % avogadro's number in mol^-1
h=6.626*10^-34 % planck's number in J-s
c_l=3*10^8 % speed of light in m/s
I=I_0*w/Na/h/c_l % convert unit for light intensity to einstein/m^2/s
dcdt=-k.*I*(1-exp(-e_1*cmeas*L))/L*3600
% unit for quantum is mol/einstein
% rate of light absorption,
% cmeas (mol/m^3) here represent sulfite concentration at time t (h),
% make sure the unit is correct
% now the unit for b is einstein/m^3/h
```

```
dcdt=dcdt'
```

m-file 2: calcmod_ode.m

```
% This coding is for solving kinetic equation
function cmod=calcmod_ode(beta,t)
ct0=beta(1);
k=beta(2);
if t(1)==0
tspan=t; % if the vector t starts with t(1)=0, then it can be used as tspan
else
tspan=[0;t]; % if t does not start with 0, tspan must start with zero
end
[tout,cmod]=ode45(@deriv_ode, tspan, ct0,[], k);
```

m-file 3: nlinfit_ode.m

```
% This script m-file inputs data and calls nlinfit_ode.m to conduct non-linear least
squares regression
data = load ('bromate.txt');
% data_name.txt is the name of a text file that contains the data used in the regression.
% It is a matrix with the first column holding the values of the independent variable
(e.g.time)
% The subsequent columns hold values of the dependent variables (e.g. concentration)
```

```
% The data file must be in a directory accessible to MATLAB
t = data(:,1); % measured values of time
cmeas = data(:,2); % measured values of concentration
beta0 = [0.0005, 1]; % initial guesses for values of parameters to be determined
[beta,resid,j]=nlinfit(t,cmeas,@calcmod_ode,beta0);
% call nlinfit.m to do least-squares regression
% calcmod.m is function that returns values of
% model concentrations given values of time and
% parameters beta. Uses format
% cmod=calcmod(beta,t), where cmod is vector of
% model values of independent variable (e.g.
% concentration)
betaci=nlparci(beta,resid,j); % call function to calculate confidence intervals
beta % print to screen values of parameters
betaci % print to screen confidence intervals for parameters
```